BUILDING THE CENTRIOLE:

PLK4 PHOSPHORYLATES STIL TO DIRECT PROCENTRIOLE ASSEMBLY

by

Tyler C. Moyer

A dissertation submitted to Johns Hopkins University in conformity with the requirements for the degree of Doctor of Philosophy.

Baltimore, Maryland

May, 2019

Abstract

Centrioles are small microtubule-based cellular structures that form the centrosome, the cell's major microtubule-organizing center responsible for forming the bipolar spindle in mitosis. Each centriole duplicates exactly once per cell cycle at the onset of S phase by forming one new centriole on the wall of each of the two pre-existing parental centrioles. Polo-like kinase 4 (PLK4) has emerged as an upstream master regulator of centriole biogenesis, but how PLK4's activity is regulated to control centriole duplication specifically at the G1/S phase transition remains unclear. Here, we used CRISPR genome engineering to create a chemical genetic system in which endogenous PLK4 can be specifically inhibited using a cell-permeable ATP analog. Using this system, we demonstrate that the centriolar localization of the core centriole component STIL requires continued PLK4 activity. Most importantly, we show that direct binding of STIL to PLK4 activates PLK4 by promoting self-phosphorylation of the kinase's activation loop. PLK4 subsequently phosphorylates STIL at two distant sites to promote centriole assembly. One site allows STIL to bind to and recruit SAS6, the major component of the centriolar cartwheel, the inner framework of the centriole governing its architecture. The other site allows STIL to increase its binding to and promote the stable integration of CPAP, the centriole protein that links the cartwheel to the centriole's outer microtubule walls. Thus, our findings describe the first key steps in the initiation of centriole assembly through activation of PLK4 and identify STIL as the first *in vivo* substrate of PLK4.

Primary Reader: Andrew Holland, Ph.D.

Secondary Reader: Jennifer Kavran, Ph.D.

Acknowledgements

I consider myself incredibly fortunate to have been guided and supported in this process by so many incredible people. First and foremost, I must acknowledge and thank my graduate school advisor, Dr. Andrew Holland. I first met Andrew on what I believe was his second or third day at Hopkins when I was interviewing for my graduate program. At the time I was convinced that my graduate career would take place at another institution, but as we sat there in his office with no more than a pair of chairs, a small table, and a whiteboard we had such a great conversation about our mutual scientific interests that I slowly began changing my mind and put Hopkins at the top of my list. I am so fortunate that I was accepted to Hopkins, was invited to rotate early in his lab, and eventually join full-time as his first graduate student. While my graduate school experience had its ups and downs, as all students' experiences do, I have to thank Andrew for always being a supportive and guiding presence, no matter how challenging things got. I have so much admiration for Andrew's constant dedication to his work and the work of his students. No matter how many grants he was writing, or faculty candidate profiles he was pouring over, or countless other behind-the-scenes minutia that he didn't bother us with, Andrew always prioritized the work of his students above all else. In terms of science, Andrew is truly top-notch. Again, I consider myself so fortunate to have been trained by someone who always sought to innovate, to incorporate new technologies into the lab, and to not be afraid to dive-in to fields entirely out of his comfort zone. We are all better off for being mentored by him and I look forward to seeing how far his lab will go in the future.

The long hours and stress of graduate school would have been insurmountable if it were not for the incredible collection of graduate students in our lab. My labmates made my graduate school experience all the more worthwhile and fun. I'd like to thank Bram and Michelle, along with our first technician, Kevin, for being such a fun team to start graduate school with. Each of them has taught me so much about lab, and life, and Adobe Illustrator that I am forever grateful. It was so much fun to start the lab with them and see us all develop into great scientists as well as usher in the new generations of graduate students into our lab. To Liz, Thao, Lauren, Collin, Gina, and Taylor, you all made my time in the lab far more enjoyable and I look forward to seeing all the great things that you all will accomplish in lab and beyond. And then there's Phillip. I am so incredibly thankful that you came to our lab and for the friendship that we developed. Your support and humor got me through so many tough days and I look forward to many more adventures in the future.

Our lab is a member of a such an incredible department, with so many world-class scientists. I am so grateful that I got to be exposed to such engaging and rigorous science, and that so many of our colleagues were so eager to lend advice, time, and reagents to help push my and my lab's research forward. To our sixth-floor colleagues – thank you for creating such a welcoming and supportive environment for us as we started to build the lab. And to our seventh-floor colleagues, thank you for being such great collaborators on multiple aspects of so many projects and for always being available to bounce ideas off of.

I would also like to thank and acknowledge my thesis committee for their support and guidance throughout my graduate career. In particular, I'd like to thank Randy Reed and Jennifer Kavran

for specific technical assistance throughout my graduate school career. I must also thank the administrators in our department and within the BCMB program for handling so much of the behind-the-scenes paperwork and such so that I, and the rest of the students, can focus on our work. A thank you is also deserving to the Professional Development and Career Office for the help and guidance in navigating career options.

Last, but certainly not least, I would like to acknowledge my friends, classmates, and family for their constant support and cheering-on throughout this whole experience. I have had a wonderful collection of people at my back always encouraging me to follow my passion and for that I am incredibly grateful.

Table of Contents

List of Figures

Intended to be blank

Chapter 1. STIL activates PLK4 kinase activity

1.1 Overview

Centrioles are among the most distinctive structures in the animal cell and are characterized by an evolutionarily conserved nine-fold rotational symmetry (Gönczy 2012). In cycling cells, a pair of centrioles forms the core of the centrosome, the cell's major microtubule-organizing center. This centriole pair duplicates once in each cell cycle by forming one new centriole on the wall of each of the two pre-existing parental centrioles (Nigg and Raff 2009; Tsou and Stearns 2006). This tightly coordinated process ensures that the single interphase centrosome reproduces exactly once prior to mitosis. The two centrosomes then separate and instruct the formation of the bipolar spindle apparatus upon which chromosomes are segregated. Abnormalities in centriole duplication can result in the production of extra copies of centrosomes, a feature commonly observed in human cancers and widely implicated in contributing to the pathogenesis of the disease (Basto et al. 2008; Castellanos, Dominguez, and Gonzalez 2008; Chan 2011; Ganem, Godinho, and Pellman 2009; Godinho et al. 2014; Silkworth et al. 2009).

Pioneering work in *C.elegans* has led to the identification of a conserved set of five core proteins required for centriole assembly: ZYG-1/PLK4, SPD2/CEP192, SAS6, SAS5/STIL/Ana2, and SAS4/CPAP (Dammermann et al. 2004; Delattre et al. 2004; Kemp et al. 2004; Kirkham et al. 2003; Leidel et al. 2005; Leidel and Gönczy 2003; O'Connell et al. 2001). Of these components,

ZYG-1/PLK4 has emerged as a central, upstream regulator of centriole biogenesis. The abundance of PLK4 must be carefully controlled: reducing PLK4 levels leads to a failure of centriole duplication, while PLK4 overexpression drives the formation of multiple centrioles in a single cycle (Bettencourt-Dias et al. 2005; Habedanck et al. 2005; Kleylein-Sohn et al. 2007; O'Connell et al. 2001; Peel et al. 2012). PLK4 levels are self-regulated by a negative feedback loop in which the kinase phosphorylates itself to trigger capture by an E3 ubiquitin ligase, leading to ubiquitylation and destruction of the active kinase (Cunha-Ferreira et al. 2013, 2009; Guderian et al. 2010; Holland et al. 2012; Klebba et al. 2013; Rogers et al. 2009).

In early G1 phase, PLK4 is localized around the entire wall of the parental centriole and transitions at the beginning of S phase to an asymmetric spot on the parental centriole that marks the site of cartwheel assembly (T.-S. Kim et al. 2013; Ohta et al. 2014; K. F. Sonnen et al. 2013). The cartwheel appears at the beginning of procentriole assembly and is formed by the oligomerization of the centriole protein SAS6 (Daiju Kitagawa et al. 2011; Van Breugel et al. 2011; van Breugel et al. 2014). In *C.elegans* and *Drosophila*, SAS6 interacts directly with another cartwheel protein SAS5/Ana2(Leidel et al. 2005; Stevens, Roque, and Raff 2010). While initial studies failed to detect a direct interaction between STIL (the human counterpart of SAS5/Ana2) and SAS6 (C. Arquint et al. 2012; Tang et al. 2011), it was recently reported that phosphorylation of the conserved STAN domain of STIL/Ana2 creates a binding site for SAS6 that is required for SAS6 recruitment to the site of procentriole assembly (Dzhindzhev et al. 2014; Ohta et al. 2014). PLK4 was also shown to phosphorylate STIL *in vitro* and when overexpressed in cells (Dzhindzhev et al. 2014; Kratz et al. 2015; Ohta et al. 2014). Nevertheless, PLK4 is a low-abundance enzyme and it remains unclear if endogenous PLK4

phosphorylates the STIL STAN domain *in vivo*. Furthermore, PLK4 localizes to the centriole throughout the cell cycle in human cells (C. Arquint et al. 2012), but how its activity is regulated to trigger procentriole formation remains unknown. A major limitation in addressing these questions is the lack of tools to rapidly and specifically control PLK4 kinase activity *in vivo*.

A recent study reported the development of CFI-400945, a potent small-molecule ATP-competitive inhibitor of PLK4 kinase activity (Laufer et al. 2013). However, along with inhibiting PLK4, CFI-400945 also strongly inhibited Aurora B kinase both *in vitro* and *in vivo*, complicating the use of this inhibitor for studying PLK4 targets in cells (Holland and Cleveland 2014). We previously showed that the mutation of a single amino acid in the ATP-binding pocket of PLK4 creates an analog-sensitive (AS) kinase that can be inhibited in a highly specific manner with cell-permeable, non-hydrolyzable, bulky ATP analogs (Holland et al. 2010). In this chapter, we knock-in the AS mutation into both endogenous PLK4 alleles in a human cell line. Upon inhibition of PLK4 we find that STIL is acutely displaced from the centriole. We further characterize the relationship between STIL and PLK4 and find that PLK4 binds to a conserved coiled-coil domain within STIL (Ohta et al. 2014). Most importantly, we show that STIL binding activates PLK4 kinase activity. Given that STIL is degraded after mitosis and accumulates at the beginning of S phase, our data offer a molecular basis for controlling the timing of PLK4 activation and centriole assembly.

1.2 A chemical genetics system for controlling PLK4 activity in cells

To study the function of PLK4 kinase activity in cells, we used CRISPR/Cas9 genome engineering to knock-in the PLK4 AS mutation (L89G) into both endogenous PLK4 alleles in

the DLD-1 colon cancer cell line (**Figure 1A**). Two homozygous PLK4$^{AS/AS}$ clones were identified that behaved similarly in all assays and are hereafter presented together. Importantly, PLK4$^{AS/AS}$ cells underwent normal centriole duplication demonstrating the functionality of the PLK4^{AS} allele *in vivo* (**Figure 1B,C**).

Inhibition of PLK4 kinase activity leads to an increase in the level of the kinase (Holland et al. 2010). We therefore used the abundance of PLK4 at the centrosome as a readout of kinase inhibition. Treatment of PLK4$^{WT/WT}$ cells with 10 μM of the bulky purine analog 3MB-PP1 did not affect centriole number or PLK4 levels (**Figure 1B,D**). By contrast, treatment of PLK4$^{AS/AS}$ cells with increasing concentrations of 3MB-PP1 led to a dose-dependent increase in PLK4 levels at the centrosome. Maximal PLK4 stabilization was achieved at 0.2 μM 3MB-PP1 indicating complete inhibition of PLK4 activity at this dose (**Figure 1D**). Consistently, PLK4$^{AS/AS}$ cells treated with 0.2 μM 3MB-PP1 for one cell cycle failed centriole duplication (> 70% cells contained 0-2 centrioles in mitosis) (**Figure 1B,C**). Treatment of PLK4$^{AS/AS}$ cells with lower doses of 3MB-PP1 partially increased PLK4 abundance and gave rise to modest centriole amplification in mitotic cells (> 20% of cells treated with between 0.025 - 0.1 μM of 3MB-PP1 contained > 4 centrioles in mitosis) (**Figure 1B-D**). This effect may be due to the formation of heterodimers between kinase inactive and catalytically-active PLK4 that leads to an increase in the abundance of the wild type (WT) kinase (Guderian et al. 2010; Laufer et al. 2013).

1.3 Human DLD-1 cells continue to proliferate in the absence of centrioles

Recent work has shown that loss of the p53 tumor suppressor is necessary for the proliferation of cells lacking centrioles (Bazzi and Anderson 2014; Izquierdo et al. 2014). DLD-1 cell lines express a mutant form of p53 with compromised function (Sur et al. 2009). Consequently, chronic treatment of DLD-1 PLK4$^{AS/AS}$ cells with 3MB-PP1 resulted in the step-wise reduction in centriole number as cells failed centriole duplication but continued to divide (**Figure 2A-B**). The cell cycle profile of PLK4^{AS} cells was unaltered at day 5 after 3MB-PP1 addition, by which point > 90 % of cells lacked centrioles (**Figure 2A-C**). DLD-1 PLK4$^{AS/AS}$ cells lacking centrioles exhibited a significant increase in the level of aneuploidy and a modestly reduced proliferation rate (**Figure 1E and 2D**) but had no reduction in long-term clonogenic survival capability (**Figure 2E-F**). These data are consistent with the view that centrosomes are not essential for cell growth, but increase the fidelity of chromosome segregation (Debec, Sullivan, and Bettencourt-Dias 2010; Khodjakov and Rieder 2001; Sir et al. 2013). Strikingly, washout of 3MB-PP1 in acentriolar DLD-1 cells led to the reactivation of PLK4 and the formation of *de novo* centrioles (**Figure 2G)**. PLK4 activity is therefore dose-limiting for canonical and *de novo* centriole biogenesis.

1.4 The centriole localization of STIL requires PLK4 kinase activity

To determine which proteins require PLK4 kinase activity for centriole recruitment, we inhibited PLK4 for one hour and measured the abundance of 12 proteins at the centrosome of S/G2 cells (**Figure 1F**). As expected, one hour after inhibiting PLK4, the abundance of the kinase at the centriole increased. RNAi depletion of STIL has been reported to dramatically decrease the centriole-localized pool of SAS6 (C. Arquint et al. 2012; Tang et al. 2011; Vulprecht et al.

2012). Surprisingly, while the abundance of STIL at the centriole declined to 26% of control levels one hour after inhibition of PLK4, the abundance of SAS6 declined to only 72% in the same time period (**Figure 1F**). Prolonged treatment with 3MB-PP1 led to a progressive decline in the level of SAS6 at the centriole, reaching 31% of control levels by 2 days after 3MB-PP1 addition (**Figure 2H**). Importantly, STIL and SAS6 cellular protein levels were not altered after chronic PLK4 inhibition (**Figure 1G**). We conclude that unlike SAS6, STIL dissociates from the centriole with extremely rapid kinetics following PLK4 inhibition.

1.5 PLK4 directly binds and facilitates the recruitment of STIL to the centriole

Since PLK4 kinase activity is required for the recruitment of STIL to the centriole, we investigated whether STIL and PLK4 form a complex in cells. Cells were transfected with full-length Myc-GFP-STIL and either kinase active ($PLK4^{WT}$) or kinase dead ($PLK4^{KD}$) PLK4-mCherry. Both active and inactive PLK4-mCherry co-purified with Myc-GFP-STIL (**Figure 3A**). PLK4 is a suicide kinase that promotes its own destruction through self-phosphorylation of a 24 a.a. multi-phosphodegron (MPD) (Holland et al. 2010). As expected, deletion of the MPD (a.a. S282-S305) specifically stabilized kinase active PLK4 ($PLK4^{\Delta 24,WT}$) and increased the amount of active PLK4 that co-immunoprecipitated with Myc-GFP-STIL (**Figure 3A**). To examine whether PLK4 directly associates with STIL we performed GST-pull down assays in the absence of ATP using purified recombinant STIL and GST-PLK4. GST-PLK4 could specifically pull-down STIL demonstrating a direct, kinase-independent association (**Figure 3B**). Together these data show that PLK4 and STIL form a complex independent of PLK4 kinase

activity. This contrasts with a recent study that proposed PLK4 interacted with STIL in a kinase-activity-dependent manner (Ohta et al. 2014).

To map the domain of STIL that interacts with PLK4, cells were transfected with a series of Myc-GFP-STIL truncation constructs and the interaction with $PLK4^{KD}$-mCherry examined. Using this approach we mapped amino acids 715-850 as a region of STIL sufficient for binding to PLK4 (**Figure 3C,D**). This region contains a highly conserved sequence (a.a. 721-746) that forms a predicted coiled-coil (**Figure 4A**). Deletion of a.a. 721-746 (ΔCC) from full-length Myc-GFP-STIL decreased binding to both kinase active and inactive $PLK4^{\Delta 24}$-mCherry (**Figure 4B,C**). We next analyzed whether PLK4 binding was required for the localization of STIL to the centriole. Myc-GFP-STIL WT and ΔCC were expressed in cells depleted of endogenous STIL by siRNA. Deletion of the predicted coiled-coil domain reduced the abundance of STIL at the centriole to 6% of that observed in control cells and failed to rescue centrosome duplication in cells depleted of endogenous STIL (**Figure 4D,E**). We conclude that binding to PLK4 is necessary for the centriole targeting and function of STIL.

1.6 STIL binding to PLK4 promotes kinase activity

Co-transfection of Myc-GFP-STIL reduced the abundance of $PLK4^{WT}$ by 50%, but had little effect on the level of $PLK4^{KD}$ (**Figure 5A,B**). Since PLK4 promotes its own destruction, we hypothesized that STIL expression stimulated PLK4 kinase activity and thus destruction. To test this hypothesis, we first examined the abundance of stably overexpressed PLK4-EYFP in the presence and absence of STIL. The total cellular pool, and levels of centrosome-localized PLK4-

EYFP increased dramatically following STIL siRNA (**Figure 5C**). To test whether STIL regulates the abundance of endogenous PLK4, Myc-GFP-STIL WT and ΔCC were expressed in cells depleted of STIL. STIL knockdown increased the level of endogenous PLK4 at the centrosome (**Figure 5D**), while overexpression of Myc-GFP-STIL WT decreased the abundance of centrosomal PLK4. This decrease required STIL binding to PLK4 as overexpression of Myc-GFP-STIL$^{\Delta CC}$ had little effect on PLK4 levels (**Figure 5D**).

To test if STIL was capable of promoting PLK4 self-phosphorylation, we stabilized kinase active PLK4 by deletion of the PLK4 MPD (PLK4$^{\Delta 24,WT}$). Strikingly, expression of Myc-GFP-STIL dramatically reduced the mobility of kinase active PLK4$^{\Delta 24}$-mCherry in a SDS-PAGE gel, but had no effect on the mobility of kinase dead PLK4$^{\Delta 24}$-mCherry (**Figure 5E**). Treatment with λ-phosphatase abolished the electrophoretic mobility shift, demonstrating that the slower migration of PLK4$^{\Delta 24}$-mCherry was a result of increased kinase self-phosphorylation. To establish whether STIL binding stimulates PLK4 activity, we co-expressed PLK4$^{\Delta 24,WT}$-mCherry with Myc-GFP-STIL WT or ΔCC in cells. While Myc-GFP-STIL increased PLK4$^{\Delta 24,WT}$-mCherry self-phosphorylation, the Myc-GFP-STIL$^{\Delta CC}$ mutant that was defective in PLK4 binding did not (**Figure 5F**). Importantly, a fragment of Myc-GFP-STIL (a.a. 715-988) that contains the coiled-coil domain and interacts with PLK4 was unable to activate the kinase, suggesting that binding to the STIL coiled-coil is not, in itself, sufficient to activate PLK4 (**Figure 5F**). We conclude that STIL binding to PLK4 stimulates kinase activity and subsequent destruction of the kinase.

PLK4 kinase activity requires phosphorylation of threonine 170 in the activation loop (T-loop) of the kinase domain (Nakamura, Saito, and Takekawa 2013; Swallow et al. 2005). We therefore

tested whether STIL binding promotes PLK4 T170 phosphorylation. PLK4$^{\Delta 24}$-mCherry was co-transfected with or without Myc-GFP-STIL and immunoprecipitated PLK4 was probed with an antibody that recognizes phosphorylated T170 (pT170) (Nakamura, Saito, and Takekawa 2013). Importantly, expression of Myc-GFP-STIL WT dramatically increased phosphorylation of T170 on kinase active, but not inactive PLK4$^{\Delta 24}$ (**Figure 5G**). By contrast, expression of the Myc-GFP-STIL$^{\Delta CC}$ mutant that was defective in PLK4 binding was unable to promote PLK4-mediated T170 phosphorylation. These data suggest that STIL binding stimulates PLK4 T170 self-phosphorylation leading to increased PLK4 activity.

Human PLK4 is targeted to the centriole through a direct interaction with the acidic N-terminal region of CEP152 and CEP192 (Cizmecioglu et al. 2010; Dzhindzhev et al. 2010; Hatch et al. 2010; T.-S. Kim et al. 2013; K. F. Sonnen et al. 2013). However, while Myc-GFP-STIL, Myc-GFP-CEP152 and Myc-GFP-CEP192 all formed a complex with PLK4$^{\Delta 24,KD}$-mCherry in cells, STIL was the only PLK4 binding partner that significantly stimulated self-phosphorylation of PLK4$^{\Delta 24}$ (**Figure 5H,I**).

1.7 Discussion

STIL is an *in vivo* regulator of PLK4 kinase activity

An important unanswered question is how PLK4 kinase activity is temporally controlled to promote centriole assembly. Our findings reveal that direct binding of PLK4 to STIL stimulates PLK4 kinase activity by promoting self-phosphorylation of the activation loop of the PLK4 kinase domain (**Figure 5E and G**). In cycling cells, STIL accumulates in late G1/early S phase

and is then degraded after anaphase onset (Arquint and Nigg 2014; C. Arquint et al. 2012; Tang et al. 2011). We therefore speculate that the cell cycle-regulated accumulation of STIL could provide the trigger for activation of PLK4 at the G1/S boundary. How STIL binding promotes PLK4 activation remains unclear. One possibility is that the binding of STIL triggers a conformational change in PLK4 that positions the PLK4 activation loop for optimal self-phosphorylation. Alternatively, STIL may promote the recruitment of an additional factor that serves to activate PLK4.

At the G1/S border, centriolar PLK4 transitions from a ring-like arrangement to a single focus on the wall of the parental centriole (T.-S. Kim et al. 2013; Ohta et al. 2014; K. F. Sonnen et al. 2013). Understanding how this transition is controlled is central to understanding how a single new centriole is created on each parental centriole. Since STIL binding stimulates PLK4 kinase and subsequent destruction (**Figure 5A**), STIL recruitment may lead to the activation and destruction of PLK4 that is localized around the wall of the parental centriole. Consistently, it was recently shown that depletion of STIL prevented the formation of a single focus of PLK4 (Ohta et al. 2014). How a single focus of PLK4 is protected from auto-destruction remains an important question for future studies.

PLK4 kinase activity is not required for continued growth of DLD-1 colon cancer cells

While the abundance of PLK4 is normally carefully controlled, alterations in PLK4 expression has been reported in several tumor types, prompting proposals that PLK4 inhibition may be an effective anticancer therapy. Surprisingly, we now show that specific inhibition of PLK4 kinase activity in a human cancer cell line with compromised p53 function results in a complete loss of

centrioles and centrosomes, but only modestly reduced cell growth (**Figure 1B and E**). This demonstrates that PLK4 and centrioles are not essential for cell cycle progression, at least in transformed cells. It therefore remains to be determined whether PLK4 inhibition will be a useful strategy in cancer therapy.

1.8 Figures and Legends

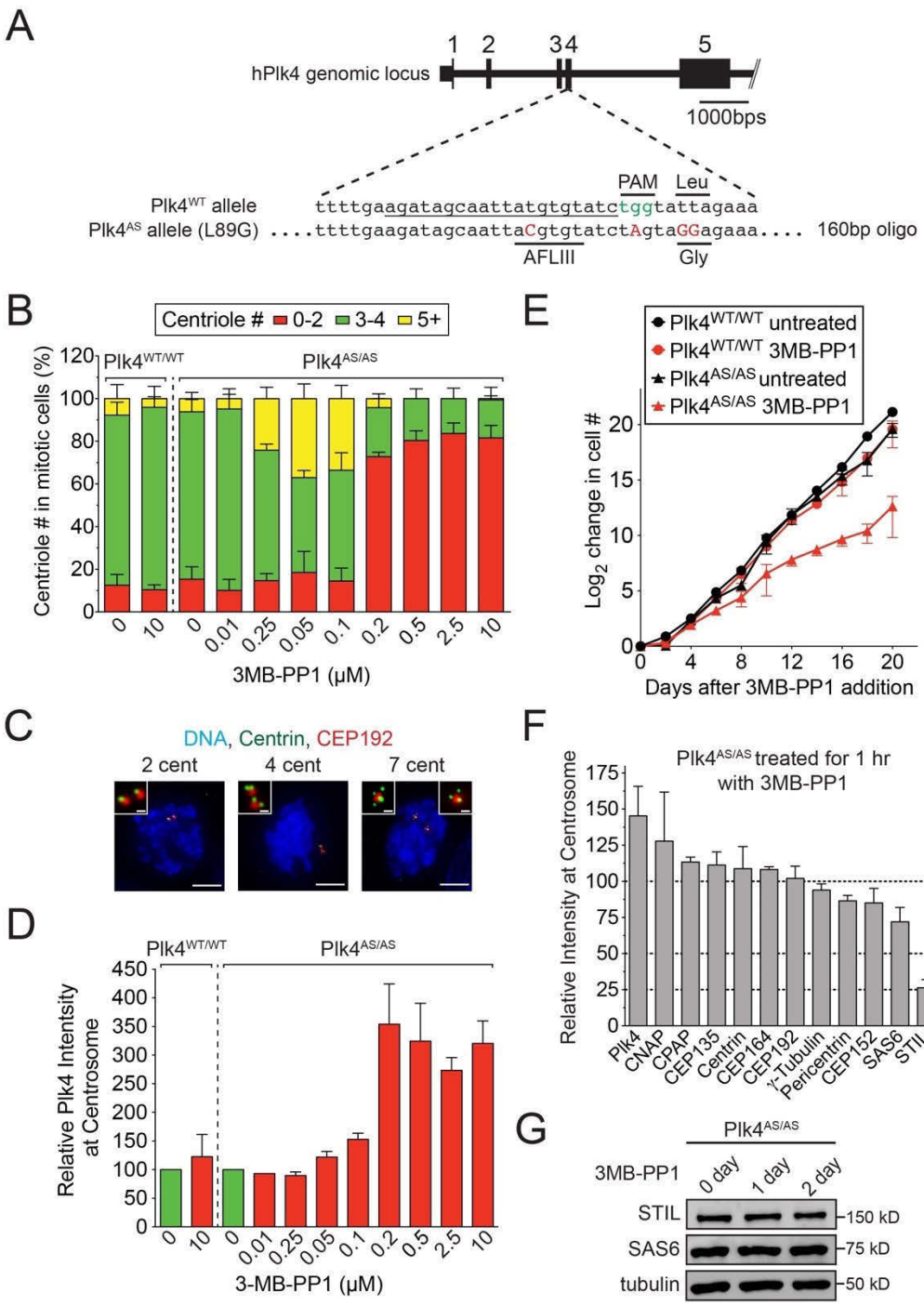

Figure 1. PLK4 kinase activity is required to maintain STIL at the centriole.

(A) Schematic of the strategy used to knock-in the analog-sensitive (AS) mutation into both alleles of PLK4 in human DLD-1 cells. The repair oligonucleotide introduced the AS mutation (L89G), a silent AflIII restriction site and a mutation in the protospacer adjacent motif (PAM) to prevent re-cutting by *Sp*Cas9 after homology directed repair.

(B) PLK4$^{WT/WT}$ or PLK4$^{AS/AS}$ cells were treated with 3MB-PP1 for 20 hours and nocodazole added for the final 4 hours of the treatment. Graph shows the fraction of mitotic cells with the indicated number of centrioles. Bars represent the mean of three independent experiments with > 20 cells counted per experiment.

(C) Selected images of mitotic PLK4$^{AS/AS}$ cells from (B) stained with Centrin and CEP192. Scale bar for large images, 5 μm. Scale bar for small images, 0.5 μm.

(D) Quantification of the relative levels of PLK4 at the centrosome of interphase cells 20 hours after addition of 3MB-PP1. Bars represent the mean of at least three independent experiments with > 40 cells counted per experiment.

(E) Graph showing the increase in cell number at various times after addition of 3MB-PP1. Points show the mean of at least three independent experiments.

(F) Quantification of relative protein abundance at the centrosome of S/G2 phase cells 1 hour after addition of 3MB-PP1. Bars represent the mean of three independent experiments with > 40 cells counted per experiment.

(G) Immunoblot showing no change in the level of endogenous STIL and SAS6 at 1 or 2 days after PLK4 inhibition with 3MB-PP1. All error bars in the figure represent the *S.E.M.*

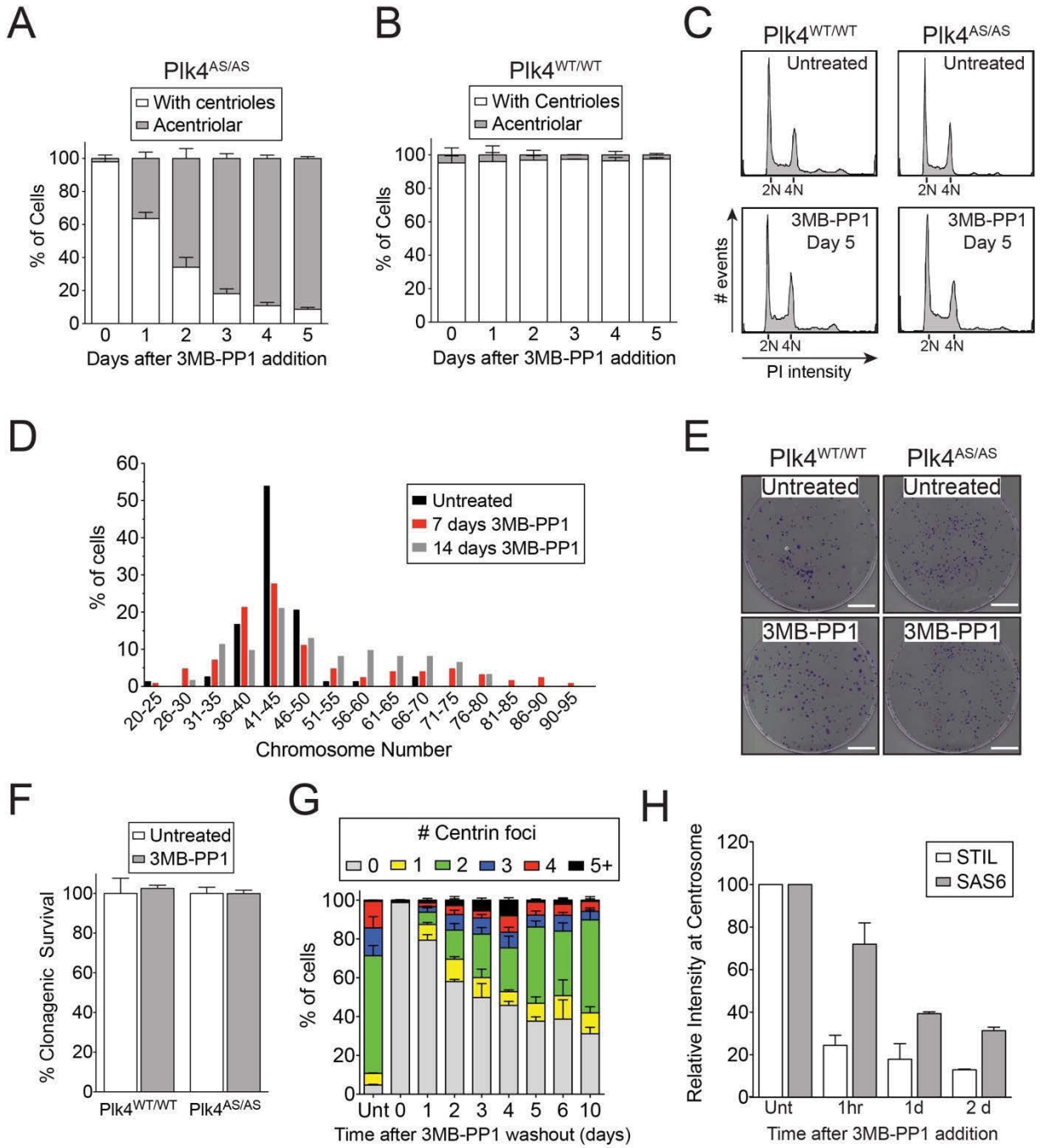

Figure 2. Continued growth of DLD-1 cells in the absence of PLK4 kinase activity.

(A-B) Quantification of the fraction of interphase cells that lack Centrin and CEP192 foci (Acentriolar) at various times after 3MB-PP1 addition. Bars represent the mean of three independent experiments with > 50 cells counted per experiment

(C) Flow cytometry profiles of $PLK4^{WT/WT}$ and $PLK4^{AS/AS}$ cells after 5 days of 3MB-PP1 treatment. Profiles shown are taken from a single representative experiment that was repeated three times.

(D) Chromosome counts of $PLK4^{AS/AS}$ cells. This experiment was completed once with at least n=60 cells per condition.

(E) Images of crystal violet-stained colonies formed two weeks after addition of 3MB-PP1. Scale bar, 2 cm.

(F) Quantification of the percent clonogenic survival of the indicated cell lines. Bars represent the mean of at least two independent experiments carried out in triplicate.

(G) Quantification of the number of Centrin foci per cell at various times after 3MB-PP1 washout. Bars represent the mean of two independent experiments with > 50 cells counted per experiment.

(H) Quantification of the relative levels of STIL and SAS6 at the centrosome of S/G2 phase cells at various times after addition of 3MB-PP1. Bars represent the mean of two independent experiments with > 40 cells counted per experiment. All error bars in the figure represent the *S.E.M.*

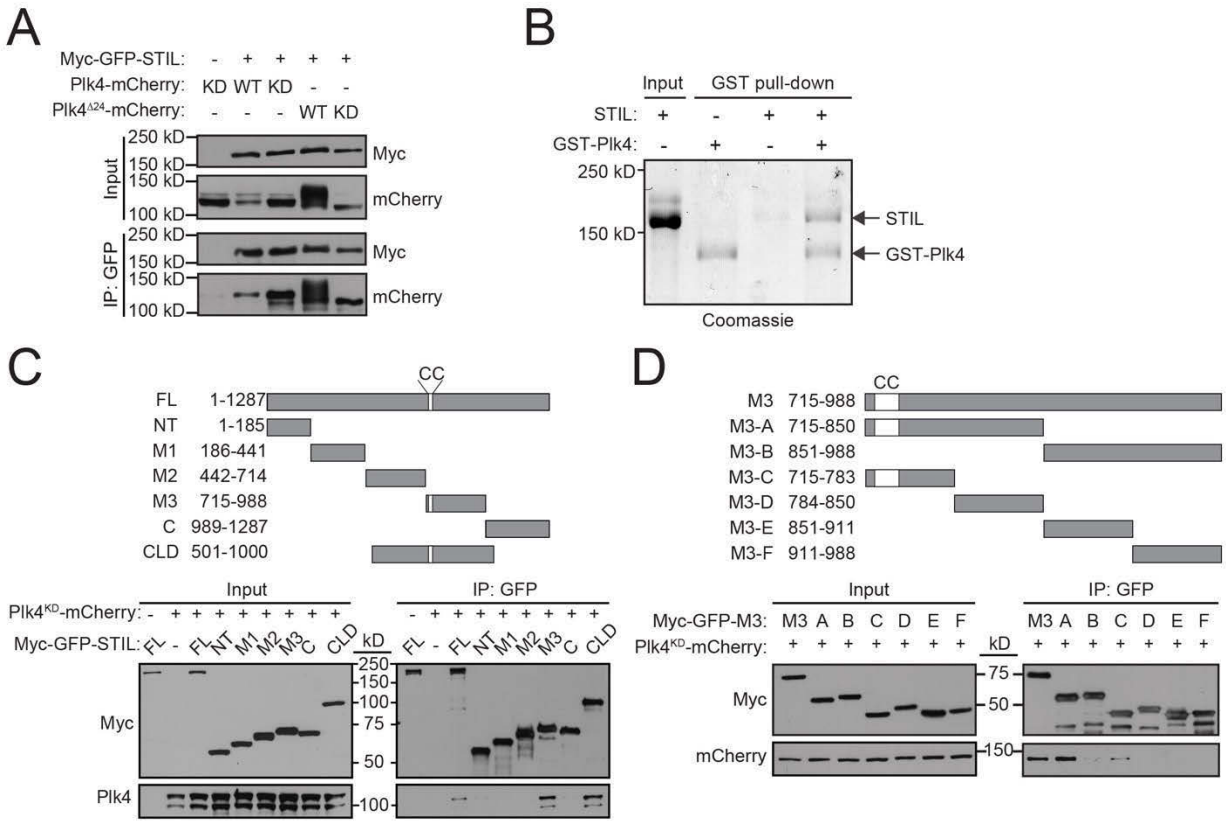

Figure 3. PLK4 directly binds to STIL *in vitro* and *in vivo*.

(A) Cells were co-transfected with the indicated constructs and subject to co-immunoprecipitation analysis with the indicated antibodies.

(B) GST-PLK4 was incubated with STIL *in vitro* and GST pull-downs analyzed by Coomassie staining.

(C-D) Cells were co-transfected with the indicated constructs and subject to co-immunoprecipitation analysis with the indicated antibodies.

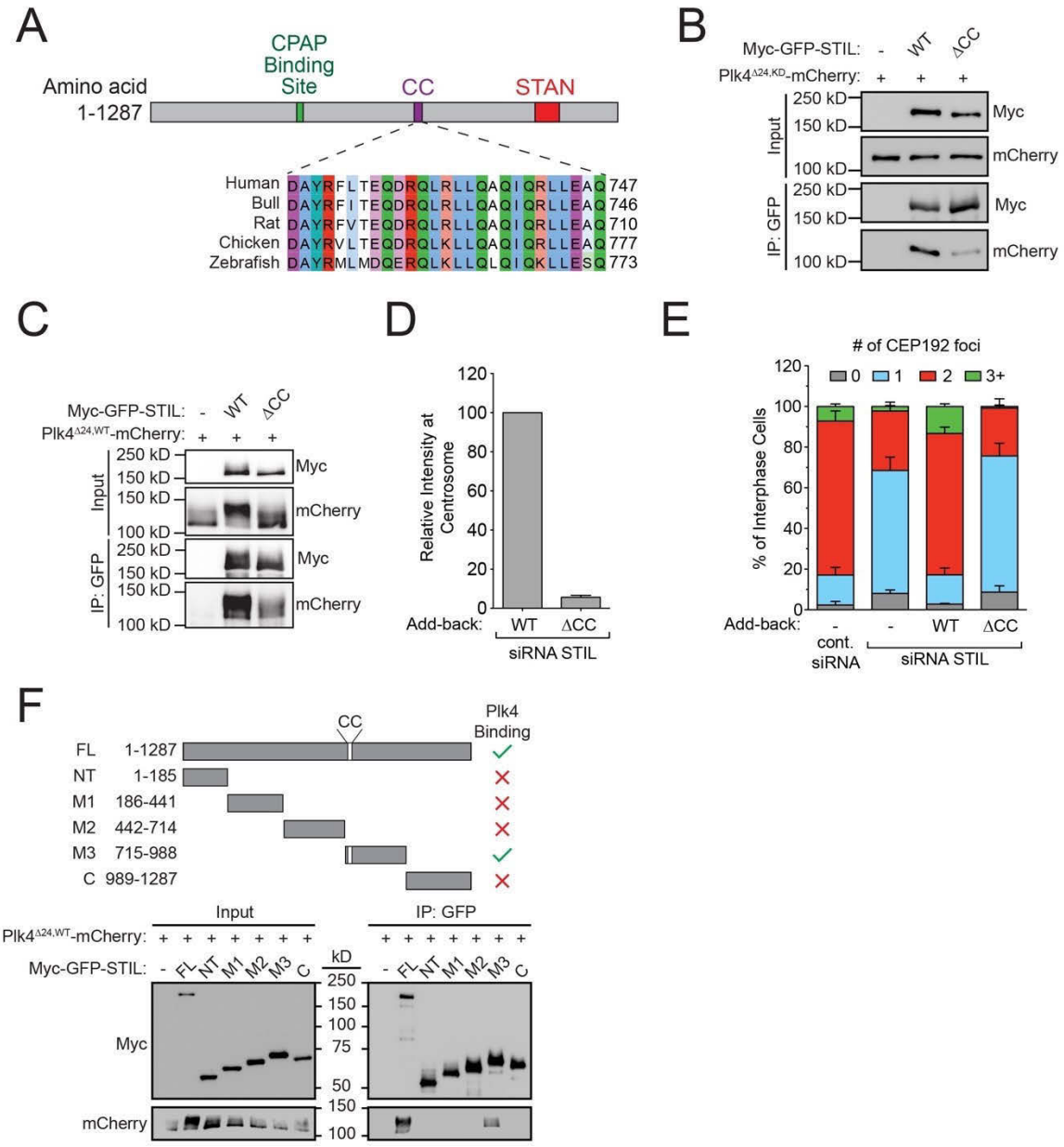

Figure 4. The coiled-coil domain of STIL is required for binding to PLK4.

(A) Schematic of STIL showing an alignment of the conserved STIL coiled-coil domain.

(B-C) Cells were co-transfected with the indicated constructs and subject to co-immunoprecipitation analysis with the indicated antibodies.

(D) Endogenous STIL was depleted by siRNA and replaced with either Myc-GFP-STIL WT or ΔCC. Graph shows quantification of the relative levels of Myc-GFP-STIL at the centrosome of S/G2 phase cells. Bars represent the mean of at least three independent experiments with > 40 cells counted per experiment.

(E) Quantification showing the number of CEP192 foci in cells in which endogenous STIL had been depleted and replaced with the indicated Myc-GFP-STIL transgene. Bars represent the mean of three independent experiments with > 100 cells counted per experiment.

(F) Cells were co-transfected with the indicated constructs and subject to co-immunoprecipitation analysis with the indicated antibodies. All error bars in the figure represent the *S.E.M.*

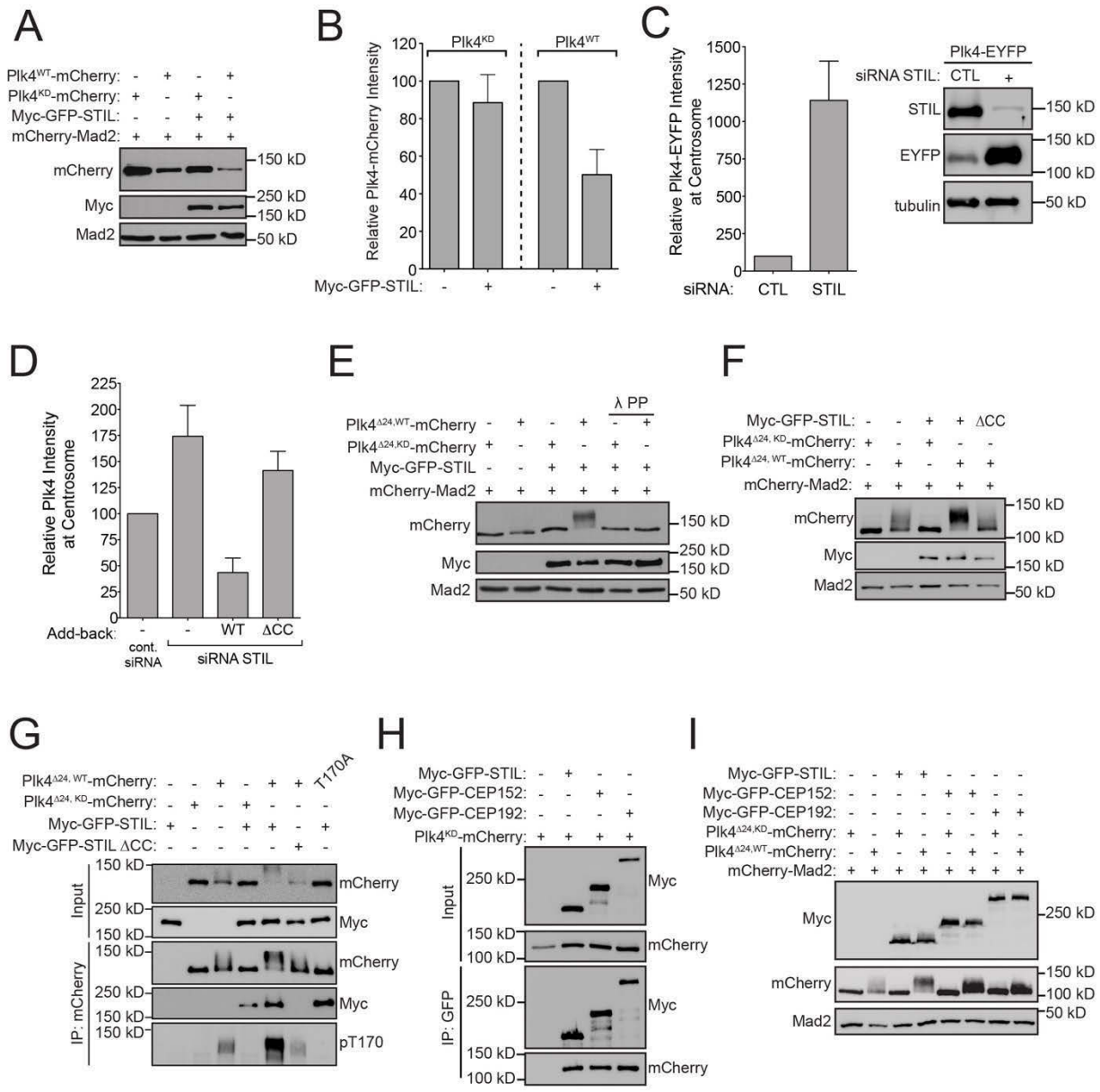

Figure 5. STIL binding stimulates PLK4 activity.

(A) Cells were co-transfected with the indicated constructs and protein levels analyzed by immunoblot. mCherry-Mad2 serves as a transfection control.

(B) Quantification of protein levels shown in (A). Bars represent the mean of three independent experiments.

(C) STIL was depleted by siRNA and 24 hours later doxycycline added to induce expression of PLK4-EYFP. Immunoblot shows the relative levels of STIL and PLK4-EYFP in control or STIL siRNA depleted cells. Graph shows quantification of the relative level of PLK4-EYFP at the centrosome of S/G2 phase cells. Bars represent the mean of at least three independent experiments with > 40 cells counted per experiment.

(D) Endogenous STIL was depleted by siRNA and replaced with either Myc-GFP-STIL WT or ΔCC using the scheme outlined in Figure 8A. Graph shows quantification of the relative levels of PLK4 at the centrosome of S/G2 phase cells. Bars represent the mean of at least three independent experiments with > 40 cells counted per experiment.

(E-F) Cells were co-transfected with the indicated constructs and protein levels analyzed by immunoblot. Where indicated, lambda protein phosphatase (λ PP) was incubated with the cell lysate for 60 minutes prior to immunoblotting.

(G-H) Cells were co-transfected with the indicated constructs and subjected to co-immunoprecipitation analysis with the indicated antibodies.

(I) Cells were co-transfected with the indicated constructs and protein levels analyzed by immunoblot. All error bars in the figure represent the *S.E.M.*

Chapter 2. PLK4 Phosphorylates STIL to promote SAS6 binding and recruitment to the procentriole

2.1 Overview

In the previous chapter, we found that STIL is an *in vivo* activator of PLK4 kinase activity and we propose a model by which accumulating levels of STIL in the cytoplasm in G1 phase could peak at the onset of S phase and trigger PLK4 activity to initiate centriole assembly at the correct time in the cell cycle (**Figure 10C**) (Tang et al. 2011; C. Arquint et al. 2012). While further experimentation is required to rigorously examine this hypothesis, the question remains as to how PLK4 activity promotes centriole duplication. Substrates have been proposed for PLK4 (Bahtz et al. 2012; Cizmecioglu et al. 2010; Hudson et al. 2001; Puklowski et al. 2011), but what specific sites PLK4 phosphorylates *in vivo* and how these phosphorylation events lead to cartwheel assembly has not been shown.

An obvious candidate substrate of PLK4 is SAS6, the major structural component of the cartwheel (Daiju Kitagawa et al. 2011; Van Breugel et al. 2011; van Breugel et al. 2014). One could imagine that PLK4 could phosphorylate SAS6 to promote its homo-oligomerization. However, crystal structures of the oligomeric interface of SAS6 have few accessible serines or threonines (Van Breugel et al. 2011; van Breugel et al. 2014; Daiju Kitagawa et al. 2011), and it is not clear how phosphorylation would support this interaction.

In this chapter, we find that PLK4 phosphorylates STIL, but not SAS6, *in vitro*. Using phospho-specific antibodies, we demonstrate that the highly conserved STIL STAN domain is a target of endogenous PLK4 *in vivo*. Importantly, we demonstrate that PLK4-mediated phosphorylation of the STIL STAN domain promotes direct binding of STIL to SAS6 and leads to SAS6 recruitment to the site of cartwheel assembly. Thus, STIL is both and activator and a substrate of PLK4.

2.2 PLK4 phosphorylates the STIL STAN domain *in vivo*

Given that STIL directly binds and stimulates PLK4 activity, we investigated whether PLK4 phosphorylates STIL to control centriole assembly. We mapped *in vitro* PLK4 phosphorylation sites on STIL using mass spectrometry (**Figure 6A**). STIL-related proteins show high sequence homology in a short ~90 a.a. region known as the STAN (STIL/Ana2) motif (Stevens et al. 2010). This region contains five conserved residues that are phosphorylated in cells: S1103, S1108, S1111, S1116 and T1119 (Hoffert et al. 2006; Huttlin et al. 2010) (**Figure 7A**). Of these five sites, S1108 and S1116 were phosphorylated by PLK4 *in vitro* and closely matched the PLK4 consensus phosphorylation sequence (Johnson et al. 2007; Kettenbach et al. 2012). To facilitate analysis of these phosphorylation sites we generated phospho-specific antibodies. The affinity purified pS1108 and pS1116 antibodies recognized recombinant GST-STIL and GST-STIL C-term only in the presence of kinase active PLK4 (**Figure 7B and 6B**). Moreover, recognition of phosphorylated GST-STIL C-term by the pS1108 and pS1116 antibody was abolished by mutation of S1108A and S1116A, respectively (**Figure 7B**). These observations confirm that PLK4 phosphorylates STIL at S1108 and S1116 *in vitro*, and demonstrate the

specificity of the pS1108 and pS1116 antibodies for revealing the phosphorylation status of STIL.

The pS1116 antibody recognized Myc-GFP-STIL WT immunoprecipitated from cells, but not Myc-GFP-STIL containing a S1116A mutation (**Figure 7D**). To establish whether PLK4 was responsible for phosphorylating STIL S1116 in cells, we treated $PLK4^{WT/WT}$ and $PLK4^{AS/AS}$ cells with 3MB-PP1 and examined phosphorylation of STIL S1116. Treatment with 3MB-PP1 abolished phosphorylation of Myc-GFP-STIL S1116 in $PLK4^{AS/AS}$ cells, but did not affect phosphorylation of this site in $PLK4^{WT/WT}$ cells, demonstrating that PLK4 phosphorylates STIL S1116 in cells (**Figure 7D**). Deletion of the coiled-coil region of STIL abolished phosphorylation of STIL S1116, suggesting that phosphorylation of this site requires PLK4 binding to STIL and/or the recruitment of STIL to the centriole (**Figure 7E**).

While the pS1116 antibody detected phosphorylated STIL by immunoblot, it cross-reacted with an additional phosphorylated centriole protein and consequently was not useful for immunofluorescence analysis. We therefore tested whether the pS1108 antibody could detect phosphorylation of STIL S1108 by immunofluorescence staining. The pS1108 antibody stained a centriole-localized signal that co-localized with Myc-GFP-STIL (**Figure 7F**). To determine the specificity this staining, we replaced endogenous STIL with a WT or S1108A Myc-GFP-STIL transgene. When normalized to the total level of STIL at the centriole, the centriole-localized pS1108 signal was reduced by > 90% in cells expressing the S1108A mutant of Myc-GFP-STIL (**Figure 7F**). Moreover, treatment of $PLK4^{AS/AS}$ cells with 3MB-PP1 for one hour resulted in a > 90% reduction in STIL S1108 phosphorylation, demonstrating that STIL S1108 is a substrate for

PLK4 *in vivo* (**Figure 7G**). To investigate the cell-cycle dependent phosphorylation of STIL S1108 we carried out fluorescence intensity measurements to determine the level of Myc-GFP-STIL and pS1108 at the centriole in late G1 (CENP-F negative) and S/G2 (CENP-F positive) cells (Hussein and Taylor 2002). While levels of Myc-GFP-STIL were higher in S/G2 compared with G1 cells, the level of pS1108 staining remained largely unchanged (**Figure 7H,I**). Importantly, we never observed centriole-localized Myc-GFP-STIL in the absence of pS1108 staining. These data suggest PLK4 is active from late G1 through G2 phase.

2.3 PLK4 phosphorylates the STIL STAN domain to promote centriole duplication

We investigated how PLK4-mediated STIL phosphorylation affects centriole biogenesis. WT or phosphorylation defective Myc-GFP-STIL transgenes were integrated at a pre-defined genomic locus in a DLD-1 host cell line and expression induced by addition of doxycycline. All of the Myc-GFP-STIL transgenes were expressed at identical, near-endogenous levels (**Figure 6C**). Expression of Myc-GFP-STIL WT in the presence of endogenous STIL drove excessive centrosome formation in 45% of cells (**Figure 6D**). By contrast, expression of a Myc-GFP-STIL variant (5A) with all 5 phosphorylation sites in the STAN domain substituted to alanine had no effect on centrosome number (**Figure 6D**). Alanine substitutions at the S1108 or S1116 PLK4 phosphorylation sites substantially reduced the ability of overexpressed Myc-GFP-STIL to promote centrosome amplification (reduced to 19% and 15%, respectively), indicating that phosphorylation of these sites is important for the function of STIL in centriole biogenesis. To further characterize STIL S1108 and S1116 phosphorylation sites, we introduced phospho-

mimicking mutations at these positions and assayed the ability of the Myc-GFP-STIL constructs to promote centrosome overduplication. The S1108D mutation promoted centrosome amplification as efficiently as Myc-GFP-STIL WT (**Figure 6D**). On the other hand, the S1116D mutation was indistinguishable from an alanine substitution at this site, suggesting that either the S1116D substitution failed to mimic the phosphorylated state, or that centriole biogenesis requires dynamic regulation of S1116 phosphorylation.

To address the role of PLK4-mediated STIL STAN domain phosphorylation in canonical centriole duplication, we replaced endogenous STIL with physiological levels of Myc-GFP-STIL transgenes (**Figure 8A,B**). Depletion of STIL led to a 47% increase in the number of cells with ≤ 1 centrosome and this effect was completely rescued by expression of an RNAi-resistant Myc-GFP-STIL WT transgene (**Figure 8C**). By contrast, expression of either Myc-GFP-STIL lacking the STAN domain (ΔSTAN, deletion of a.a. 1061-1147), or the Myc-GFP-STIL 5A mutant lacking 5 phosphorylation sites in this region, failed to rescue centriole duplication (**Figure 8C**). Single alanine substitutions at each of the five-phosphorylation sites in the STIL STAN domain revealed that S1116 was the most important phosphorylation site for controlling centriole duplication (53% of S1116A cells contain ≤ 1 centrosome) (**Figure 8F**). The Myc-GFP-STIL S1108A mutant was also partially defective in centriole duplication (32% S1108A cells contain ≤ 1 centrosome) and this defect was further exacerbated when combined with the S1116A mutation (61% of S1108A/S1116A cells contain ≤ 1 centrosome) (**Figure 8F***).* We conclude that PLK4-mediated phosphorylation of STIL S1116, and to a lesser extent STIL S1108, is required for centriole duplication.

2.4 PLK4 phosphorylation of the STIL STAN domain is required for centriole recruitment of STIL

We next analyzed if STAN phosphorylation contributes to STIL centriole targeting. Since STIL is degraded after mitosis (Arquint and Nigg 2014; C. Arquint et al. 2012; Tang et al. 2011), we measured Myc-GFP-STIL levels in S/G2 cells marked by the presence of CENP-F (Hussein and Taylor 2002). While all WT and mutant Myc-GFP-STIL transgenes localized to the centriole in the absence of endogenous STIL, the relative abundance of each phosphorylation site mutant at the centriole varied considerably. Surprisingly, while deletion of the STAN domain did not alter the centriole abundance of STIL, mutation of 5 phosphorylation sites in this region reduced the abundance of centriole STIL to < 25% of that WT STIL (**Figure 8D,E**). The difference in centriole abundance of STIL 5A and STIL ΔSTAN suggests that the STAN domain acts to inhibit STIL centriole localization and that phosphorylation of the STAN domain is able to overcome this inhibition to promote localization. Preventing phosphorylation of both the S1108 and S1116 PLK4 phosphorylation sites reduced the abundance of STIL at the centriole to 32% of control cells (**Figure 8G,H**). This suggests that phosphorylation by PLK4 of S1108 and S1116 overcomes the STAN domain mediated inhibition of STIL centriole localization. Taken together, these observations offer an explanation for why the centriole levels of STIL are reduced after PLK4 inhibition (**Figure 1F**).

Mutating STIL S1108 to aspartic acid increased the centriolar abundance of Myc-GFP-STIL in excess of the WT protein (**Figure 6E**). Nevertheless, Myc-GFP-STIL S1108D was as defective in centriole duplication as the S1108A mutant protein, suggesting that STAN phosphorylation

performs functions in addition to centriole recruitment (**Figure 6F**). Since the Myc-GFP-STIL S1108D promoted centrosome amplification as effectively as Myc-GFP-STIL WT when overexpressed in the presence of endogenous STIL (**Figure 6D**), our data highlight differences in assays using STIL overexpression versus functional replacement.

To examine how STAN domain phosphorylation affects the binding dynamics of centriolar STIL, we performed Fluorescence Recovery after Photobleaching in cells expressing Myc-GFP-STIL transgenes. Myc-GFP-STIL WT and S1108A only partially recovered following bleaching, showing that STIL exists in both a mobile and immobile pool at the centriole (**Figure 8I**, Myc-GFP-STIL WT R% = 48%, $t_{1/2}$ = 127 s). Deletion of the STAN domain or mutation of the S1116 phosphorylation site both increased the mobile fraction of centriolar STIL (**Figure 8I**, Myc-GFP-STIL ΔSTAN R% = 93%, $t_{1/2}$ = 110 s; Myc-GFP-STIL S1116A, R% = 69%, $t_{1/2}$ = 80 s). Together, these data suggest that phosphorylation of the STAN domain is required for stable interaction of STIL with the centriole. The increased turnover of Myc-GFP-STIL ΔSTAN is likely to limit the centriolar accumulation of this mutant protein. This provides an explanation for why, despite loss of a domain that is inhibitory to centriole recruitment, Myc-GFP-STIL ΔSTAN localizes to the centriole to a similar level as Myc-GFP-STIL WT.

2.5 Stable centriole recruitment of STIL requires direct binding of SAS6

Recently, it was proposed that phosphorylation of the STIL/Ana2 STAN domain facilitates STIL binding to SAS6 (Dzhindzhev et al. 2014; Ohta et al. 2014). To test if phosphorylation of STIL S1108 and S1116 by PLK4 promotes the association of SAS6, we reconstituted SAS6 binding to

STIL *in vitro*. GST-STIL was incubated with kinase active or inactive PLK4 and then combined with SAS6. GST-STIL was then captured on beads and the association with SAS6 determined by immunoblotting. Incubation with kinase active but not kinase dead PLK4 promoted direct binding of SAS6 to GST-STIL (**Figure 9A**). To establish if SAS6 binding was dependent on phosphorylation of STIL S1108 or S1116, we tested the ability of SAS6 to bind *in vitro* to WT or phosphorylation site mutants of recombinant GST-STIL C-term (a.a. 898-1287). Phosphorylation of GST-STIL C-term by PLK4 increased the binding of SAS-6 by > 9-fold (**Figure 9B**). Importantly, mutation of STIL S1108A and S1116A reduced SAS6 binding to 37% and 22% of that observed with WT GST-STIL C-term (a.a. 898-1287). To map the domain of SAS6 that interacts with STIL, cells were transfected with a series of FLAG-SUMO-SAS6 truncation constructs and the interaction with Myc-GFP-STIL examined in the presence of $PLK4^{\Delta 24,WT}$-mCherry. Using this approach STIL binding was mapped to the C-terminal part of SAS6 protein (a.a. 316-657) (**Figure 10A**). We conclude that phosphorylation of the STIL STAN domain by PLK4 promotes direct binding of STIL to the C-terminal region of SAS6.

We next analyzed the requirement of STIL phosphorylation for binding to SAS-6 in cells. Deletion of the STIL STAN domain or mutation of phosphorylation sites in this region did not affect STIL binding to PLK4, or activation of PLK4 kinase activity (**Figure 9C**)**.** Expression of kinase active $PLK4^{\Delta 24}$ promoted a ~2-fold increase in the binding of FLAG-SUMO-SAS6 to Myc-GFP-STIL (**Figure 9C, lane 2 and 3**). The Myc-GFP-STIL 5A mutant associated with SAS6 at only 23% of the level observed with Myc-GFP-STIL WT (**Figure 9C, lane 2 and 7**). Importantly, preventing phosphorylation of STIL S1116 alone also reduced SAS6 binding to a similar degree, while deletion of the STAN domain reduced SAS6 binding to 12% of that

observed with Myc-GFP-STIL WT (**Figure 9C lane 2, 5 and 8**). These data indicate that PLK4-mediated phosphorylation of STIL S1116 plays a key role in promoting SAS6 binding to STIL.

Finally, we investigated how PLK4-mediated phosphorylation of STIL contributes to SAS6 recruitment to the centriole. We monitored the presence of PLK4 and SAS6 at the centriole of cells in which endogenous STIL had been functionally replaced with various Myc-GFP-STIL transgenes. Despite the fact that the centriolar abundance of the STIL transgenes varied dramatically (**Figure 8G,H**), cells contained near identical levels of endogenous centriolar PLK4 (**Figure 9D**). Since binding to PLK4 is unaffected by STIL STAN domain phosphorylation (**Figure 9C**), our data suggest that abundance of centriolar PLK4 is mainly controlled through binding to STIL in the cytosol. In accord with previous reports, depletion of STIL dramatically reduced SAS6 recruitment to the centriole (an average of 13% SAS6 remaining) without altering SAS6 protein levels (**Figure 9E and 10B**). While expression of Myc-GFP-STIL WT rescued the centriole recruitment of SAS6 in cells depleted of endogenous STIL, the Myc-GFP-STIL 5A mutant failed to do so (19% centriolar SAS6 remaining) (**Figure 9E,F**). Preventing phosphorylation of STIL S1108 or S1116 also reduced SAS6 recruitment (64% and 36% of centriolar SAS6 remaining, respectively). This suggests that PLK4-mediated phosphorylation of the STIL STAN domain contributes to the efficient targeting of SAS6 to the centriole.

2.6 Discussion

Here, we have provided direct evidence to show that endogenous PLK4 directly phosphorylates STIL S1108 and S1116 *in vivo* and reveal two key roles for these phosphorylation events in

promoting centriole assembly (**Figure 5G**). First, phosphorylation of S1108 and S1116 increased the efficiency of STIL centriole targeting (**Figure 4G,H**). This explains why PLK4 kinase activity is required for the robust targeting of STIL to the centriole (**Figure 1F**). Second, and consistent with two recent reports (Dzhindzhev et al. 2014; Ohta et al. 2014), we show that phosphorylation of STIL S1108 and S1116 is required for subsequent binding of STIL to SAS6 and for efficient recruitment of SAS6 to the centriole (**Figure 5A,B**). We speculate that STIL binding to SAS6 facilitates cartwheel assembly, leading to the stable incorporation of STIL into the centriole structure.

In human cells, SAS6 is transiently recruited to the lumen of the mother centriole in early S phase, before repositioning to the outer wall of the mother centriole to initiate cartwheel formation and procentriole assembly (Fong et al. 2014). PLK4 and STIL are both required for the release of luminal SAS6. It is therefore tempting to speculate that STIL-mediated activation of PLK4 triggers the release of luminal SAS6 and subsequent capture by STIL at a site on the wall of the mother. Further studies will be required to test this idea.

STIL localization to the centriole requires both PLK4 binding and STAN domain phosphorylation

PLK4 has been shown to interact with a conserved coiled-coil domain in the central region of STIL (Kratz et al. 2015; Ohta et al. 2014). We demonstrate that PLK4 and STIL form a complex both *in vitro* and *in vivo* in the absence of PLK4 activity (**Figure 3A,B**). This contrasts with a previous study that indicated the binding of PLK4 to STIL required PLK4 kinase activity (Ohta et al. 2014). While the reason for this discrepancy remains unclear, we note that in *C.elegans*,

ZYG-1/PLK4 binds directly to the coiled-coil of SAS6 independent of kinase activity (Lettman et al. 2013). It is thus tempting to speculate that while the location of the ZYG-1/PLK4 binding site differs, a conserved role of the ZYG-1/PLK4-SAS5/STIL-SAS6 module is to position ZYG-1/PLK4 for optimal phosphorylation of SAS5/STIL family proteins.

A mutant form of STIL lacking the central coiled-coil had a dramatically reduced localization to the centriole, suggesting that PLK4 may act as a centriole receptor for STIL (**Figure 4D**). In flies, Ana2/STIL localizes to the centriole in the absence of phosphorylation by PLK4 (Dzhindzhev et al. 2014). In addition, a study in human cells reported that phosphorylation of the STIL STAN domain was not required for centriole targeting of STIL. How, then, do we explain the observation that PLK4 activity is also required for the localization of STIL to the centriole (**Figure 1F**)? Our evidence shows that, although not essential for STIL centriole recruitment, phosphorylation of the STAN domain by PLK4 dramatically increased the efficiency of STIL centriole targeting (**Figure 4G,H**). Importantly, we show that PLK4 binding to STIL does not require STIL STAN domain phosphorylation (**Figure 5C**), demonstrating that centriole targeting of STIL requires both PLK4 binding and phosphorylation of its STAN domain by PLK4.

How does phosphorylation of the STAN domain control the localization of STIL? We speculate that cytoplasmic STIL exists in an auto-inhibited conformation that prevents recruitment to the centriole **(Figure 6)**. Deletion of the STIL STAN domain or phosphorylation of this region by PLK4 is proposed to release this auto-inhibition to allow efficient centriole targeting. Phosphorylation of the STIL STAN domain also triggers the binding of STIL to SAS6. This interaction could promote cartwheel assembly and lead to the stable incorporation of STIL in the

cartwheel structure (**Figure 6)**. This explains why STIL mutants that are defective in STAN domain phosphorylation have a reduced pool of protein stably bound at the centriole (**Figure 4I**).

2.7 Figures and Legends

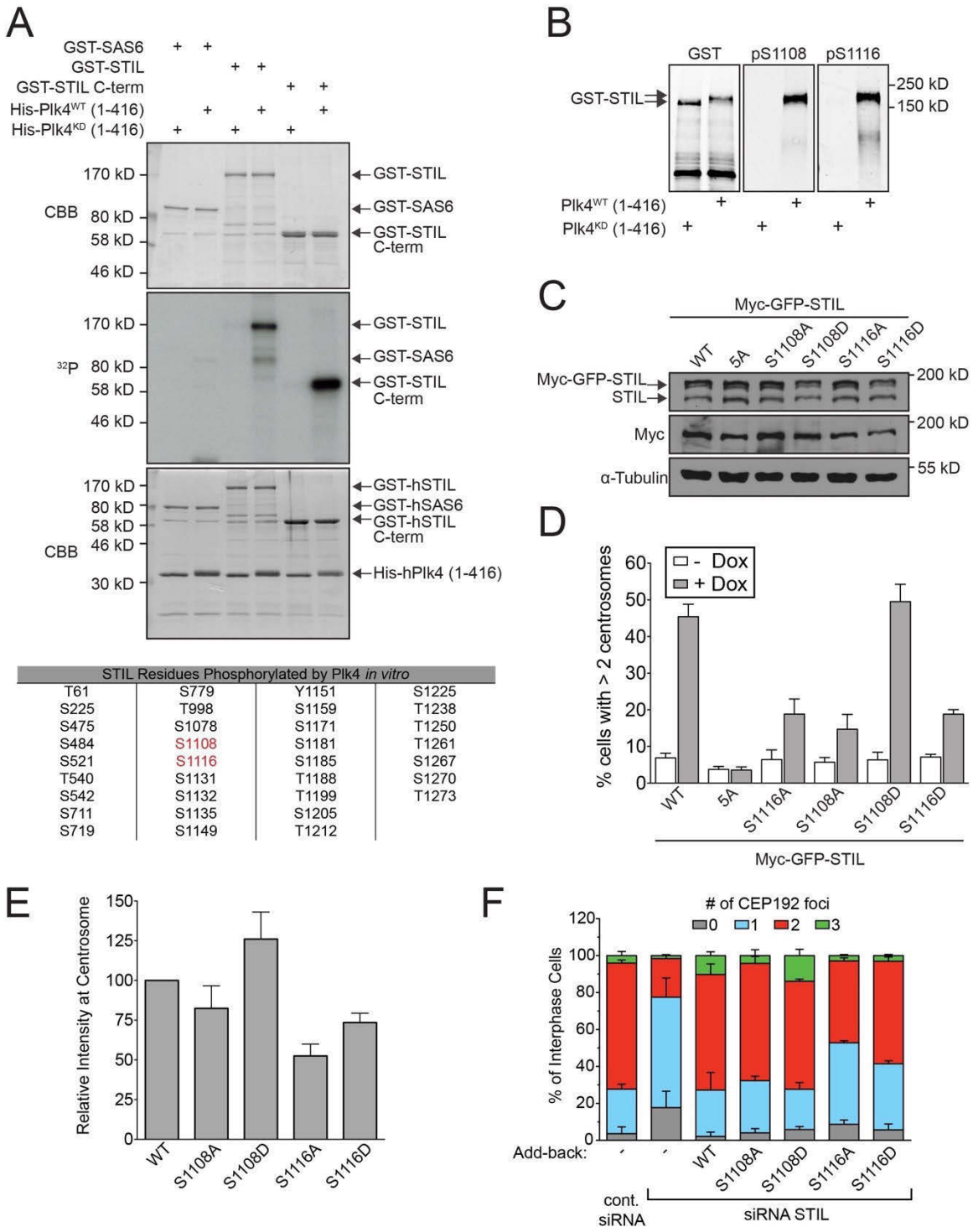

STIL Residues Phosphorylated by Plk4 *in vitro*			
T61	S779	Y1151	S1225
S225	T998	S1159	T1238
S475	S1078	S1171	T1250
S484	S1108	S1181	T1261
S521	S1116	S1185	T1267
T540	S1131	T1188	T1270
S542	S1132	T1199	T1273
S711	S1135	S1205	
S719	S1149	T1212	

Figure 6. STIL phosphorylation is required for centriole duplication.

(A) GST-SAS6, GST-STIL or GST-STIL C-term (a.a. 898-1287) was phosphorylated *in vitro* with kinase active or inactive His-PLK4. Coomassie (CBB) stained gel shows the purified protein and autoradiogram (^{32}P) shows the incorporation of γ-^{32}P-ATP.

(B) GST-STIL was phosphorylated *in vitro* with kinase active or inactive His-PLK4 and analyzed by immunoblot with the indicated antibodies.

(C) Expression of Myc-GFP-STIL was induced for 48 hours with doxycycline and protein levels analyzed by immunoblot.

(D) Quantification of the fraction of cells with > 2 centrosomes 48 hours after induction of Myc-GFP-STIL expression with doxycycline (Dox). Bars show the mean of three independent experiments with > 50 cells counted per experiment.

(E) Quantification from (E) showing the relative level of Myc-GFP-STIL at the centrosome of S/G2 phase cells. Bars represent the mean of at least three independent experiments with > 40 cells counted per experiment. The Myc-GFP-STIL S1108 and S1116 mutants from Figure 8H are shown alongside as a comparison. All error bars in the figure represent the *S.E.M.*

(F) Quantification showing the number of CEP192 foci in cells in which endogenous STIL had been depleted and replaced with the indicated Myc-GFP-STIL transgene. Bars represent the mean of at least three independent experiments with > 100 cells counted per experiment. The Myc-GFP-STIL S1108 and S1116 mutants from Figure 8F are shown alongside as a comparison.

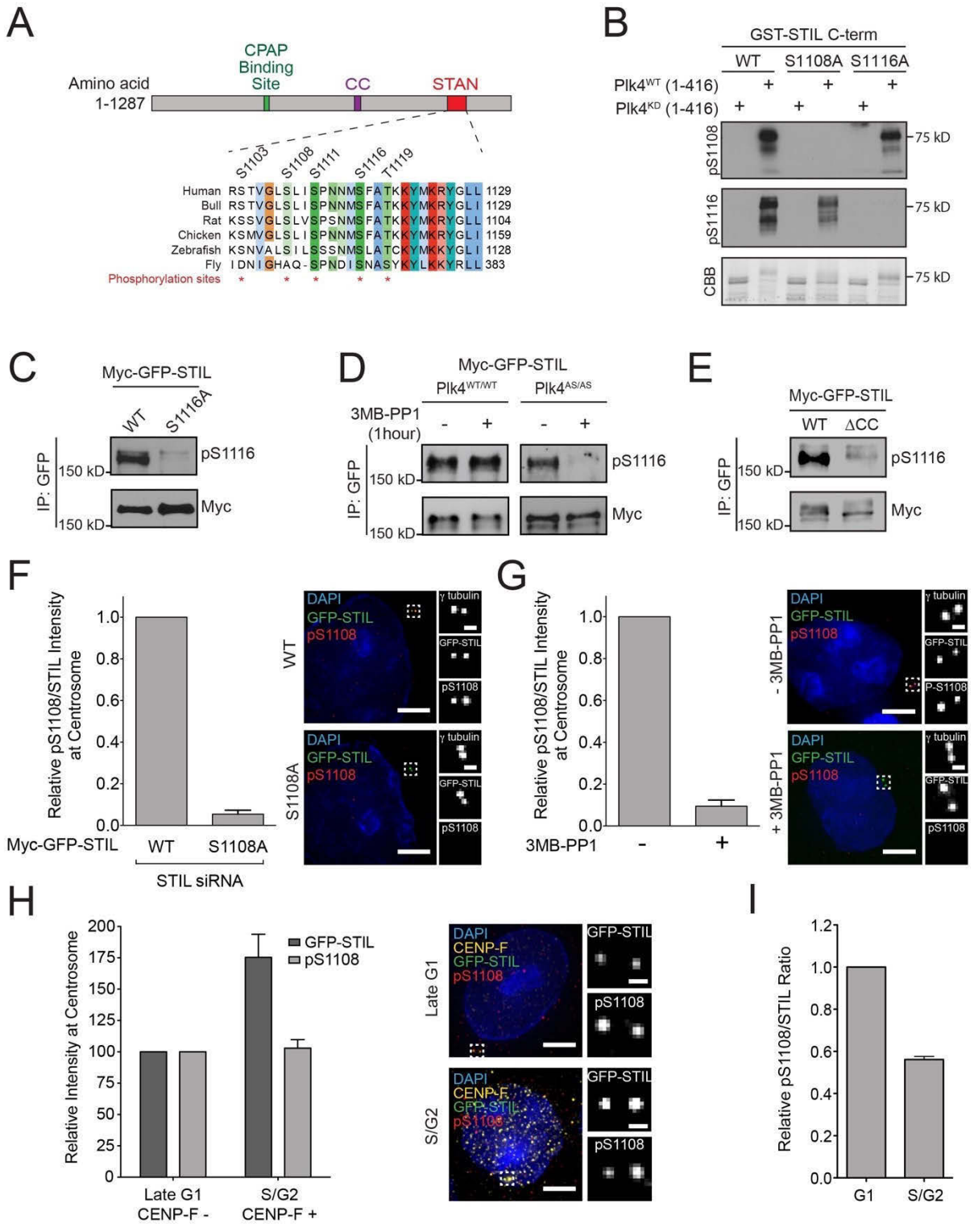

Figure 7. PLK4 phosphorylates the STIL STAN domain *in vivo*.

(A) Schematic of STIL showing the CPAP binding domain, coiled-coil domain (CC) and the conserved STAN domain. Alignment shows the position of five amino acids in the STAN domain that are phosphorylated *in vivo*.

(B) GST-STIL C-term (a.a. 898-1287) was phosphorylated *in vitro* with kinase active or inactive His-PLK4 and analyzed by immunoblot with the indicated antibodies. Coomassie (CBB) stained gel shows the purified protein.

(C) Myc-GFP-STIL WT or S1116A was immunopurified from cells and analyzed by immunobloting with the indicated antibodies.

(D) $PLK4^{WT/WT}$ or $PLK4^{AS/AS}$ cells were treated with 3MB-PP1 for 1 hour. Myc-GFP-STIL was then immunopurified from cells and analyzed by immunoblotting with the indicated antibodies.

(E) Myc-GFP-STIL WT or ΔCC was immunopurified from cells and analyzed by immunobloting with the indicated antibodies.

(F) (Left) Endogenous STIL was replaced with either Myc-GFP-STIL WT or S1108A. Graph shows quantification of the relative levels of pS1108/STIL at the centrosome of S/G2 phase cells. Bars represent the mean of at least three independent experiments with > 40 cells counted per experiment. (Right) Selected images of cells showing Myc-GFP-STIL and pS1108 staining. Left images, scale bar, 5 μm. Right images, scale bar, 0.5 μm.

(G) (Left) $PLK4^{AS/AS}$ cells were treated with or without 3MB-PP1 for 1 hour. Graph shows quantification of the relative levels of pS1108/STIL at the centrosome of S/G2 phase cells. Bars represent the mean of at least three independent experiments with > 40 cells counted per experiment. (Right) Selected images of cells showing Myc-GFP-STIL and pS1108 staining. Left images, scale bar, 5 μm. Right images, scale bar, 0.5 μm.

(H) (Left) Quantification showing the relative levels of Myc-GFP-STIL and pS1108 at the centrosome of G1 (CENP-F negative) and S/G2 (CENP-F positive) phase cells. Bars represent the mean of at least three independent experiments with > 40 cells counted per experiment. (Right) Selected images of cells showing Myc-GFP-STIL and pS1108 staining. Left images, scale bar, 5 μm. Right images, scale bar, 0.5 μm.

(I) Quantification showing the relative levels of pS1108/STIL at the centrosome of G1 or S/G2 phase cells. Ratio is calculated from the data shown in (H). All error bars in the figure represent the *S.E.M.*

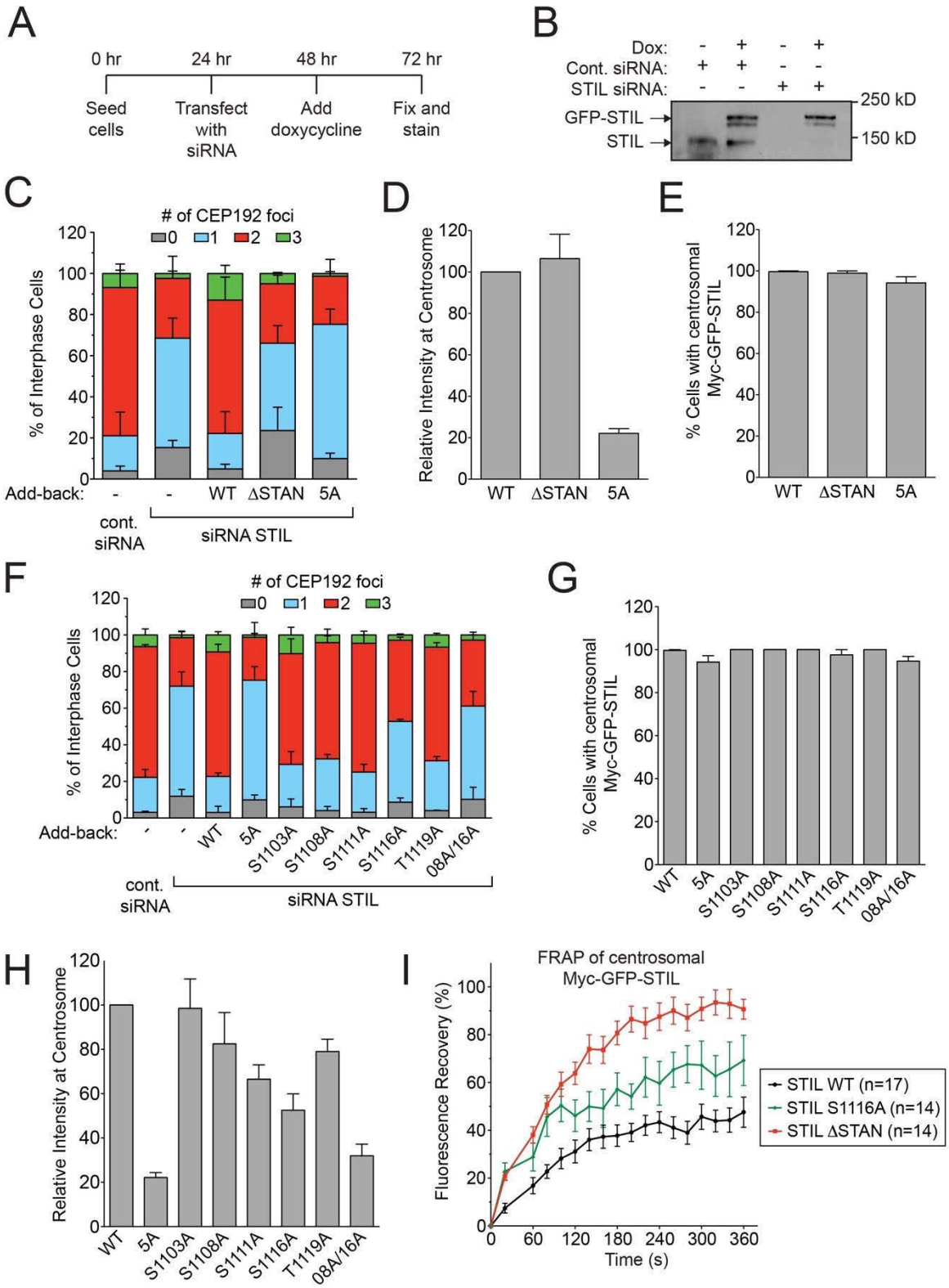

Figure 8. Phosphorylation of the STIL STAN domain is required for centriole duplication.

(A) Outline of the experimental timeline for the STIL siRNA and add-back experiments.

(B) Immunoblot showing the relative STIL expression level after replacement of endogenous STIL with a Myc-GFP-STIL WT transgene.

(C) Quantification showing the number of CEP192 foci in cells in which endogenous STIL had been depleted and replaced with the indicated Myc-GFP-STIL transgene. Bars represent the mean of at least three independent experiments with > 100 cells counted per experiment.

(D-E) Quantification from (C) showing (D) the relative level of Myc-GFP-STIL at the centrosome of S/G2 phase cells and (E) the fraction of S/G2 phase cells with detectable Myc-GFP-STIL at the centrosome. Bars represent the mean of at least three independent experiments with > 40 cells counted per experiment.

(F) Quantification showing the number of CEP192 foci in cells in which endogenous STIL had been depleted and replaced with the indicated Myc-GFP-STIL transgene. '08A/16A' refers to a Myc-GFP-STIL S1108A/S1116A double mutant. Bars represent the mean of at least three independent experiments with > 100 cells counted per experiment. The Myc-GFP-STIL 5A mutant from Figure 8C is shown alongside as a comparison.

(G-H) Quantification from (F) showing (G) the relative level of Myc-GFP-STIL at the centrosome of S/G2 phase cells and (H) the fraction of S/G2 phase cells with detectable cells Myc-GFP-STIL at the centrosome. Bars represent the mean of at least three independent experiments with > 40 cells counted per experiment. The Myc-GFP-STIL 5A mutant from Figure 8D,E is shown alongside as a comparison.

(I) Endogenous STIL was replaced with Myc-GFP-STIL WT, ΔSTAN or S1116A. Graph shows the fluorescence recovery of centrosomal Myc-GFP-STIL after photobleaching. Points represent

the mean > 10 cells from two independent experiments. All error bars in the figure represent the *S.E.M.*

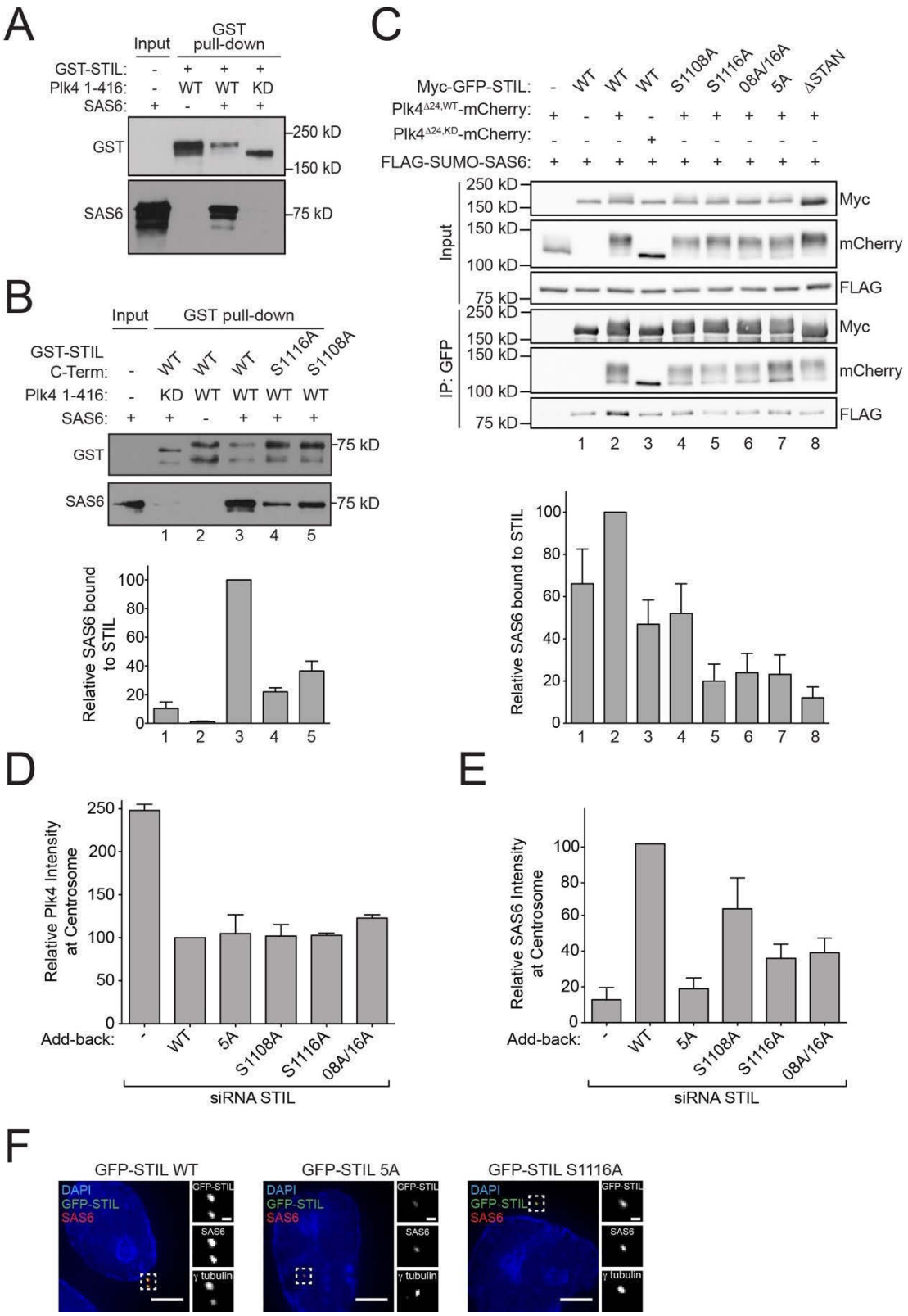

Figure 9. STIL STAN domain phosphorylation is required for direct binding to SAS6.

(A-B) GST-STIL or GST-STIL C-term (a.a. 898-1287) was phosphorylated *in vitro* with kinase active or inactive His-PLK4 and incubated with SAS6. GST pull-downs were analyzed by immunoblot with the indicated antibodies. Graph shows the quantification from (B) of the relative amount of SAS6 bound to GST-STIL C-term. Bars represent the mean of three independent experiments.

(C) (Top) Cells were co-transfected and subject to co-immunoprecipitation analysis with the indicated antibodies. (Bottom) Quantification of the relative amount of SAS6 bound to Myc-GFP-STIL. Bars represent the mean of three independent experiments.

(D-E) Quantification showing the relative level of PLK4 or SAS6 at the centrosome of cells in which endogenous STIL had been depleted and replaced with the indicated Myc-GFP-STIL transgene. Bars represent the mean of at least three independent experiments with > 50 cells counted per experiment.

(F) Selected images of cells showing Myc-GFP-STIL and SAS6 staining. Left images, scale bar, 5 μm. Right images, scale bar, 0.5 μm. All error bars in the figure represent the *S.E.M.*

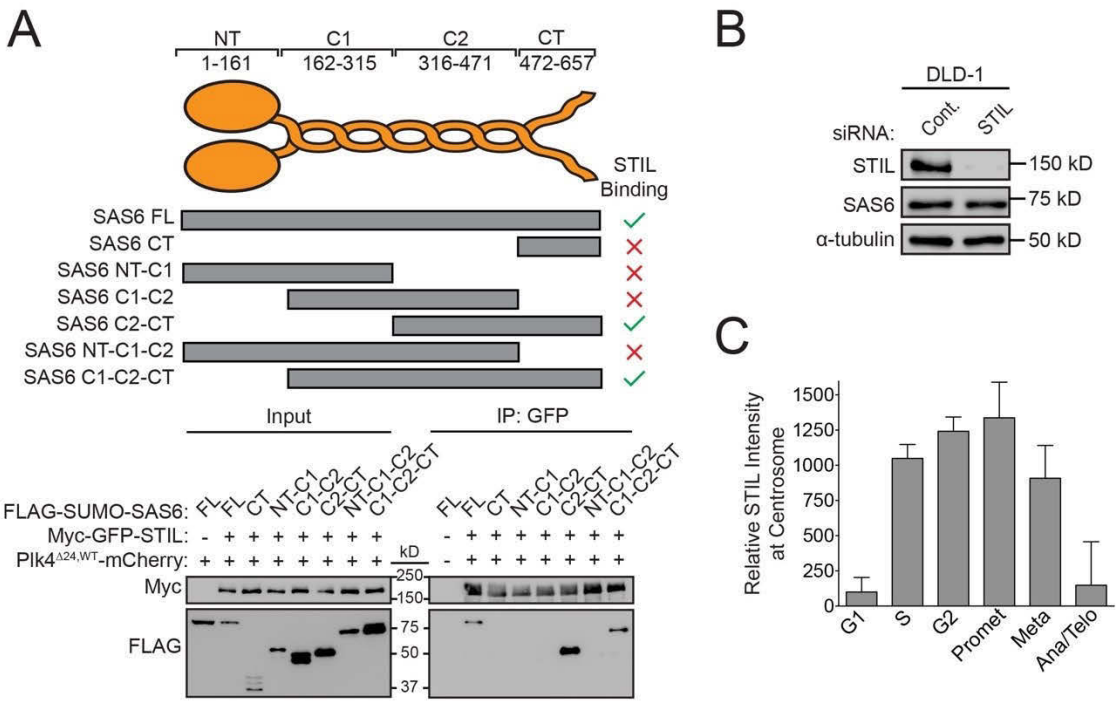

Figure 10. The C-terminal domain of SAS6 interacts with STIL.

(A) Cells were co-transfected with the indicated constructs and subject to co-immunoprecipitation analysis with the indicated antibodies.

(B) Immunoblot showing the levels of the indicated proteins at 48 hours after STIL siRNA.

(C) Quantitative immunofluorescence analysis of the levels of STIL at the centrosome in different cell cycle phases. Bars show the mean of > 85 cells from at least two independent experiments. Error bars in the figure represent the *S.E.M.*

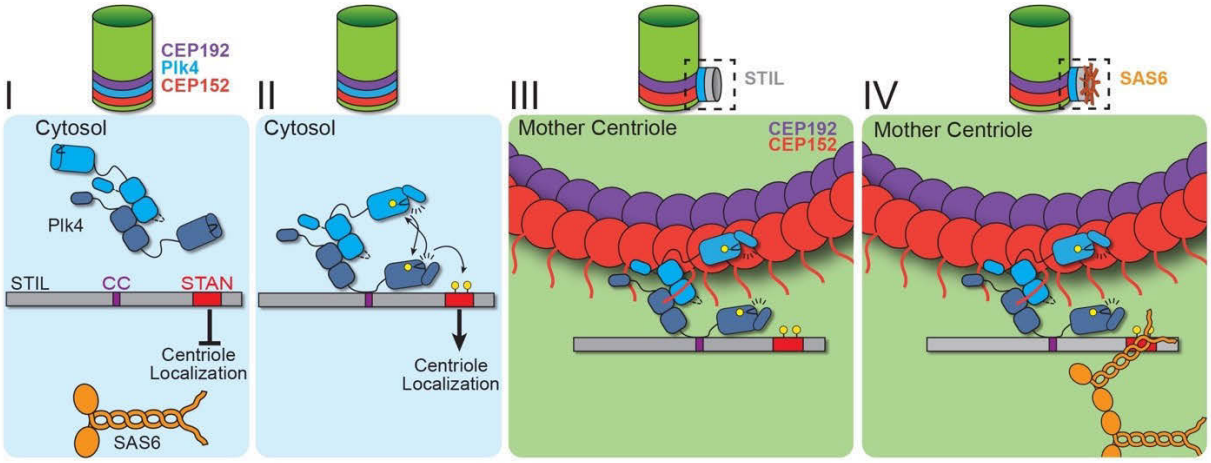

Figure 11. A model for how PLK4 and STIL cooperate to promote centriole assembly.

(I) We propose that cytoplasmic STIL exists in an auto-inhibited conformation that prevents recruitment to the centriole. (II) PLK4 directly binds to STIL and this binding leads to activation of kinase activity through self-phosphorylation of the PLK4 activation loop. PLK4 then directly phosphorylates two sites in the STAN domain of STIL. (III) Phosphorylation of these sites releases STIL auto-inhibition to promote efficient centriole targeting. (IV) In a second step, STIL STAN domain phosphorylation promotes the binding of centriolar STIL to the C-terminal region of SAS6. We propose that binding of STIL to SAS6 triggers cartwheel assembly and the stable binding of STIL to the centriole.

Chapter 3. PLK4 Phosphorylates STIL to promote CPAP binding and recruitment to the procentriole

3.1 Overview

Centrioles are microtubule-based structures that recruit a surrounding pericentriolar material (PCM) to form the centrosome (Nigg and Holland 2018; Gönczy 2012). Centrosomes nucleate the formation of the microtubule cytoskeleton in interphase cells and form the poles of the mitotic spindle during cell division. In quiescent cells, centrioles dock at the plasma membrane and act as basal bodies that template the formation of cilia and flagella (Breslow and Holland 2019). Cycling cells tightly couple centriole biogenesis with cell cycle progression. Centriole duplication begins at the G1-S phase transition when a new procentriole grows perpendicularly from a single site at the proximal end of each of the two parent centrioles. In late G2 phase, the two centriole pairs separate and increase PCM recruitment to promote the formation of the mitotic spindle. At the end of mitosis, the centrosomes are equally partitioned so that each daughter cell inherits a pair of centrioles. Defects in centriole biogenesis can result in the formation of supernumerary centrosomes which promote mitotic errors that can contribute to tumorigenesis (Levine et al. 2017; Levine and Holland 2018; Basto et al. 2008; Serçin et al. 2016; Coelho et al. 2015). Moreover, mutations in centriole proteins are linked to growth retardation syndromes and autosomal recessive primary microcephaly (MPCH) in human patients (Nigg and Raff 2009; Gergely 2014).

The initiation of centriole duplication requires a conserved set of five core proteins: PLK4, CEP192, CPAP (also known as CENPJ), STIL, and SAS6 (Leidel and Gönczy 2003; Leidel et al. 2005; Dammermann et al. 2004; Delattre et al. 2004; Kemp et al. 2004; O'Connell et al. 2001; Pelletier et al. 2004; Kirkham et al. 2003). Of these components, PLK4 has been identified as the central regulator of centriole assembly (Habedanck et al. 2005; Bettencourt-Dias et al. 2005). In mammalian cells, PLK4 is recruited to the centriole during G1 phase through binding to its centriole receptors CEP152 and CEP192, which encircle the proximal end of the parent centriole (Cizmecioglu et al. 2010; Hatch et al. 2010; T.-S. Kim et al. 2013; Park et al. 2014; K. F. Sonnen et al. 2013). At G1-S transition, PLK4 transforms from a ring-like localization to a single focus on the wall of the parent centriole that marks the site of procentriole formation (T.-S. Kim et al. 2013; Ohta et al. 2014; Katharina F. Sonnen et al. 2012; Dzhindzhev et al. 2017). This transition bears features of a symmetry breaking reaction and can be recreated *in silico* using two positive feedback loops that act on PLK4 (Goryachev and Leda 2017; Leda, Holland, and Goryachev 2018). Binding of PLK4 to its centriole substrate STIL promotes activation of the kinase and is required for its ring-to-dot transformation (Moyer et al. 2015; Ohta et al. 2014; Lopes et al. 2015). PLK4 phosphorylates STIL in a conserved STAN motif to promote the binding and recruitment of SAS6 (Ohta et al. 2014; Kratz et al. 2015; Moyer et al. 2015; Dzhindzhev et al. 2014). SAS6 homo-oligomerizes to organize the central cartwheel, a stack of ring-like assemblies with nine-fold symmetry that provides the structural foundation for the procentriole (Kitagawa et al. 2011; Van Breugel et al. 2011; van Breugel et al. 2014; Cottee et al. 2015; Guichard et al. 2017).

Following cartwheel assembly, the centriole protein CPAP plays a critical role in the formation and stabilization of the triplet microtubule blades that make up the procentriole wall. CPAP interacts with multiple centriole proteins including STIL (Cottee et al. 2013; Tang et al. 2011; Vulprecht et al. 2012), CEP152 (Cizmecioglu et al. 2010; Dzhindzhev et al. 2010), CEP120 (Y. N. Lin et al. 2013), CEP135 (Y. C. Lin et al. 2013), and Centrobin (Gudi et al. 2015). The C-terminal TCP domain of CPAP directly binds to a highly conserved PRP motif in STIL (Cottee et al. 2013; Tang et al. 2011; Vulprecht et al. 2012), while the N-terminal domain of CPAP interacts with α/β-tubulin heterodimers (Sharma et al. 2016; Xiangdong Zheng et al. 2016; Hung 2004). These interactions allow CPAP to act as a molecular link between the cartwheel and the triplet microtubule blades of the centriole wall. Importantly, an MCPH mutation in the CPAP TCP domain weakens the STIL-CPAP interaction, highlighting the importance of this complex in centriole assembly and function (Cottee et al. 2013; Tang et al. 2011; Bond et al. 2005). CPAP positively regulates centriolar microtubule growth and, consequently, overexpression of CPAP leads to the formation of overly long centrioles in human cells (Tang et al. 2009; Schmidt et al. 2009; Kohlmaier et al. 2009). In addition to its role in controlling microtubule growth, CPAP also functions in recruiting PCM, either through the direct tethering of PCM proteins or by recruiting Plk1/Polo which is critical in promoting PCM assembly (X. Zheng et al. 2014; Gopalakrishnan et al. 2011; Chou et al. 2016; Novak et al. 2016).

At present, the binding of SAS6 to the STAN motif of STIL is the only interaction known to be controlled by PLK4 kinase activity. While the regulation of this assembly step is conserved in humans and flies (Ohta et al. 2014; Dzhindzhev et al. 2014; Moyer et al. 2015; Kratz et al. 2015), it is unclear whether this takes place in *C.elegans*, where ZYG-1/PLK4 directly binds and

recruits SAS6 to promote cartwheel assembly (Lettman et al. 2013). Moreover, although phosphomimetic mutations in the crucial PLK4 phosphorylation sites in the STAN motif of STIL are functional, they cannot support centriole duplication in the absence of PLK4 kinase activity (M. Kim et al. 2016). This suggests that PLK4 must phosphorylate STIL, or other substrates, at additional sites to promote centriole assembly. Indeed, recent work in *Drosophila* identified additional PLK4 phosphorylation sites required for centriole biogenesis in the N-terminus of Ana2/STIL, but exactly how these phosphorylation events contribute to centriole formation remains unclear (Dzhindzhev et al. 2017; McLamarrah et al. 2018).

In this chapter, we identify a conserved PLK4 phosphorylation site on STIL that promotes binding to CPAP *in vitro* and *in vivo*. This phospho-dependent binding interaction is conserved in flies and allows STIL to link the growing cartwheel to the outer microtubule wall of the centriole. Together, our findings offer insight into a novel step in centriole assembly that is regulated by PLK4 kinase activity.

3.2 PLK4 phosphorylates STIL to promote CPAP binding.

PLK4 phosphorylates conserved residues in the STIL STAN motif to promote binding to SAS6 (Moyer et al. 2015; Ohta et al. 2014; Dzhindzhev et al. 2014). To determine whether phosphorylation of STIL by PLK4 might affect the interaction of STIL with other components of the centriole duplication machinery, we tested the ability of Myc-GFP-STIL to interact with its known centriolar binding partners in the presence of kinase active ($PLK4^{WT}$) or kinase dead ($PLK4^{KD}$) PLK4 (Holland et al. 2010). Active PLK4 triggers its own degradation and thus, we

used a PLK4$^{\Delta 24}$ mutant that stabilizes the active kinase by preventing PLK4-induced autodestruction (Holland et al. 2010). Expression of kinase active PLK4$^{\Delta 24}$-mCherry increased the binding of STIL to SAS6 in cells **(Figure 12A)**, but did not increase binding to the STIL-interacting partners RTTN (Chen et al. 2017) or CEP85 (Liu et al. 2018) **(Figure 12B,C)**. Unexpectedly, we observed that PLK4 kinase activity promoted a robust increase in STIL binding to CPAP, suggesting that PLK4 kinase activity also controls the interaction of CPAP with STIL **(Figure 12D)**.

To determine how PLK4 phosphorylation promotes binding of CPAP to STIL, we mapped *in vitro* PLK4 phosphorylation sites on STIL using mass spectrometry. Recombinant full-length GST-STIL was phosphorylated with the His-PLK4 kinase domain *in vitro*. Of the 89 *in vitro* phosphorylation sites we identified on STIL, S428 was of particular interest as it is highly conserved, matches the PLK4 consensus phosphorylation sequence and is positioned close to the known CPAP binding region on STIL **(Figure 13, Figure 14A)** (Cottee et al. 2013; Kettenbach et al. 2012; Johnson et al. 2007; Hatzopoulos et al. 2013). To determine if phosphorylation of STIL S428 was responsible for enhancing the binding of CPAP to STIL, we co-expressed FLAG-CPAP and a wild type (WT) or S428A mutant of Myc-GFP-STIL in the presence of kinase active or inactive PLK4$^{\Delta 24}$-mCherry. The expression of kinase active PLK4 promoted a > 7-fold increase in the amount of CPAP bound to WT STIL, but this increased binding was not observed with STIL S428A **(Figure 14B).** To test if this phospho-regulated binding interaction can be reconstituted with purified components, we performed GST-pull down experiments on recombinant WT or S428A GST-STIL that had been phosphorylated with the His-PLK4 kinase domain and then incubated with a recombinant Flag-CPAP TCP domain. Phosphorylation of WT

GST-STIL with PLK4 increased binding to the Flag-TCP domain by ~2.5-fold, but this increased binding was not observed with STIL S428A **(Figure 14C)**. The use of the CPAP TCP domain rather than full-length protein may explain the more modest increase in CPAP binding to STIL *in vitro* compared to *in vivo*. These data show that phosphorylation of STIL S428 promotes CPAP binding to STIL *in vitro* and *in vivo*.

To demonstrate STIL S428 is a *bona fide* PLK4 phosphorylation site, we raised a phospho-specific antibody to this site. The affinity-purified pS428 antibody recognized recombinant GST-STIL in the presence of ATP and the His-PLK4 kinase domain, but not in the absence of ATP (**Figure 14D**). Moreover, recognition of phosphorylated GST-STIL by the pS428 antibody was abolished by the S428A mutation, demonstrating the specificity of the pS428 antibody (**Figure 14D**). To determine if PLK4 can phosphorylate STIL S428 in cells, we co-expressed WT or a S428A mutant of Myc-GFP-STIL with kinase active or inactive PLK4$^{\Delta 24}$-mCherry **(Figure 14E)**. The pS428 antibody recognized WT STIL in the presence of kinase active, but not kinase inactive, PLK4, showing that PLK4 phosphorylates STIL at S428 *in vitro* and *in vivo*.

3.3 The phosphorylation-dependent binding of CPAP to STIL is conserved in flies.

D.melanogaster PLK4 (DmPLK4) was recently shown to phosphorylate the STIL homolog Ana2 at S38, a residue equivalent to S428 in the human STIL (McLamarrah et al. 2018; Dzhindzhev et al. 2017) **(Figure 14A).** Phosphorylation of S38 was shown to be required for Ana2 recruitment (Dzhindzhev et al. 2017) but was reported not to alter Ana2 binding to the CPAP orthologue

DmSas4 (McLamarrah et al. 2018). We reasoned that this discrepancy might arise because PLK4 is a low-abundance protein that is activated at the centriole and is unable to efficiently phosphorylate a significant fraction of the transfected Ana2. To test this possibility, we transfected *D.melanogaster* S2 cells with either WT or S38A Myc-GFP-Ana2 and Flag-DmSas4 in the presence or absence of a stabilized version of *Dm*PLK4^{SBM}-mCherry (Rogers et al. 2009). *Dm*PLK4 promoted a > 6-fold increase in the amount of *Dm*Sas4 bound to WT Ana2, but this increased binding was not observed with Ana2 S38A **(Figure 14F).** These data suggest that the increased binding of CPAP/*Dm*Sas4 to phosphorylated STIL/Ana2 is conserved between human and flies.

3.4 PLK4 phosphorylates STIL S428 to promote centriole duplication.

To test the requirement of STIL S428 phosphorylation by PLK4 for centriole biogenesis, we integrated doxycycline-inducible, siRNA-resistant WT or S428A Myc-GFP-STIL transgenes a pre-defined genomic locus in a DLD-1 host cell line**.** As a control, we also generated DLD-1 cells expressing a Myc-GFP-STIL S1116A transgene, which contains a mutation at a conserved PLK4 phosphorylation site in the STIL STAN motif required for efficient binding to SAS6 (Moyer et al. 2015; Dzhindzhev et al. 2014; Ohta et al. 2014). WT, S1116A and S428A Myc-GFP-STIL transgenes were all expressed to similar levels in cells **(Figure 16A, B)**. Depletion of STIL by siRNA resulted in 100% of mitotic cells with ≤ 2 centrioles, and this effect was almost completely rescued by expression of the WT STIL transgene (**Figure 15A**). By contrast, expression of either STIL S428A or S1116A only led to a partial rescue of centriole duplication (61% S428A cells and 70% S1116A cells contain ≤ 2 centrioles in mitosis) (**Figure 15A**).

Importantly, preventing S428 phosphorylation did not affect the ability of STIL to bind to or stimulate PLK4 kinase activity, suggesting that a failure to activate PLK4 kinase activity is not responsible for the failure of centriole duplication **(Figure 17A)** (Moyer et al. 2015). These data show that phosphorylation of STIL S428 by PLK4 promotes centriole duplication.

3.5 Preventing STIL S428 phosphorylation phenocopies mutations in the CPAP binding motif of STIL.

CPAP interacts with STIL via a short proline-rich region containing a highly conserved PRxxPxP motif **(Figure 14A)** (Cottee et al. 2013). To test whether defective CPAP binding causes the failure to rescue centriole duplication with STIL S428A, we created a PRP mutant of STIL by mutating the conserved PRPIPSP CPAP binding motif to AAPIASP (P404A, R405A, P408A). This mutation did not affect PLK4's ability to phosphorylate STIL on S428 **(Figure 17B)**. As expected, the STIL PRP mutant showed impaired binding to CPAP **(Figure 15E).** Expression of Myc-GFP-STIL PRP led to only a partial rescue of centriole duplication in cells depleted of endogenous STIL by siRNA, similar to that of the STIL S428A mutation **(Figure 15A)**. Combining the S428A or PRP mutation with the S1116A mutation in the STIL STAN motif that impairs binding to SAS6 prevented any rescue of centriole duplication **(Figure 15A,B)**. By contrast, a Myc-GFP-STIL transgene containing both the S428A and PRP mutation rescued centriole duplication to a level similar to that observed with a STIL transgene that contained either mutation on its own **(Figure 15A,B)**. Collectively, these data suggest that S428 phosphorylation and the PRxxPxP motif of STIL function in the same pathway to promote CPAP

binding to STIL, and that they both are in a separate pathway from mutations that disrupt SAS6 binding to STIL.

To evaluate the impact of disrupting CPAP and SAS6 binding on the centriole targeting of STIL, we measured the levels of Myc-GFP-STIL transgenes at the centriole in S/G2 phase cells depleted of endogenous STIL. Preventing phosphorylation at S428 reduced the localization of Myc-GFP-STIL by 28%, compared to that of the WT transgene **(Figure 15C,D)**. Preventing phosphorylation at S1116 in the STAN motif reduced the abundance of STIL at the centriole by ~2-fold, as previously reported (**Figure 15C**) (Moyer et al. 2015). However, preventing phosphorylation of both sites reduced the centriole localization of STIL by 80%, suggesting that stable incorporation of STIL into the centriole requires strong binding to both CPAP and SAS6 (**Figure 15B,C,D, Figure 18**). Combining the S428A and PRP mutations did not diminish the levels of centriolar STIL below that observed with either mutation alone (**Figure 15C**). This provides further evidence that the S428A and PRP mutations function in the same pathway and act to reduce the stability of CPAP binding to STIL.

3.6 Phosphorylation of the STIL STAN motif by PLK4 does not require STIL S428 phosphorylation.

Experiments in flies suggested that *Dm*PLK4 phosphorylates S38 to promote Ana2 recruitment to the centriole and then phosphorylates conserved residues in the STAN motif to enable SAS6 recruitment (Dzhindzhev et al. 2017; McLamarrah et al. 2018). However, we found that phosphorylation of STIL S428 in human cells does not play a significant role in the centriolar

recruitment of STIL **(Figure 15C,D)**. To determine whether phosphorylation of the STAN motif requires phosphorylation of STIL S428, or vice versa, we monitored phosphorylation of STIL S428 and S1116 using phospho-specific antibodies. Expression of kinase active PLK4$^{\Delta 24}$-mCherry promoted phosphorylation of a Myc-GFP-STIL transgene at both S428 and S1116, and mutation of either site did not prevent phosphorylation of the other **(Figure 19)**. To test if PLK4-mediated phosphorylation of the STIL STAN motif at the centriole requires phosphorylation of S428, we monitored phosphorylation of S1108 in the STAN motif using a phospho-specific antibody (Moyer et al. 2015). Although treatment with the PLK4 inhibitor centrinone abolished STIL S1108 phosphorylation, the S428A or PRP motif mutation did not affect phosphorylation of STIL S1108 **(Figure 19)**. These data show that phosphorylation of the STIL STAN motif by PLK4 does not require prior phosphorylation of STIL S428.

3.7 Stable centriole recruitment of STIL requires STIL S428 phosphorylation.

To examine how S428 phosphorylation affects the binding dynamics of centriolar STIL, we performed Fluorescence Recovery after Photobleaching (FRAP) in cells depleted of endogenous STIL and expressing Myc-GFP-STIL transgenes. Myc-GFP-STIL WT partially recovered following bleaching, showing that STIL exists in both mobile and immobile pool at the procentriole (**Figure 20A**, Myc-GFP-STIL WT, recovery percentage (R%) = 38%). Consistent with previous observations, mutation of the S1116 phosphorylation site increased the mobile fraction of centriolar STIL (**Figure 20A**, Myc-GFP-STIL S1116A, R% = 71%) (Moyer et al. 2015). Importantly, the S428A and PRP mutants of STIL also showed an increased recovery of centriolar STIL (**Figure 20A, Figure 21)**; Myc-GFP-STIL S428A, R% = 57%; Myc-GFP-STIL

PRP, R% = 58%), suggesting that CPAP binding allows more stable incorporation of STIL into the procentriole.

To understand how mutations in STIL affect centrosomal CPAP dynamics, we monitored centrosomal GFP-CPAP turnover using FRAP by knocking down endogenous CPAP and expressing a siRNA-resistant Myc-GFP-CPAP transgene. As previously reported, Myc-GFP-CPAP partially recovered after photobleaching (**Figure 22A)**, Myc-GFP-CPAP, R% = 51%) (D. Kitagawa et al. 2011). Surprisingly, performing the same measurements in cells depleted of STIL led to an almost complete turnover of Myc-GFP-CPAP (**Figure 22A**, Myc-GFP-CPAP, STIL siRNA, R% = 96%). While STIL is uniquely localized to the procentriole, CPAP is present at both the parent centriole and procentriole. In addition, CPAP has been reported to localize in the PCM material (Sonnen et al. 2012), consistent with a proposed role in recruiting PCM (X. Zheng et al. 2014; Gopalakrishnan et al. 2011; Chou et al. 2016; Novak et al. 2016). Since we bleach all of the pools of CPAP in our FRAP experiments, we cannot distinguish which centrosomal populations of CPAP are dynamic and which are stably bound. Nevertheless, given STIL localizes exclusively to the procentriole, one interpretation of our data is that STIL is required for the stable incorporation of CPAP at the procentriole, while the parental centriole and PCM pool of CPAP are dynamic and display a transient association with the centrosome.

To test the role of STIL S428 phosphorylation in modulating CPAP turnover at the centrosome, we integrated into DLD1 cells a Myc-STIL-T2A-GFP-CPAP transgene in which siRNA-resistant Myc-STIL and GFP-CPAP were both expressed from the same doxycycline-inducible promoter. As expected, Myc-STIL expression significantly suppressed the increased turnover of GFP-

CPAP observed in cells depleted of endogenous STIL (**Figure 22A**, GFP-CPAP, Myc-STIL WT background, R% = 50%). However, mutation of S428 or the PRP motif on STIL increased the turnover of GFP-CPAP compared with WT STIL (**Figure 20B, Figure 22B**, GFP-CPAP, Myc-STIL S428A background, R% = 69%; GFP-CPAP, Myc-STIL PRP background, R% = 67%). Expression of Myc-STIL S1116A did not increase GFP-CPAP turnover, indicating that the increase in GFP-CPAP turnover in a Myc-STIL S428A background reflects a specific defect in the STIL/CPAP interaction (**Figure 20B**, GFP-CPAP, Myc-STIL S1116A background, R% =55%). These data suggest that STIL binding allows a more stable incorporation of CPAP into the centrosome, possibly by facilitating interactions with CPAP at the procentriole. However, since the depletion of STIL resulted in a higher level of CPAP turnover than specifically disrupting the STIL/CPAP interaction, it is likely STIL recruits additional proteins that collectively act to stabilize the incorporation of CPAP into the centrosome. Together, our data show that the interaction of CPAP with STIL allows both proteins to incorporate more stably into the centrosome.

3.8 Mutations in the CPAP TCP domain cause less stable CPAP incorporation into the centrosome.

To better understand the requirement of the STIL/CPAP interaction in centriole duplication, we constructed an RNAi-replacement system in DLD-1 cells where endogenous CPAP was depleted by siRNA and replaced with physiological levels of a siRNA-resistant Myc-GFP-CPAP transgene **(Figure 23A, Figure 23B)**. Knockdown of CPAP by siRNA resulted in 81% of mitotic cells with ≤ 2 centrioles, and this was largely rescued by expression of the CPAP WT transgene

(**Figure 23C**). By contrast, expression of a CPAP transgene with mutations in the TCP domain that reduced binding to STIL (F1229A or E1235K), led to a partial rescue of centriole duplication (58% of F1229A cells and 48% of E1235K cells contain ≤ 2 centrioles in mitosis) (**Figure 23C**, **Figure 23D**) (Cottee et al. 2013; Hatzopoulos et al. 2013). Importantly, the presence of these TCP domain mutations increased the turnover of Myc-GFP-CPAP at the centrosome (**Figure 23E,** Myc-GFP-CPAP R% = 51%; Myc-GFP-CPAP F1229A, R% = 76%; Myc-GFP-CPAP E1235K, R% = 67%), but did not alter the abundance of the Myc-GFP-CPAP or STIL at the centrosome (**Figure 23F-H**). Collectively, these data support the conclusion that the STIL-CPAP interaction facilitates the stable centrosomal integration of CPAP, but that this interaction does not have a major impact on the level to which CPAP accumulates at the centrosome.

3.9 STIL depletion reduces the localization of CPAP to the centrosome.

To further test whether the overall level of CPAP present at the centrosome depends on STIL, we measured centrosomal CPAP levels in S/G2 cells depleted of STIL by siRNA. STIL knockdown reduced the level of CPAP at the centrosome by ~30% **(Figure 24A-C)**. Importantly, we observed that centrosomal CPAP levels were not significantly reduced following depletion of endogenous STIL and expression of a WT or mutant Myc-GFP-STIL transgene **(Figure 24D,E)**. This is consistent with a model in which CPAP is localized to the parent centriole independently of STIL, while procentriole localized CPAP requires STIL for stable binding. However, our data argue that the role of STIL in recruiting CPAP to the centrosome is largely independent of the STIL/CPAP interaction and likely depends on the recruitment of other proteins. This is

consistent with our FRAP analysis which showed that depletion of STIL increased the turnover of CPAP at the centriole from 51% to 96%, while disruption of STIL binding to CPAP increased CPAP turnover to only ~70%. We conclude that the recruitment of the majority of CPAP present at the centrosome does not require CPAP binding to STIL.

3.10 Recruitment of CPAP to *de novo* formed centrioles requires STIL S428 phosphorylation.

The multiple populations of CPAP present at the centrosome prevented us from specifically testing the requirement of STIL S428 phosphorylation for CPAP recruitment to the procentriole. To analyze the role of STIL S428 phosphorylation in recruiting CPAP specifically to assembling procentrioles, we induced the formation of freestanding *de novo* centrioles in cells expressing various STIL mutants. DLD-1 cells expressing a Myc-GFP-STIL transgene were chronically treated with the PLK4 inhibitor centrinone to remove centrioles (Wong et al. 2015). Acentriolar cell lines were then depleted of endogenous STIL by siRNA for twenty-four hours, and centrinone was removed to induce the formation of freestanding *de novo* centrioles **(Figure 25A)**. *De novo* centrioles were defined as foci marked by both PLK4 and Centrin **(Figure 26)**. As expected, depletion of STIL suppressed *de novo* centriole assembly, and this was rescued by expression of a WT Myc-GFP-STIL transgene (48% and 87% of cells expressing WT STIL contained *de novo* centrioles at 24 and 72 hours after centrinone washout, respectively) (**Figure 25B**). S428A, S1116A, and PRP Myc-GFP-STIL were all deficient in assembling *de novo* centrioles, with only 25%, 12%, and 33% of cells containing PLK4 and Centrin positive foci at 72 hours after centrinone removal, respectively. While cells expressing Myc-GFP-STIL S1116A

STIL formed very few STIL/PLK4 foci, the number of foci observed in cells expressing S428A and PRP Myc-GFP-STIL was comparable to that observed with the WT STIL transgene (**Figure 25C, Figure 26**). This suggests that cells which express the S428A and PRP mutant STIL fail centriole assembly at a later stage than those that cells express the S1116A mutant of STIL.

To determine why the S428A and PRP mutations fail *de novo* centriole formation after forming STIL/PLK4 foci, we measured the recruitment of SAS6 and CPAP to the newly formed STIL foci. WT Myc-GFP-STIL recruited both CPAP and SAS6 to as expected (**Figure 25D-H**). While recruitment of SAS6 was identical in WT, S428A and PRP Myc-GFP-STIL, the S428A and PRP mutations resulted in a > 90% reduction in the amount of CPAP recruitment to the STIL foci (**Figure 25D-H**). Together, these data suggest that S428A and PRP mutant STIL bind to SAS6 and assemble a cartwheel but fail to recruit CPAP and form *de novo* centrioles.

3.11 Discussion

Significant progress has been made in understanding the composition of centrioles and how protein interactions can direct centriole assembly (Andersen et al. 2003; Jakobsen et al. 2011; Firat-Karalar et al. 2014; Galletta et al. 2016; Gupta et al. 2015). However, we have a limited understanding of which assembly steps are controlled by PLK4 to maintain the number of centrioles in cycling cells. Our data now establish that PLK4 phosphorylates its centriole substrate STIL on a conserved site close to the PRP motif to promote STIL binding to CPAP *in vitro* and *in vivo*. The STIL/CPAP complex is only the second binding interaction shown to be controlled by PLK4 and highlights a new regulated step in centriole assembly.

Our data lead us to propose a model whereby active PLK4 phosphorylates STIL at the site of procentriole assembly in two different regions with distinct functional consequences **(Figure 7)**: phosphorylation of multiple residues in the STAN motif, most notably S1116, allows STIL binding to SAS6 to promote cartwheel assembly. Second, phosphorylation of S428 promotes the binding of the STIL PRP motif to CPAP, thereby linking the growing cartwheel to the triplet microtubules of the centriole wall. This model is consistent with our analysis of *de novo* centriole assembly, which showed that phosphorylation of the STIL STAN motif is required to recruit SAS6 to the site of procentriole assembly while phosphorylation of STIL S428 is required at a later stage to recruit CPAP to the cartwheel. Moreover, super-resolution imaging of *Drosophila* centrioles has revealed that the C-terminal region of Ana2/STIL containing the STAN motif is located closer to the cartwheel hub, while the N-terminal region containing the PRP motif is positioned close to the C-terminus of Sas-4/CPAP at the periphery of the cartwheel (Gartenmann et al. 2017). A mutation in the CPAP TCP domain that causes microcephaly in humans has been shown to decrease the affinity of CPAP to STIL (Tang et al. 2011; Cottee et al. 2013; Bond et al. 2005). Moreover, mutations in STIL that reside in the CPAP and SAS6 interacting motifs have also been identified in patients with microcephaly, although the significance of these alterations remains to be determined (Cristofoli et al. 2017).

Although recruitment of CPAP to assembling *de novo* centrioles requires STIL S428 phosphorylation, this modification is not required for recruiting the bulk of CPAP to the centrosome. We envisage two possible explanations for these observations. First, although sharing obvious similarities, *de novo* centriole assembly may have some distinct requirements compared with canonical centriole biogenesis. For example, the presence of a parent centriole

may help direct CPAP recruitment to the site of procentriole assembly; CPAP localized in the PCM could be recruited to the procentriole by some of CPAP's other interacting partners in the absence of STIL S428 phosphorylation. A second possibility is that multiple pools of CPAP at the centrosome (parent centriole, procentriole and PCM associated) may obscure the ability to accurately monitor the role of STIL phosphorylation in CPAP recruitment at the nascent procentriole. In any case, it is clear that even if the STIL-CPAP interaction is not strictly necessary for the recruitment of either protein to canonically duplicating centrioles, it does allow for the more stable integration of these proteins into the centrosome.

A previous study solved the structure of the CPAP TCP domain bound to a short STIL peptide (residues 395 - 416) containing the PRP motif but lacking the S428 phosphorylation site (Cottee et al. 2013). A central question that now emerges is how phosphorylation of S428, which is positioned ~20 amino acids downstream of the core PRP interaction motif in STIL, promotes binding to CPAP in cells. We envisage two non-mutually exclusive possibilities. First, phosphorylation creates an extended binding interface that increases the affinity of STIL to CPAP. Indeed, sequence conservation in the CPAP TCP domain is not confined to the region that directly interacts with the PRP motif of STIL but extends further along the surface of the TCP domain beta sheet, suggesting that additional contacts with STIL may occur in this region (Cottee et al. 2013). Moreover, there is high conservation around the S428 phosphorylation site on STIL, and this conserved motif was proposed to be well positioned to form an extended interaction interface with conserved residues in the CPAP TCP domain (Cottee et al. 2013). Phosphorylation of STIL S428 could, therefore, seed the binding of this conserved region and cooperatively enhance the binding of STIL to CPAP.

An alternative hypothesis is that S428 phosphorylation generates a conformational change that unmasks the PRP motif in STIL and exposes it for binding to CPAP. In support of this model, work in *Drosophila* has shown that phosphorylation of the homologous site (S38) on Ana2/STIL leads to a dramatic mobility shift in an SDS page gel that is likely to reflect a significant conformational change in Ana2 (Dzhindzhev et al. 2017). It is notable that *C.elegans* SAS-5/STIL lacks an obvious PRP motif, but directly binds to SAS-4/CPAP through a disordered region (Cottee et al. 2013). Moreover, the SAS-4/CPAP TCP domain is required for the incorporation of SAS-4 into the centriole in *C.elegans*. SAS-5 has also been shown to bind to microtubules through a region that overlaps with the SAS-4 binding domain, suggesting that the interaction of SAS-5 with microtubules and SAS-4 may be mutually exclusive (Rothbauer et al. 2007). In the future, it will be interesting to investigate if ZYG-1/PLK4 kinase activity regulates the critical SAS-5/SAS-4 interaction in *C.elegans* and switches SAS-5 from binding microtubules to an association with SAS-4.

3.12 Figures and Legends

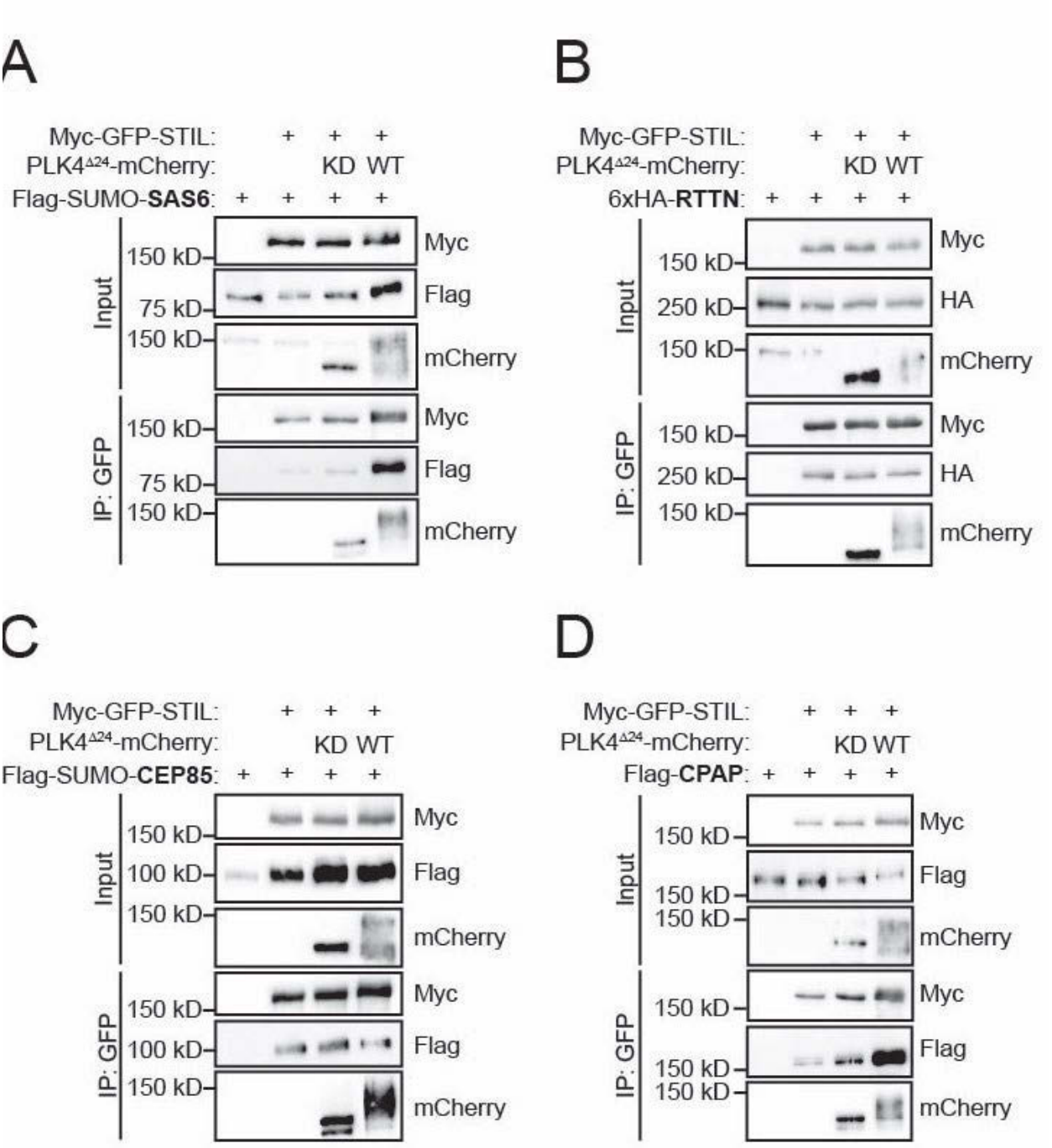

Figure 12. PLK4 kinase activity promotes STIL binding to CPAP.

(A-D) HEK293FT cells were transfected with indicated constructs, subjected to co-immunoprecipitation and immunoblotted with indicated antibodies. PLK4 activity increased binding of both SAS6 and CPAP to STIL.

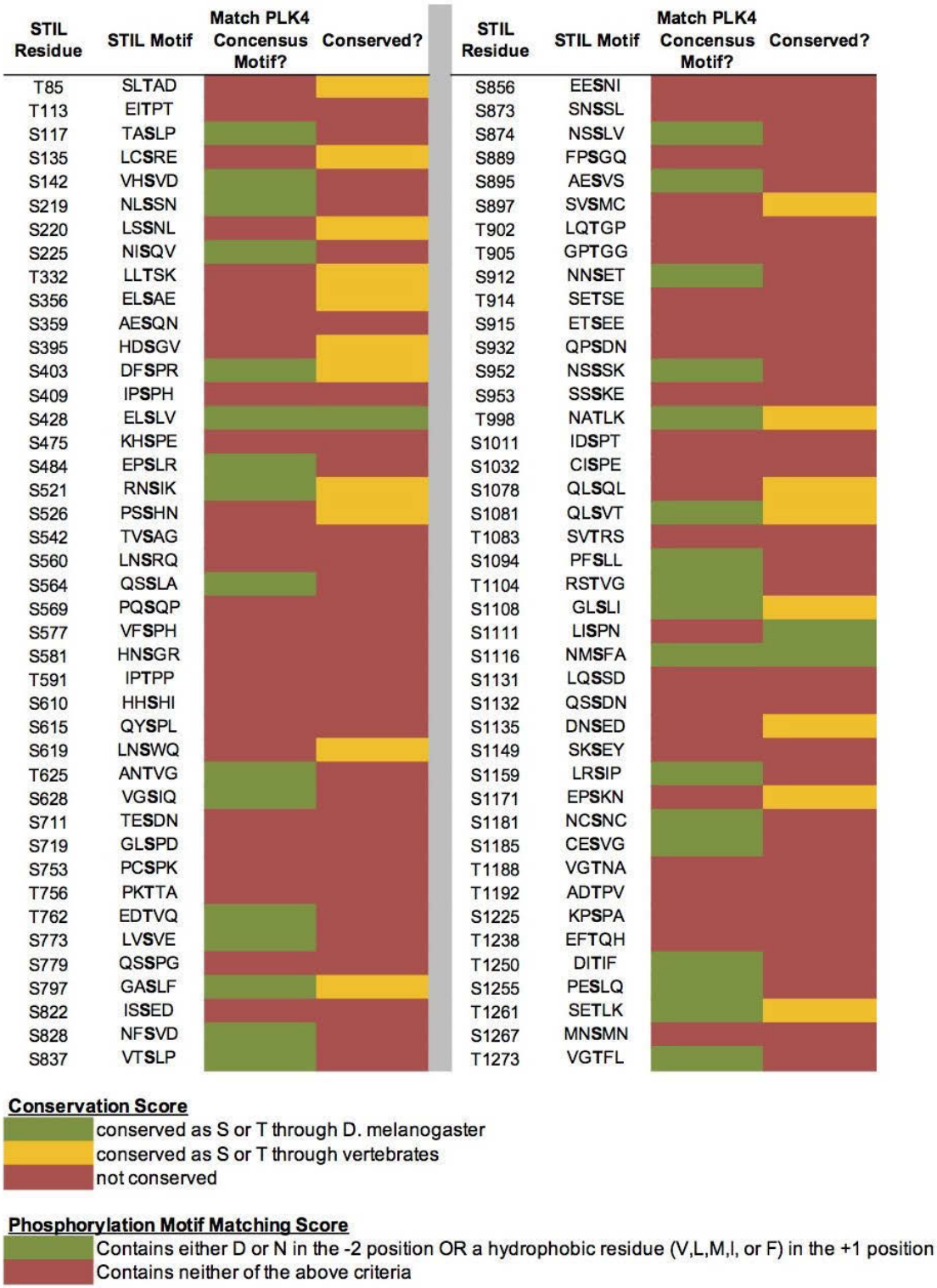

Figure 13. *In vitro* PLK4 phosphorylation sites on STIL.

Recombinant GST-STIL was phosphorylated by PLK4 kinase domain *in vitro,* and phosphorylation sites were mapped with mass spectrometry. Phosphorylated residues were scored as to whether or not they are conserved (see Figure 14A for sample alignment) and whether they match the PLK4 phosphorylation consensus motif.

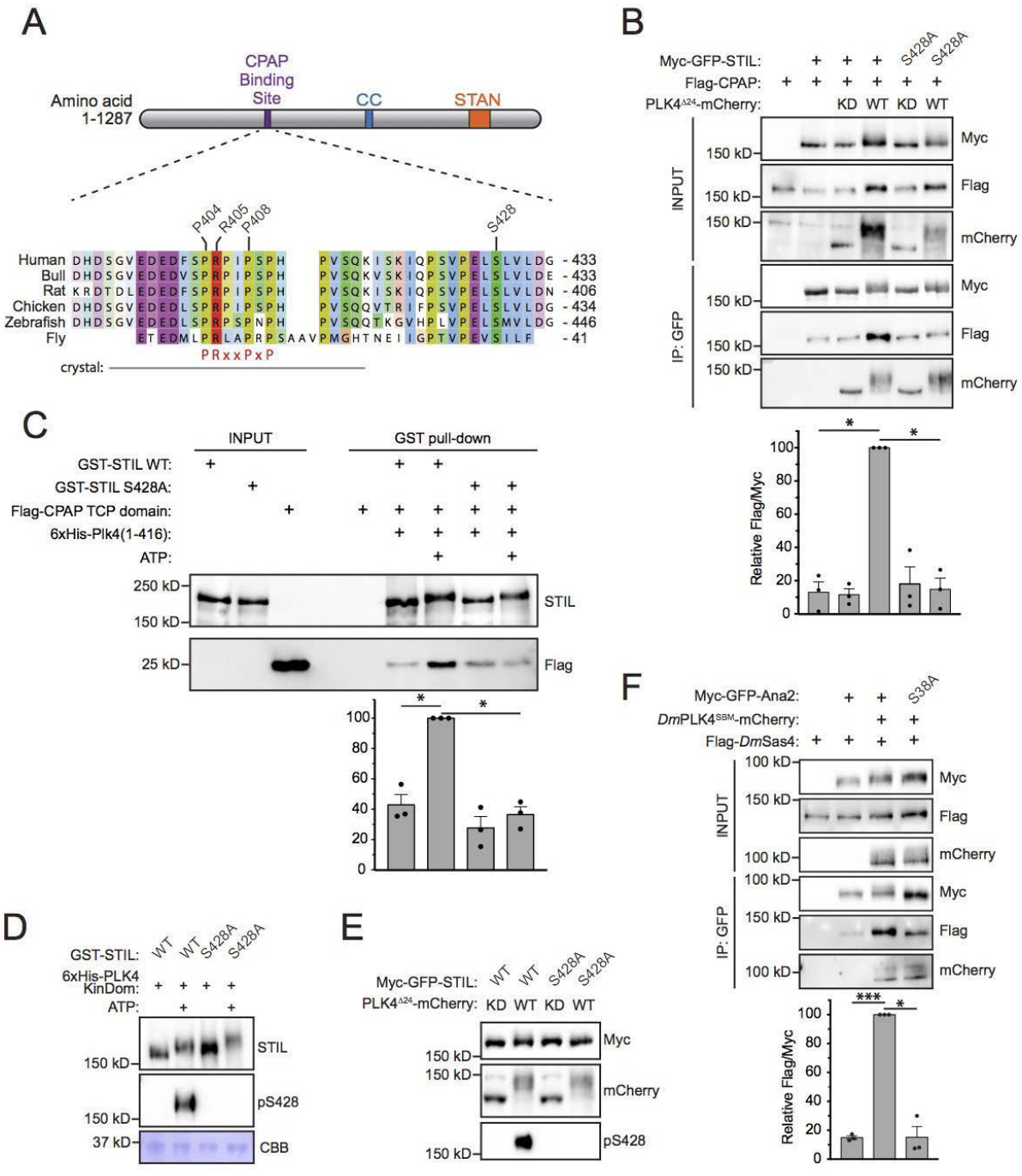

Figure 14. Phosphorylation of STIL by PLK4 promotes increased CPAP binding.

(A) Schematic of full-length STIL showing locations of the known CPAP binding motif, coiled-coil (CC), and STAN motif important for SAS6 binding. Sequence alignment shows the

conserved CPAP binding motif. The fragment of STIL crystalized with CPAP is shown by the grey bar. STIL residues key to the STIL-CPAP interaction (P404, R405, and P408) are highlighted. The conserved PRxxPxP motif is indicated in red. Alignment was generated using Muscle under standard parameters.

(B) HEK293FT cells were transfected with indicated constructs, subjected to co-immunoprecipitation and immunoblotted with indicated antibodies. The graph represents the mean of relative levels of immunoprecipitated Flag/Myc signal across three independent experiments. A dot displays measurements from each experiment. (C) Recombinant full-length GST-STIL (WT or S428A) was bound to beads, phosphorylated by recombinant 6xHis-PLK4 kinase domain, and then incubated with Flag-CPAP TCP domain. GST-pulldowns were analyzed by immunoblotting with indicated antibodies. The graph represents the mean of relative levels of Flag-TCP pulled down with GST-STIL. A dot displays measurements from each experiment. (D) Recombinant full-length GST-STIL (WT or S428A) was phosphorylated *in vitro* by recombinant 6xHis-PLK4 kinase domain. Samples were immunoblotted with indicated antibodies. CBB represents 'coomassie brilliant blue' staining and shows the recombinant PLK4 kinase domain.

(E) HEK293FT cells were transfected with indicated constructs and immunoblotted with indicated antibodies.

(F) *Drosophila melanogaster* S2 cells were transfected with indicated constructs, subjected to co-immunoprecipitation and immunoblotted with indicated antibodies. The graph represents the mean of relative levels of immunoprecipitated Flag/Myc signal across three independent experiments. A dot displays measurements from each experiment. All error bars in the figure represent the standard error of the mean. Asterisks indicate statistically significant differences

between measurements (*: P<0.05; **: P<0.005; ***: P<0.0005). Statistics were calculated using a one-sample t-test where mean values were tested as being different from a value of 100.

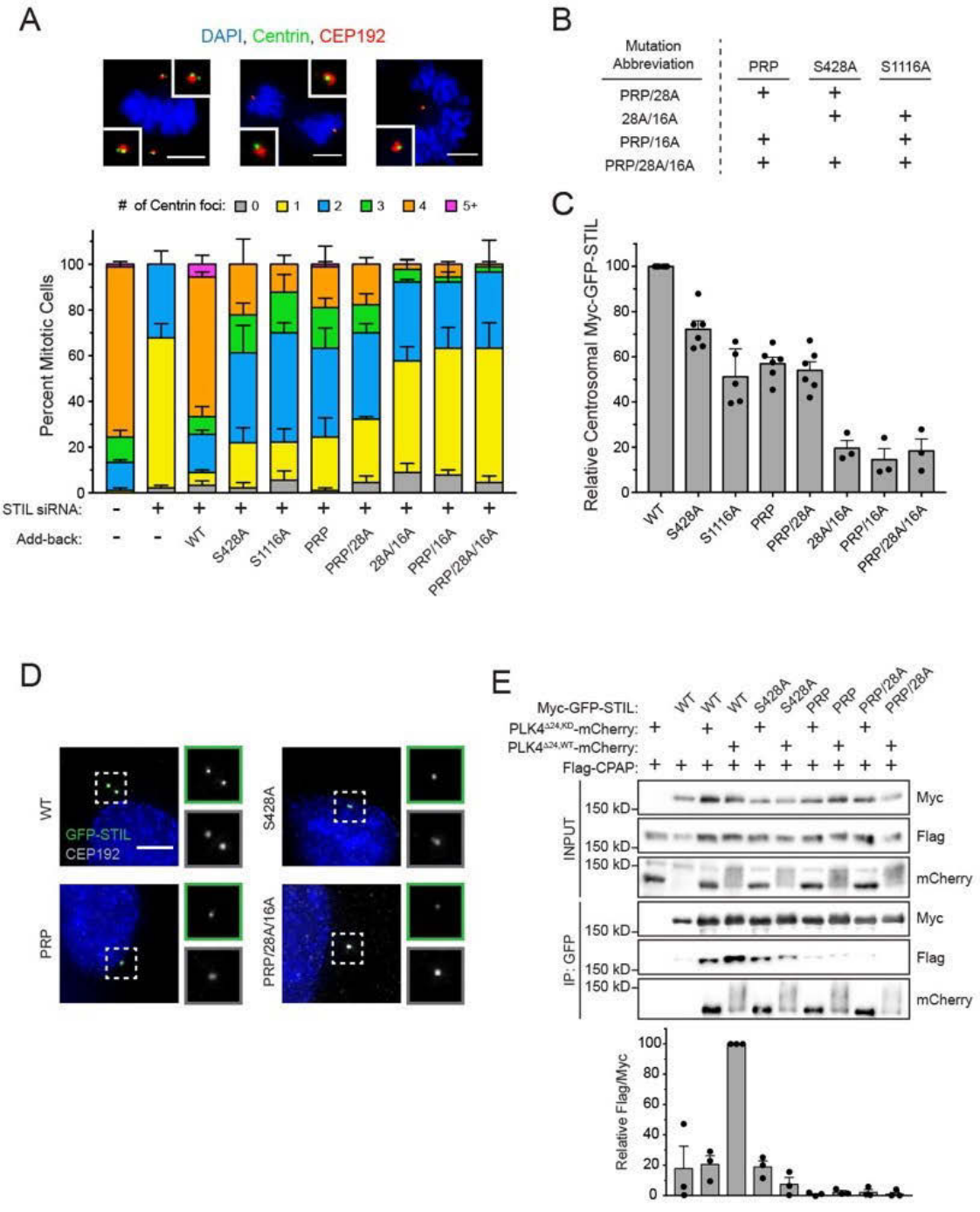

Figure 15. STIL S428 phosphorylation promotes centriole duplication.

(A) Quantification showing the number of mitotic Centrin foci in cells that were depleted of endogenous STIL and induced to express a siRNA-resistant Myc-GFP-STIL transgene as indicated. Representative images show mitotic cells. Scale bars represent 5 μm.

(B) The table shows abbreviations for Myc-GFP-STIL transgenes with multiple mutations. 'PRP' represents a triple mutation of P404A, R405A, and P408A.

(C) Quantification of the relative centrosomal levels of Myc-GFP-STIL constructs from (A) in S/G2 phase cells with at least 40 cells measured per experiment. Bars represent the mean of at least three independent experiments with the average within each experiment shown as a dot.

(D) Representative images of data shown in (C). Scale bar represents 5 μm. All error bars in the figure represent the standard error of the mean.

(E) HEK293FT cells were transfected with indicated constructs and subjected to co-immunoprecipitation and immunoblotted with indicated antibodies. Graph represents the mean of relative levels of immunoprecipitated Flag/Myc signal across three independent experiments. A dot displays measurement from each experiment.

Figure 16. STIL transgenes are expressed to similar levels.

(A) Experimental outline for the STIL RNAi-replacement experiments.

(B) Immunoblot showing Myc-GFP-STIL transgene expression levels after knockdown of endogenous STIL.

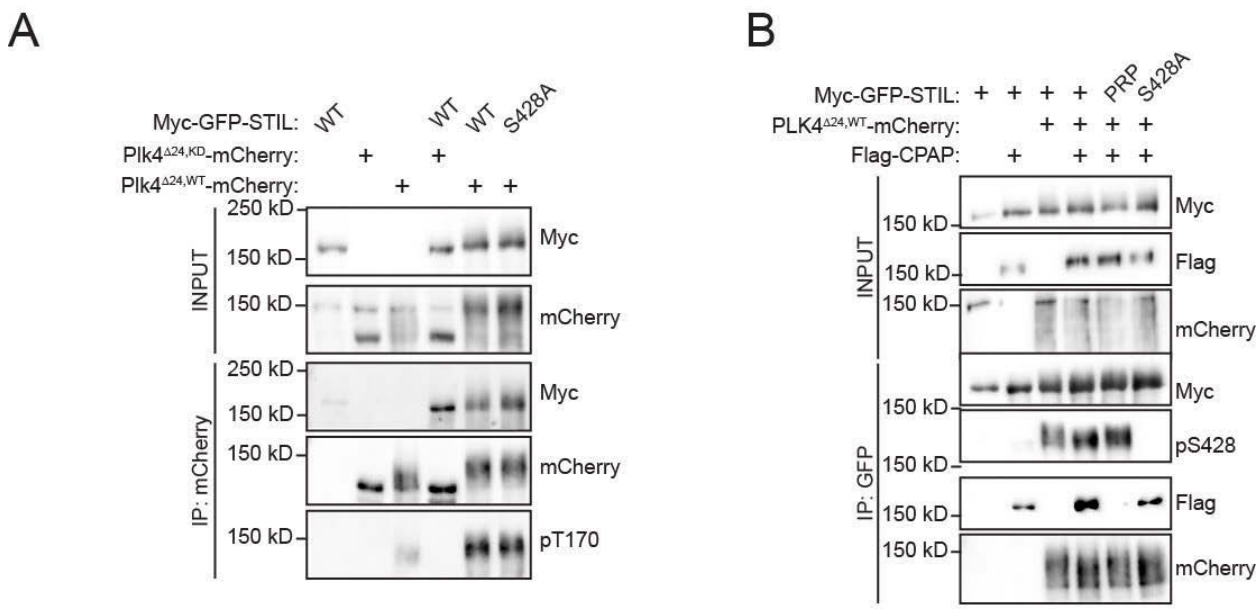

Figure 17. STIL PRP mutations do not affect S428 phosphorylation.

HEK293FT cells were transfected with indicated constructs, subjected to co-immunoprecipitation and immunoblotted with indicated antibodies. (A) Both WT and S428A STIL are capable of activating PLK4 and increasing autophosphorylation of T170. (B) The STIL PRP mutations do not affect S428 phosphorylation.

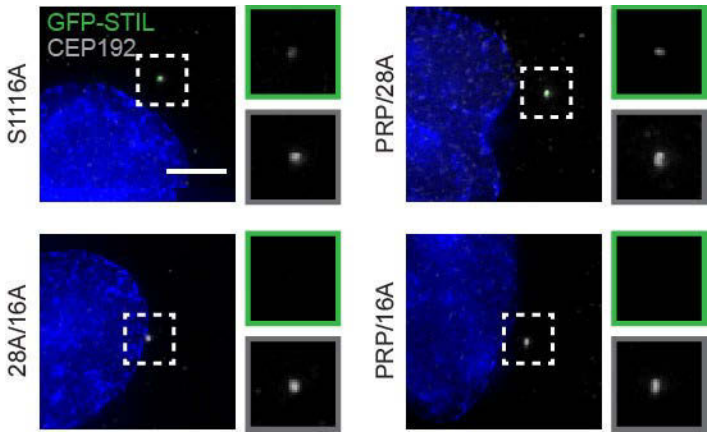

Figure 18. Preventing STIL phosphorylation inhibits accumulation of STIL at the centriole.

Representative images of data shown in (Figure 15C). Scale bar represents 5 μm. All error bars in the figure represent the standard error of the mean.

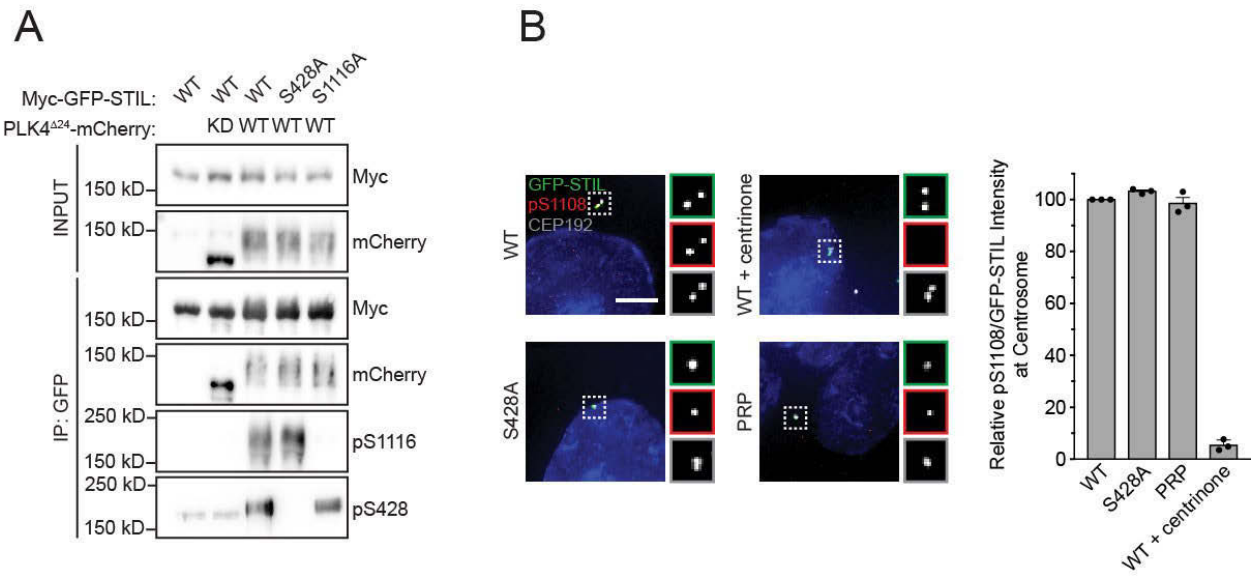

Figure 19. Phosphorylation of the STIL STAN motif by PLK4 does not require STIL S428 phosphorylation.

(A) HEK293FT cells were transfected with indicated constructs, subjected to co-immunoprecipitation and immunoblotted with indicated antibodies. Preventing phosphorylation of STIL S428 does not block STIL S1116 phosphorylation, and vice-versa.

(B) Endogenous STIL was knocked down and replaced with indicated Myc-GFP-STIL transgene. Where indicated, cells were treated with centrinone for 1 hour. Left, representative images showing Myc-GFP-STIL and pS1108 staining. Scale bar represents 5 μm. Right, quantification of the relative centrosomal ratio of pS1108/GFP-STIL in S/G2 phase cells. Bars represent the mean of three independent experiments in which at least 40 cells were quantified per experiment, and the average within each experiment is shown as a dot. Error bars represent the standard error of the mean.

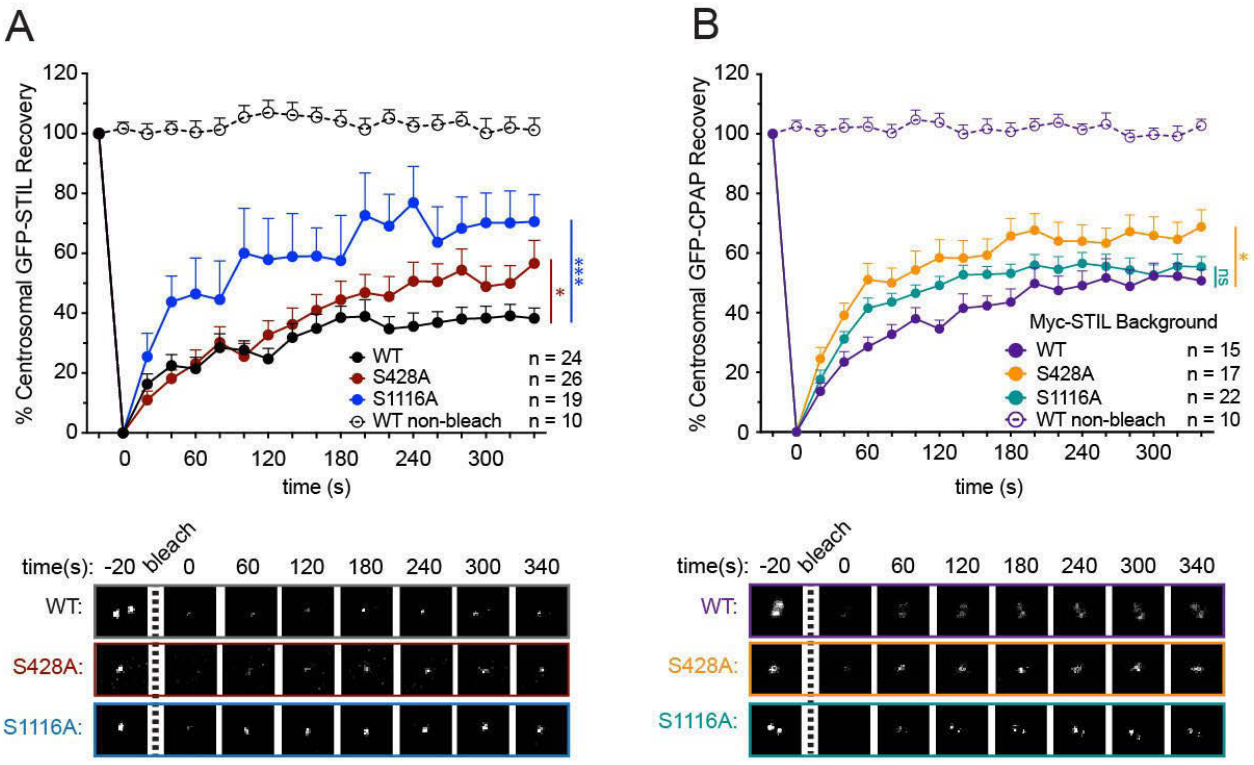

Figure 20. STIL S428 phosphorylation promotes the stable integration of CPAP into the centrosome.

(A) Cells were depleted of endogenous STIL and replaced with the indicated transgene. Myc-GFP-STIL centrosomal foci were photobleached, and fluorescence recovery was measured. The number of quantified photobleaching and recovery events are indicated. Representative timepoints are shown below.

(B) Cells were depleted of endogenous STIL and CPAP and replaced with indicated Myc-STIL-T2A-GFP-CPAP transgene. GFP-CPAP centrosomal foci were photobleached, and fluorescence recovery was measured. The number of quantified photobleaching events is indicated. Representative timepoints are shown below. All error bars in the figure represent the standard error of the mean. Asterisks indicate statistically significant differences between measurements

(*: $P<0.05$; **: $P<0.005$; ***: $P<0.0005$). Statistics were calculated using an unpaired t-test against the population of recovery measurements between indicated samples at the 360 second timepoint.

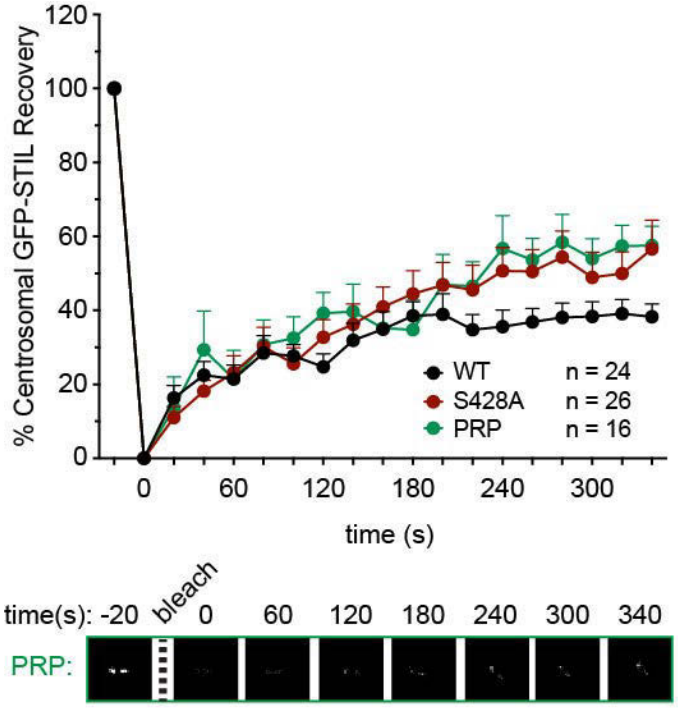

Figure 21. The STIL PRP mutation mimics the turnover dynamics of the STIL S428A mutation.

(A) Cells were depleted of endogenous STIL and replaced with the indicated transgene. Myc-GFP-STIL centrosomal foci were photobleached, and fluorescence recovery was measured. The number of quantified photobleaching and recovery events is indicated. Representative timepoints are shown below. Note that 'WT' and 'S428A' recovery traces are repeated from Figure 20A.

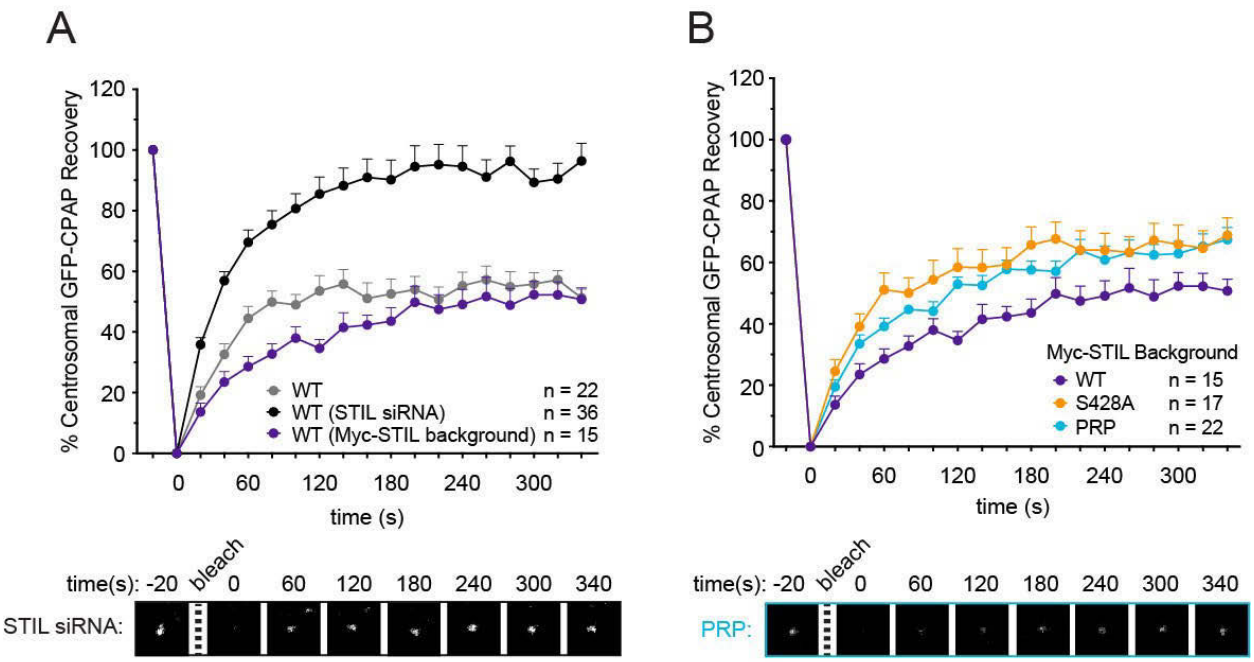

Figure 22. Centrosomal CPAP turns over in response to STIL depletion.

(A) (WT, grey) Cells were depleted of endogenous CPAP and replaced with a Myc-GFP-CPAP transgene. (WT, STIL siRNA) Cells were depleted of endogenous CPAP and STIL, and CPAP was replaced with a Myc-GFP-CPAP transgene. (WT, Myc-STIL background)

(B) Cells were depleted of endogenous STIL and CPAP with replaced with a Myc-STIL-T2A-GFP-CPAP transgene. Centrosomal GFP-CPAP foci were photobleached, and fluorescence recovery was measured. The number of quantified photobleaching and recovery events is indicated. Representative timepoints are shown below. Note that 'WT' and 'S428A/ (Myc-STIL background)' traces are repeated from Figure 20B.

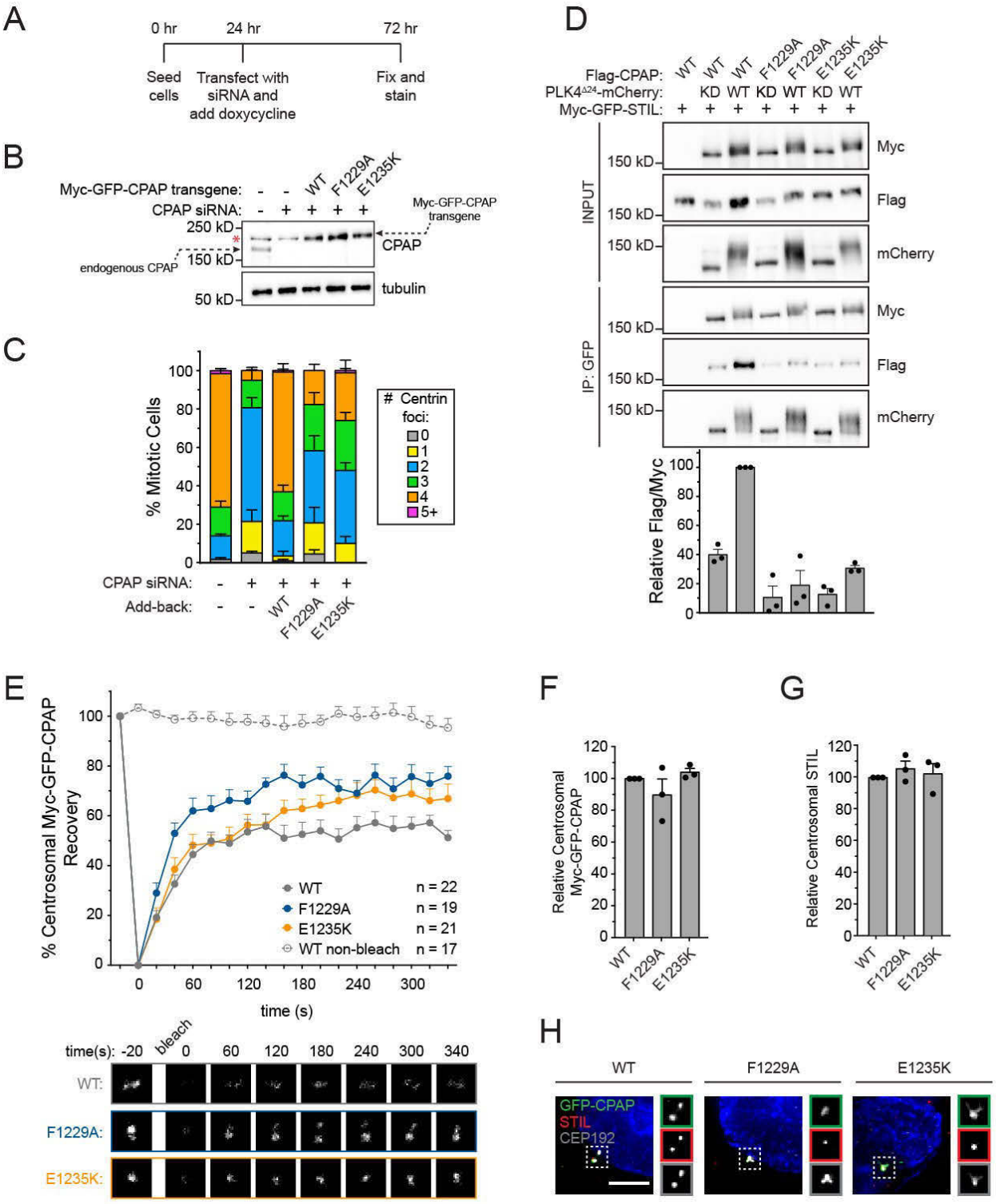

Figure 23. Mutations in the CPAP TCP domain cause less stable CPAP incorporation into the centrosome.

(A) Experimental outline for the STIL RNAi-replacement experiments.

(B) Immunoblot showing the Myc-GFP-CPAP transgene expression levels after knockdown of endogenous CPAP. Note that a background band (denoted by a red asterisk) appears in control lanes that overlaps with the Myc-GFP-CPAP transgene.

(C) Quantification showing the number of mitotic Centrin foci in which cells were depleted of endogenous CPAP and induced to express a siRNA-resistant Myc-GFP-CPAP transgene as indicated.

(D) HEK293FT cells were transfected with indicated constructs, subjected to co-immunoprecipitation and immunoblotted with indicated antibodies. Graph represents the mean of relative levels of immunoprecipitated Flag/Myc signal across three independent experiments. A dot indicates the average within each experiment.

(E) Cells were depleted of endogenous CPAP and replaced with indicated transgene. Myc-GFP-CPAP centrosomal foci were photobleached, and fluorescence recovery was measured. The number of quantified photobleaching and recovery events is indicated. Representative timepoints are shown below. Note that 'WT' trace is repeated from Figure 22.

(F) Quantification of the relative centrosomal levels of Myc-GFP-CPAP from S/G2 phase cells with at least 40 cells measured per experiment. Bars represent the mean of at least three independent experiments with the average within each experiment shown as a dot.

(G) Quantification of the relative centrosomal levels of STIL from S/G2 phase cells with at least 40 cells measured per experiment. Bars represent the mean of at least three independent experiments with the average within each experiment shown as a dot. (H) Representative images from data quantified in (F) and (G). Scale bar represents 5 μm. All error bars represent the standard error of the mean.

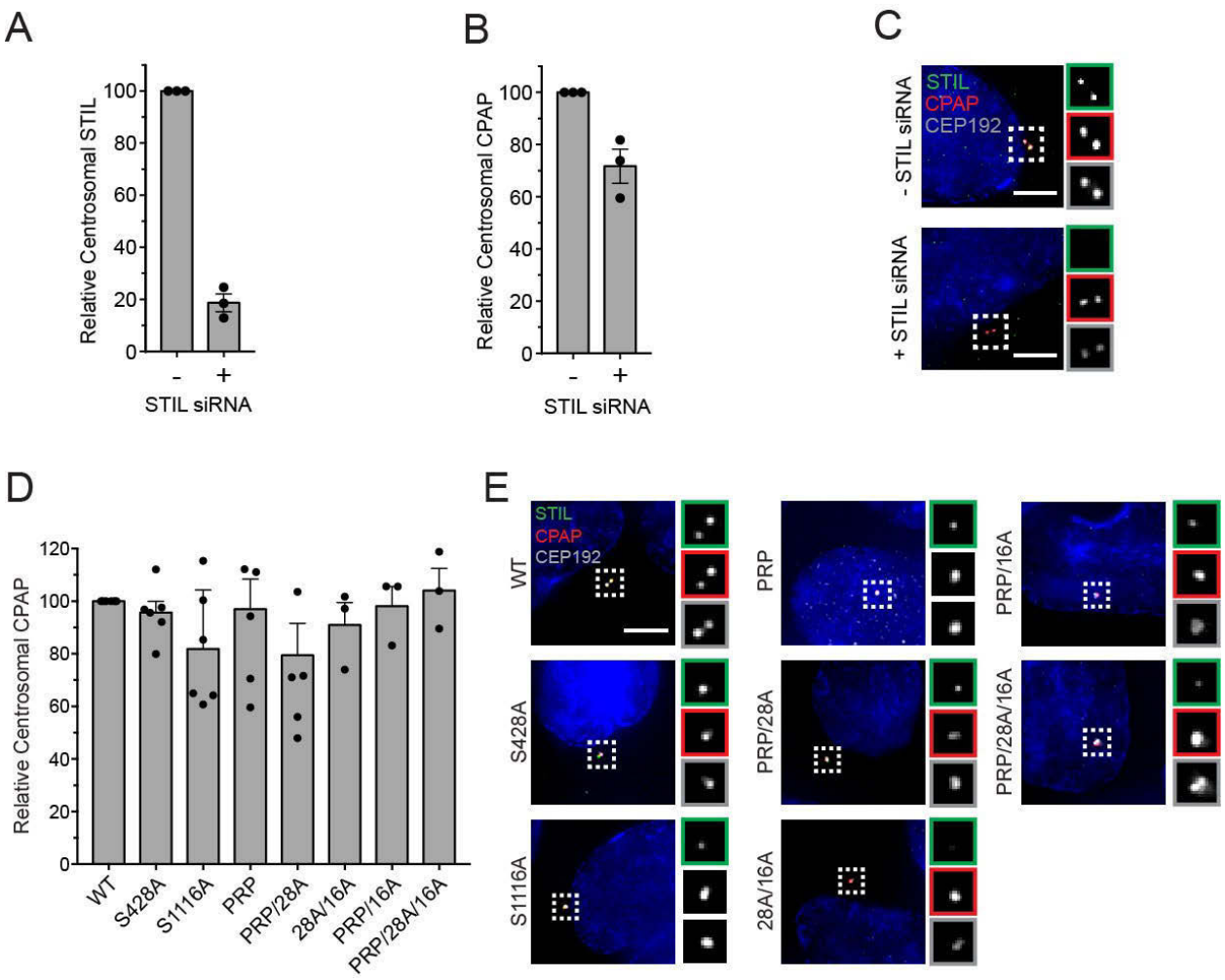

Figure 24. Centrosomal CPAP localization does not depend on the STIL-CPAP interaction.

(A) Quantification of the relative centrosomal levels of endogenous STIL in S/G2 phase cells 48 hours after STIL siRNA. Bars represent the mean of three independent experiments in which at least 40 cells were quantified per experiment, and the average within each experiment is shown as a dot.

(B) Quantification of the relative centrosomal levels of CPAP in S/G2 phase cells 48 hours after STIL siRNA. Bars represent the mean of three independent experiments in which at least 40 cells were quantified per experiment, and the average within each experiment is shown as a dot.

(C) Representative images from the quantification shown in (A) and (B).

(D) Quantification of the relative centrosomal levels of CPAP from experiment described in Figure 15A-C in S/G2 phase cells with at least 40 cells measured per experiment. Bars represent the mean of at least three independent experiments with the average within each experiment shown as a dot.

(E) Representative images of data shown in (D). Scale bar represents 5 μm. All error bars represent the standard error of the mean.

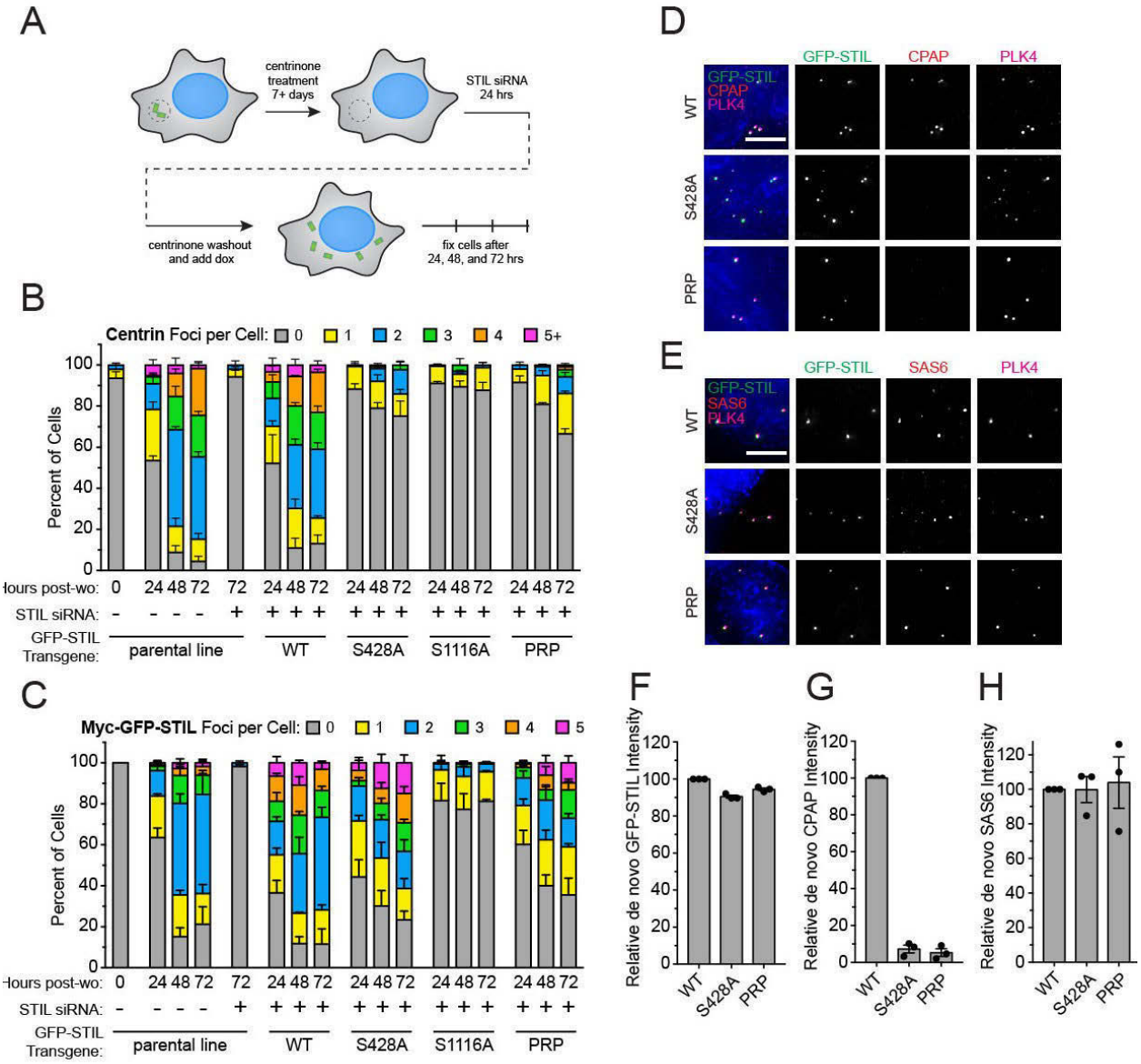

Figure 25. STIL S428 phosphorylation is required for recruitment of CPAP to *de novo* centrioles.

(A) Experimental outline for *de novo* centriole assembly assay. DLD-1 cells were maintained in 500 nM centrinone for seven or more days to deplete centrioles, and then endogenous STIL was knocked down with siRNA. Twenty-four hours later, centrinone was washed out, and the

expression of a siRNA-resistant Myc-GFP-STIL transgene was induced with doxycycline. Cells were analyzed at 24, 48, and 72 hours post-centrinone washout.

(B) Quantification showing the number of Centrin foci in interphase cells under the indicated conditions. Bars represent the mean of three independent experiments in which at least 40 cells were counted per condition. 'Post-wo' refers to post-washout. A Centrin focus was counted as a *de novo* centriole if it overlapped with a PLK4 focus (see Figure 26).

(C) Quantification showing the number of Myc-GFP-STIL foci, or endogenous STIL foci in parental line, in cells under the indicated conditions. 'Post-wo' refers to post-washout. Bars represent the mean of three independent experiments in which at least 40 cells were counted per condition.

(D) Representative images of *de novo* centriole formation showing CPAP localization. Cells were fixed at 24 hours post-centrinone washout. Scale bar represents 5 μm.

(E) Representative images of *de novo* centriole formation showing SAS6 localization. Cells were fixed at 24 hours post-centrinone washout. Scale bar represents 5 μm.

(F-H) Quantification of the relative localization of (F) Myc-GPF-STIL, (G) CPAP, and (H) SAS6 at *de novo* centrioles. Bars represent the mean of three independent experiments in which at least 40 cells were quantified per mutant, and a dot indicates the average within each experiment. All error bars represent the standard error of the mean.

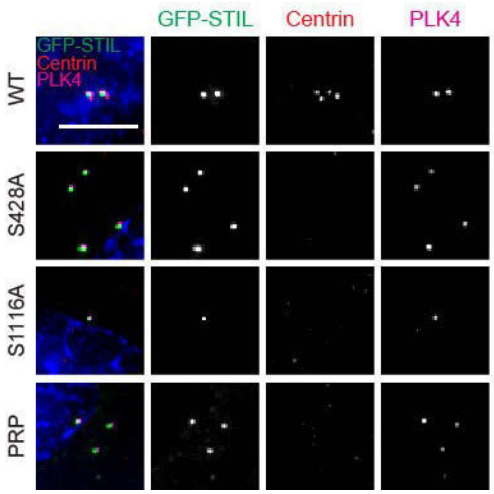

Figure 26. *De novo* centriole formation requires phosphorylation of STIL S428 and S1116 by PLK4.

Representative images of *de novo* centriole formation at 72 hours after centrinone washout. Scale bar represents 5 μm.

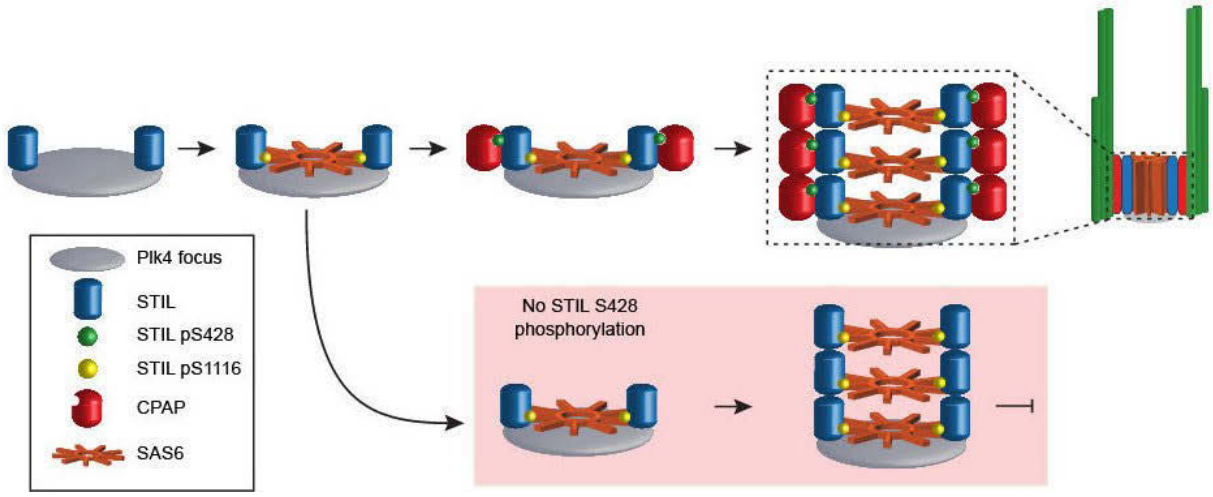

Figure 27. Model depicting the early stages of *de novo* centriole formation.

PLK4 activity recruits STIL to a PLK4 focus and phosphorylates STIL at S1116 in the STAN motif to recruit SAS6 and initiate cartwheel assembly. Phosphorylation of STIL at S428 by PLK4 promotes CPAP binding and connects the growing cartwheel to the triplet microtubules of the centriole wall. In the absence of STIL S428 phosphorylation, STIL is able to recruit SAS6 and promote cartwheel assembly. However, STIL S428A fails to recruit CPAP and link the cartwheel to the microtubule wall, leading to a failure of *de novo* centriole assembly. In the absence of STIL S1116 phosphorylation, STIL is not effectively recruited to a PLK4 focus and cartwheel assembly fails. All error bars represent the standard error of the mean.

Chapter 4. Materials and Methods

Antibody production

A C-terminal hPlk4 fragment (a.a. 510-970) was cloned into a pET-23b bacterial expression vector (Novagen) containing a C-terminal 6xHis tag. Recombinant protein was purified from *E. coli* using Ni–NTA beads (QIAGEN) and used for immunization (ProSci). A STIL C-terminal peptide VGTFLDVKRLRQLPKLF (a.a. 1271-1287) was synthesized and conjugated to KLH for immunization. Rabbit immune sera were affinity-purified using standard procedures. Affinity-purified antibodies were directly conjugated to DyLight 550 and DyLight 650 fluorophores (Thermo Scientific) for use in immunofluorescence.

Human Centrin2 (a.a. 1-172) was cloned into a pET-23b bacterial expression vector (Novagen) containing an N-terminal 6xHis-SUMO1 tag. Recombinant protein was purified from *E. coli* using Ni–NTA beads (BioRad), cleaved from beads with SUMO protease and used for immunization in rabbits (ProSci). An N-terminal CEP192 fragment (a.a. 1-211) was cloned into a pGEX GST bacterial expression vector containing an N-terminal GST tag. Recombinant protein was purified from *E. coli* using glutathione sepharose beads (GoldBio), cleaved from beads with PreScission protease (GE) and used for immunization in goats. Rabbit and goat immune sera were affinity-purified using standard procedures. Affinity-purified antibodies were directly conjugated to Alexa Fluor488, DyLight 550, or DyLight 647 fluorophores (Thermo Scientific) for use in immunofluorescence.

A synthetic phospho-peptide based on the human hSTIL sequence flanking serine 1108 [CDRSTVGL(pS)LISPN], 1116 [CSPNNM(pS)FATKK] , or 428 [CSVPEL(pS)LVDG] was

synthesized, coupled to KLH and injected into rabbits (ProSci). Polyclonal pS1108, pS1116, and pS428 antibodies were affinity-purified using the appropriate phosphopeptide coupled to a SulfoLink Coupling Resin (Thermo Scientific). Additionally, a synthetic phospho-peptide based on the human PLK4 sequence flanking threonine 170 [HEKHY(pT)LCGTC] was synthesized, coupled to KLH and injected into rabbits (ProSci). Polyclonal pT170 antibodies were affinity-purified using the human PLK4 phosphopeptide coupled to a SulfoLink Coupling Resin (Thermo Scientific).

Cell culture and drug treatments

Cells were maintained at 37°C in a 5% CO_2 atmosphere with 21% oxygen. Cells were grown in Dulbecco's Modified Eagle Medium (DMEM) containing 10% fetal bovine serum (Sigma) or 10% FB Essence serum (VWR), 100 U/ml penicillin, 100 U/ml streptomycin and 2 mM L-glutamine. 293FT cells were used in co-transfection experiments, while Flp-In™ TRex™-DLD-1 cells (a kind gift from Stephen Taylor, the University of Manchester, UK) were used in all other experiments. Flp-In™ TRex™-DLD-1 cells were engineered using the Flp-In™ TRex™ Core Kit (Life Technologies) to stably express the Tetracycline repressor protein and contain a single, genomic FRT/*lac*Zeo site. 3MB-PP1 (Sigma) was dissolved in DMSO and used at a final concentration of 10 μM unless otherwise stated. Centrinone (a kind gift from Karen Oegema) was dissolved in DMSO and used at a final concentration of 500 nM.

Gene targeting

Gene targeting was performed in Flp-In^{TM} TRex^{TM}-DLD-1 cells using CRISPR/Cas9. Briefly, a gRNA targeting Plk4 (AGATAGCAATTATGTGTATC) was cloned into the PX459 expression vector that co-expresses the gRNA from a U6 promoter and *Sp*Cas9 from a CMV promoter. Cells were co-transfected with a 1:20 ratio of the PX459 plasmid and a 160 bp single-stranded oligonucleotide repair template. The repair template introduced the L89G mutation, a silent AflIII restriction site and a mutation in the *Sp*Cas9 protospacer adjacent motif (PAM) to prevent re-cutting after homology directed repair. Transfected cells were selected for two days with puromycin and single clones isolated by limiting dilution. Genomic DNA was isolated from single clones and subjected to PCR using the following primers (For: GCAGGAATGGTACAGAGAGTCC, Rev: GCAAAACTTTTATCCACCCAAA). PCR products were digested with AflIII for 2 hours. Clones with digested PCR products were sequenced to verify insertion of the L89G mutation. Two independent homozygous L89G clones were identified and behaved identically in all assays performed.

L89G donor oligonucleotide:

CTGAATTTTTGTATATTTTAATTTATTATGCCCTTTCACATTTCAGCTTTATAACTATT
TTGAAGATAGCAATTACGTGTATCTAGTAGGAGAAATGTGCCATAATGGAGAAATG
AACAGGTATCTAAAGAATAGAGTGAAACCCTTCTCAGAAAATGAAG

Drosophila S2 cell culture and transfection

Drosophila S2 cells (a kind gift from Ji Hoon Kim) were cultured at room temperature in vented T-25 flasks with Schnedier media (Gibco) containing 10% Fetal Bovine Serum (Sigma). $1.5x10^6$

cells were seeded in a 6-well plate in 2 mL media. The following day cells were transfected with the indicated constructs using Effectene (QIAGEN) according to the manufacturer's protocol. Cells were harvested 48 hours later and subjected to co-immunoprecipitation (procedure below).

Cloning

All DNA constructs were cloned into a pcDNA^{TM}5/FRT/TO vector backbone (Life Technologies) and expressed from a CMV promoter under the control of two Tetracycline operator sites. All constructs were full-length proteins unless otherwise noted. DNA constructs for Drosophila S2 transfection were cloned into a pAc^{TM} vector backbone (Invitrogen).

Generation of stable cell lines and siRNA treatment

Stable, isogenic cell lines expressing Myc-GFP-STIL from a CMV promoter under the control of two Tetracycline operator sites were generated according to the manufacturer's recommendation using the FRT/Flp-mediated recombination in Flp-In^{TM} TRex^{TM}-DLD-1 cells (Life Technologies Flp-In^{TM} TRex^{TM} Core Kit). Expression of Myc-GFP-STIL was induced with 1 μg/ml Tetracycline (Sigma), and expression of Myc-GFP-CPAP was induced with 2 ng/mL Tetracycline. Expression of Myc-STIL-T2A-GFP-CPAP constructs were induced with 1 μg/mL Tetracycline. For RNA interference, 2 x 10^5 cells were seeded in a 6-well plate and duplexed siRNAs introduced using RNAiMax (Life Technologies). siRNA directed against STIL (5'-GCUCCAAACAGUUUCUGCUGGAAU-3') and CPAP (5'-AGAAUUAGCUCGAAUAGAAUU-3') were purchased from Dharmacon and control siRNA (Universal Negative Control #1) was purchased from Sigma. Tetracycline was added to induce expression of RNAi-resistant Myc-GFP-STIL or Myc-STIL-T2A-GFP-CPAP. Expression of

Myc-GFP-CPAP transgene was induced concurrently with siRNA treatment. Cells were harvested and processed for immunoblotting or fixed for immunofluorescence 24 hours later.

De novo centriole formation assay

Acentriolar Flp-In^{TM} TRex^{TM}-DLD-1 cell lines were generated by culturing lines in centrinone at 500 nM for seven or more days. Cells were subjected to the siRNA protocol (above). 24 hours later, centrinone was washed out where noted by replacing media twice on cells for ten minutes each and then resuspending cells across multiple coverslips and adding Tetracycline at given concentrations depending on the cell line (concentrations above). Cells were fixed at 24, 48, and 72 hours post-washout as described below.

Cell biology

To prepare cells for flow cytometry, cell pellets were fixed in cold 70% EtOH for 24 hours, washed once in PBS and suspended in PBS supplemented with 0.5 mg/ml RNAse A and 50 mg/ml Propidium Iodide (PI). Samples were incubated at room temperature for 30 minutes and analyzed on a flow cytometer (FACSCalibur; Becton Dickinson). For metaphase spreads, cells were treated for up to 4 hours with 3.3 μM nocodazole, then incubated in 0.45% hypotonic buffer (32 mM KCl, 16 mM Hepes, 0.5 mM EDTA pH 7.4) at 37°C for 20 minutes. Cells were fixed in methanol:acetic acid (3:1) and stored at –20°C overnight. Fixed cells were dropped onto acetic-acid-coated slides and air-dried. Chromosomes were stained with Hoechst, mounted and imaged. For clonogenic assays 500 cells were seeded in a 10cm^2 culture dish and left to grow for ~ 2 weeks until colonies were visible by eye. Cells were fixed in methanol for 10 minutes at room temperature and colonies stained with crystal violet (Sigma).

Co-immunoprecipitation

2 x 10^6 293-FT cells were seeded into 10 cm^2 dishes and 24 hours later transfected with 2 µg of plasmid DNA. 48 hours later, transfected cells were lysed in lysis buffer [10 mM Tris pH 7.5, 0.1% Triton X-100, 300 mM NaCl, 1 mM EDTA, 50 mM NaF, 50 mM β-glycerophosphate, 1 mM DTT, 500 nM microcystin, 1 mM PMSF and EDTA-free protease inhibitor tablet (Roche)], sonicated and soluble extracts prepared. The supernatant was incubated with beads coupled to GFP-binding protein (Rothbauer et al. 2007). Alternatively, 2 µg of anti-mCherry antibody (rabbit, a kind gift from Joo Soek-Han) was added per sample and collected using Affi-Prep Protein A (Bio-Rad) (Figure 5G). Beads were washed 3 times in lysis buffer and immunopurified protein analyzed by immunoblot. For lambda phosphatase treatment, cells were lysed in lambda phosphatase buffer (New England BioLabs) and soluble lysates incubated with 2µL of Lambda Protein Phosphatase (New England BioLabs) for 60 minutes at 30°C.

Immunoblotting and immunofluorescence

For immunoblot analysis, protein samples were separated by SDS-PAGE, transferred onto nitrocellulose membranes with a Trans-Blot Turbo Transfer System (BioRad) and then probed with the following antibodies: DM1A (mouse anti-α-tubulin, Sigma, T6199, 1:5000), STIL (rabbit, Bethyl, A302-441A, 1:2500), FLAG M2 (mouse, Sigma, F1804, 1:1000), CPAP (rabbit, a kind gift from Karen Oegema, 1:1000), HA (rat, 3F10, Roche, 1:1000), Myc 4A6 (mouse, EMD Millipore 1:1000), SAS6 (mouse, Santa Cruz, sc-81431, 1:1000), Plk4 pT170 (rabbit, a kind gift from Mutsuhiro Takekawa, 1:1000) in Figure 5G (Nakamura, Saito, and Takekawa 2013), Plk4 pT170 (rabbit, this study, 1:1000) for all other figures, Plk4 (rabbit, this study,

1:3200), mCherry (rabbit, a kind gift from Joo Soek-Han, 1:1000), STIL pS1116 (rabbit, this study, 1:250), and STIL pS428 (rabbit, this study, 1:1000). Blots were blocked with 3% BSA in PBST and washed with PBST. Phospho-antibody blots were blocked in TBS Starting Block (Thermo) supplemented with 0.05% Tween 20 and washed in TBST. Antibodies were diluted in respective blocking buffers.

For immunofluorescence, cells were grown on 18-mm glass coverslips and fixed in 100% ice cold methanol for 10 min. Cells were blocked in 2.5% FBS, 200 mM glycine, 0.1% Triton X-100 in PBS for 1 h. Antibody incubations were conducted in the blocking solution for 1 h. DNA was detected using DAPI, and cells were mounted in Prolong Antifade (Invitrogen). Staining was performed with the following primary antibodies: GTU-88 (mouse anti-γ-tubulin, Abcam, 1:250), Centrin (mouse, Millipore, 04-1624, 1:1000), Centrin (rabbit, directly-conjugated, this study, 1:1000), CNAP (guinea pig, raised against the CNAP peptide sequence SPTQQDGRGQKNSDAKC, a kind gift from Olaf Stemmann, University of Bayreuth, Germany, 1:1000), CEP152 (rabbit, Bethyl, A302-479A, 1:5000), Plk4-650 (directly-labeled rabbit, this study, 1:1000), STIL-550 (directly-labeled rabbit, this study, 1:1000), STIL pS1108 (rabbit, this study, 1:250), CEP135 (rabbit, raised against CEP135 a.a. 695-838, a kind gift from Anthony Hyman, Max Planck Institute for Molecular Cell Biology and Genetics, Germany, 1:1000), CEP192-Cy3 (directly-labeled rabbit, raised against CEP192 a.a. 1-211, a kind gift from Karen Oegema, Ludwig Institute for Cancer Research, CA, 1:1000), SAS6 (mouse, sc-81-431 Santa Cruz, 1:1000), SAS6-Cy3 (directly-labeled rabbit, raised against SAS6 a.a. 501-657, a kind gift from Karen Oegema, Ludwig Institute for Cancer Research, CA,1:1000), CPAP-Cy3 (directly-labeled rabbit, a kind gift from Karen Oegema, Ludwig Institute for Cancer Research,

CA,1:1000) and, CEP192 (goat, directly-labeled, this study, 1:000), CENP-F (sheep, raised against CENP-F a.a. 1363-1640, a kind gift from Stephen Taylor, the University of Manchester, UK,1:1000). Secondary donkey antibodies were conjugated to Alexa Fluor® 488, 555 or 650 (Life Technologies).

For the cell cycle analysis of STIL levels shown in Figure 10C, cells were pulsed with EdU for 1 hour prior to fixation in 100% ice cold methanol at -20°C for 10 minutes. Cells were washed 3 x with 0.1% Triton X-100 in PBS and stained using a Click-It EdU Alexa Fluor 555 imaging kit (Life Technologies) according to the manufacturer's recommendations. Cells were blocked in 2.5% FBS, 200 mM glycine, 0.1% Triton X-100 in PBS for 1 hour and immunofluorescence microscopy performed using the following antibodies: CENP-F, GTU-88 and STIL-550. G1 phase cells were classified as CENP-F and EdU negative, S phase cells were classified as EdU positive and G2 phase cells were classified as CENP-F positive and EdU negative. The γ-tubulin staining was used to define the position of the centrosome.

Immunofluorescence images were collected using a Deltavision Elite system (GE Healthare) controlling a Scientific CMOS camera (pco.edge 5.5). Acquition parameters were controlled by SoftWoRx suite (GE Healthare). Images were collected at room temperature using an Olympus 60 x 1.42 NA or Olympus 100x 1.4 NA oil objective at 0.2 μM z-sections and subsequently deconvolved in SoftWoRx suite. Images were acquired using Applied Precision immersion oil (N=1.516). For quantitation of signal intensity at the centrosome, deconvolved 2D maximum intensity projections were saved as 16-bit TIFF images. Signal intensity was determined using ImageJ, by drawing a circular region of interest (ROI) around the centriole (ROI S). A larger

concentric circle (ROI L) was drawn around ROI S. ROI S and L were transferred to the channel of interest and the signal in ROI S was calculated using the following formula: IS – [(IL-IS/AL-AS) x AS]

A =Area, I=Integrated pixel intensity.

Fluorescence recovery after photobleaching

Cells were seeded into 4-chamber, 35mm glass bottom culture dishes (Greiner) and maintained in cell culture medium at 37°C and 5% CO_2 in an environmental control station. Images were collected using a Zeiss 40x 1.4 NA PlanApochromat oil-immersion objective on a Zeiss LSM 780 confocal equipped with a solid-state 488 nm laser and a spectral GaAsP detector. Images were acquired using Carl Zeiss immersion oil (N=1.518). Acquisition parameters, shutters, and focus were controlled by Zen black software (Zeiss). 10 X 0.5 μM z-sections were acquired for EGFP at each time point. Two consecutive pre-bleach scans were collected at 5% of the maximum ATOF value. Centrosome localized Myc-EGFP-STIL or EGFP-CPAP was bleached within a circular region encompassing the centrosome (~ 3 μM in diameter) at 100% laser power with 100 μsec dwell time. Post-bleach scans were performed at 20-second time intervals for a total period of 400 seconds. Maximum intensity projections were created using Zen black. The integrated intensity value within a circular region of interest in the cytosol of the cell was subtracted from an identically sized region of interest drawn around the bleached centrosome. Recovery values were plotted relative to the difference between the fluorescence pre- and post-bleach.

Recombinant protein expression and purification

GFP-binding protein (GBP), recombinant His-hPlk4 (a.a. 1-416), and GST-Flag-CPAP TCP domain (aa 1142-1338) were expressed and purified from *E.coli* [strain Rosetta (DE3)] using standard procedures. Recombinant GST-hPlk4, GST-hSAS6, GST-hSTIL and GST-hSTIL C-term (a.a. 898-1287) were expressed and purified from High Five insect cells (Invitrogen) using the Bac-to-Bac expression system (Invitrogen). Infected cell pellets were suspended in lysis buffer (10 mM $PO4^{3-}$ pH 7.4, 137 mM NaCl, 2.7 mM KCl, 10% glycerol, 2 mM $MgCl_2$, 5 mM DTT, 100 nM Microcystin, 1 mM Na_3V0_4, 250 U of Benzonaze nuclease (Sigma), 1 mM PMSF and EDTA-free protease inhibitor tablet (Roche)) and lysed by sonication. After centrifugation at 15,000 rpm for 30 min, the supernatant was supplemented with 110 mM KCL and 0.1% Triton X-100 and incubated with Glutathione Sepharose beads (GE Healthcare) for 4 h at 4°C. Beads were washed extensively in wash buffer [10 mM $PO4^{3-}$ pH 7.4, 137 mM NaCl, 2.7 mM KCl, 10% glycerol, 5 mM DTT, 0.1% Trition X-100, 100 mM KCL, 1 mM PMSF and EDTA-free protease inhibitor tablet (Roche)] and protein eluted in elution buffer (10 mM $PO4^{3-}$ pH 7.4, 137 mM NaCl, 2.7 mM KCl, 10% glycerol, with 40 mM reduced glutathione and 5 mM DTT). Protein was dialyzed into a final buffer of 10 mM $PO4^{3-}$ pH 7.4, 137 mM NaCl, 2.7 mM KCl, 10% glycerol. When necessary, the GST tag was removed by overnight incubation with GST-PreScission protease (GE Healthcare).

In vitro kinase assay

Assays were conducted for 30 minutes at 30°C in 20 mM Tris pH 7.5, 25 mM KCl, 1 mM DTT, and in the presence of 10 mM $MgCl_2$ and 100 µM ATP. 2 µg of substrate was incubated with 1 µg of of His-hPlk4 (a.a. 1-416). Kinase reactions were stopped with sample buffer and analyzed by SDS-PAGE and western blotting.

In vitro binding assay

For STIL-SAS6 binding, recombinant GST-hSTIL or GST-hSTIL C-term (a.a. 898-1287) was incubated with kinase active or kinase dead His-hPlk4 (a.a. 1-416) in kinase buffer with or without cold ATP as above. Reactions were then supplemented with 500 µl of binding buffer (50 mM Na-HEPES pH 7.5, 100 mM NaCl, 2 mM $MgCl_2$, 1 mM EGTA, 1 mM DTT, 0.1 % Triton-X 100, 100 nM Microcystin (Calbiochem) and 0.5 mg/ml BSA) and incubated at 4°C for 1 hour. Glutathione Sepharose beads (GE Healthcare) was incubated with the protein for a further 1 hour at 4°C. Beads were washed three times in binding buffer without BSA and proteins eluted in SDS sample buffer.

For STIL-CPAP binding, Recombinant GST-hSTIL was bound to GSH resin (GoldBio) for four hours at 4°C in PBS, 10% glycerol, and 1 mM DTT. Beads were washed twice in kinase buffer (see above) supplemented with 10% glycerol and incubated with 6xHis-hPlk4 (a.a. 1-416) in kinase buffer with or without 10 µM cold ATP at 33°C for two hours. Reactions were then spun down and washed twice with cold binding buffer (50 mM Na-HEPES pH 7.5, 400 mM NaCl, 2 mM $MgCl_2$, 1 mM EGTA, 1 mM DTT, 0.15 % Triton-X 100, 100 nM Microcystin (Calbiochem) and 0.5 mg/ml BSA) and spun in binding buffer at 4°C for 2 hours in the presence of recombinant Flag-CPAP TCP domain. Beads were washed three times in binding buffer without BSA, and then proteins were eluted in SDS sample buffer and immunoblotted.

Mass spectrometry

In-solution protein digestion was carried out using "Filter Assisted Sample Preparation" (FASP) method . Data dependent MS/MS analysis of peptides was carried out on the LTQ-Orbitrap Velos (www.thermoscientific.com) interfaced with Eksigent 2D nanoflow liquid chromatography system (www.eksigent.com system). Peptides were enriched on a 2 cm trap column (YMC gel ODS-A S-10µm), fractionated on a 75 µm x 15 cm column packed with 5µm, 100Å Magic AQ C18 material (Michrom Bioresources), and electrosprayed through a 15 µm emitter (PF3360-75-15-N-5, New Objective). Reversed-phase solvent gradient consisted of 0.1% formic acid with increasing levels of 0.1% formic acid, 90% acetonitrile over a period of 90 minutes. LTQ orbitrap Velos was set at 2.0 kV spray voltage, full MS survey scan range was set at 350-1800 m/z, data dependent HCD MS/MS analysis set for top 8 precursors with minimum signal of 2,000. Other parameters include peptide isolation width of m/z 1.9; dynamic exclusion limit 30s and normalized collision energy 35; precursor and the fragment ions resolutions were 30,000 and 15,000, respectively. Internal mass calibration was applied using lock mass ion m/z = 371.101230.

Mass spectrometry raw files were automatically processed through Proteome Discoverer 1.4 software. Raw MS and MS/MS data was isotopically resolved with deconvolution and deisotoping using Thermo Scientific Xtract and MS2-processor software in addition to default spectrum selector node. The data was searched in Refseq human entries using Mascot (v2.2.6, Matrix Sciences) search engine interfaced with different processing nodes of Proteome Discoverer 1.4. Mass tolerances on precursor and fragment masses were set to 15 ppm and 0.03 Da, respectively. Peptide validator node was used for identification confidence and 1% false

discovery rate cutoff was used to filter the peptides. Phosphorylation site probability was analyzed using phosphoRS 3.0 node in Proteome discoverer software (Taus et al. 2011).

References

Andersen, Jens S, Christopher J Wilkinson, Thibault Mayor, Peter Mortensen, Erich A Nigg, and Matthias Mann. 2003. "Proteomic Characterization of the Human Centrosome by Protein Correlation Profiling." *Nature*. https://doi.org/10.1038/nature02166.

Arquint, C., K. F. Sonnen, Y.-D. Stierhof, and E. A. Nigg. 2012. "Cell-Cycle-Regulated Expression of STIL Controls Centriole Number in Human Cells." *Journal of Cell Science*. https://doi.org/10.1242/jcs.099887.

Arquint, Christian, and Erich A. Nigg. 2014. "STIL Microcephaly Mutations Interfere with APC/C-Mediated Degradation and Cause Centriole Amplification." *Current Biology*. https://doi.org/10.1016/j.cub.2013.12.016.

Bahtz, R., J. Seidler, M. Arnold, U. Haselmann-Weiss, C. Antony, W. D. Lehmann, and I. Hoffmann. 2012. "GCP6 Is a Substrate of Plk4 and Required for Centriole Duplication." *Journal of Cell Science*. https://doi.org/10.1242/jcs.093930.

Basto, Renata, Kathrin Brunk, Tatiana Vinadogrova, Nina Peel, Anna Franz, Alexey Khodjakov, and Jordan W. Raff. 2008. "Centrosome Amplification Can Initiate Tumorigenesis in Flies." *Cell*. https://doi.org/10.1016/j.cell.2008.05.039.

Bazzi, H., and K. V. Anderson. 2014. "Acentriolar Mitosis Activates a P53-Dependent Apoptosis Pathway in the Mouse Embryo." *Proceedings of the National Academy of Sciences*. https://doi.org/10.1073/pnas.1400568111.

Bettencourt-Dias, M., A. Rodrigues-Martins, L. Carpenter, M. Riparbelli, L. Lehmann, M. K. Gatt, N. Carmo, F. Balloux, G. Callaini, and D. M. Glover. 2005. "SAK/PLK4 Is Required for Centriole Duplication and Flagella Development." *Current Biology*. https://doi.org/10.1016/j.cub.2005.11.042.

Bond, Jacquelyn, Emma Roberts, Kelly Springell, Sophia Lizarraga, Sheila Scott, Julie Higgins, Daniel J. Hampshire, et al. 2005. "A Centrosomal Mechanism Involving CDK5RAP2 and CENPJ Controls Brain Size." *Nature Genetics*. https://doi.org/10.1038/ng1539.

Breslow, David K., and Andrew J. Holland. 2019. "Mechanism and Regulation of Centriole and Cilium Biogenesis." *Annual Review of Biochemistry*. https://doi.org/10.1146/annurev-biochem-013118-111153.

Breugel, Mark Van, Masafumi Hirono, Antonina Andreeva, Haru Aki Yanagisawa, Shoko Yamaguchi, Yuki Nakazawa, Nina Morgner, et al. 2011. "Structures of SAS-6 Suggest Its Organization in Centrioles." *Science*. https://doi.org/10.1126/science.1199325.

Breugel, Mark van, Rainer Wilcken, Stephen H McLaughlin, Trevor J Rutherford, and Christopher M Johnson. 2014. "Structure of the SAS-6 Cartwheel Hub from Leishmania Major." *ELife*. https://doi.org/10.7554/elife.01812.

Castellanos, Elisabeth, Paloma Dominguez, and Cayetano Gonzalez. 2008. "Centrosome Dysfunction in Drosophila Neural Stem Cells Causes Tumors That Are Not Due to Genome Instability." *Current Biology*. https://doi.org/10.1016/j.cub.2008.07.029.

Chan, Jason Yongsheng. 2011. "A Clinical Overview of Centrosome Amplification in Human Cancers." *International Journal of Biological Sciences*.

Chen, Hsin Yi, Chien Ting Wu, Chieh Ju C. Tang, Yi Nan Lin, Won Jing Wang, and Tang K. Tang. 2017. "Human Microcephaly Protein RTTN Interacts with STIL and Is Required to Build Full-Length Centrioles." *Nature Communications*. https://doi.org/10.1038/s41467-

017-00305-0.
Chou, En Ju, Liang Yi Hung, Chieh Ju C. Tang, Wen Bin Hsu, Hsin Yi Wu, Pao Chi Liao, and Tang K. Tang. 2016. “Phosphorylation of CPAP by Aurora-A Maintains Spindle Pole Integrity during Mitosis.” *Cell Reports*. https://doi.org/10.1016/j.celrep.2016.02.085.
Cizmecioglu, Onur, Marc Arnold, Ramona Bahtz, Florian Settele, Lena Ehret, Uta Haselmann-Weiß, Claude Antony, and Ingrid Hoffmann. 2010. “Cep152 Acts as a Scaffold for Recruitment of Plk4 and CPAP to the Centrosome.” *Journal of Cell Biology*. https://doi.org/10.1083/jcb.201007107.
Coelho, Paula A., Leah Bury, Marta N. Shahbazi, Kifayathullah Liakath-Ali, Peri H. Tate, Sam Wormald, Christopher J. Hindley, et al. 2015. “Over-Expression of Plk4 Induces Centrosome Amplification, Loss of Primary Cilia and Associated Tissue Hyperplasia in the Mouse.” *Open Biology*. https://doi.org/10.1098/rsob.150209.
Cottee, Matthew A., Nadine Muschalik, Steven Johnson, Joanna Leveson, Jordan W. Raff, and Susan M. Lea. 2015. “The Homo-Oligomerisation of Both Sas-6 and Ana2 Is Required for Efficient Centriole Assembly in Flies.” *ELife*. https://doi.org/10.7554/eLife.07236.
Cottee, Matthew A, Nadine Muschalik, Yao Liang Wong, Christopher M Johnson, Steven Johnson, Antonina Andreeva, Karen Oegema, Susan M Lea, Jordan W Raff, and Mark van Breugel. 2013. “Crystal Structures of the CPAP/STIL Complex Reveal Its Role in Centriole Assembly and Human Microcephaly.” *ELife*. https://doi.org/10.7554/elife.01071.
Cristofoli, Francesca, Bart De Keersmaecker, Luc De Catte, Joris R. Vermeesch, and Hilde Van Esch. 2017. “Novel STIL Compound Heterozygous Mutations Cause Severe Fetal Microcephaly and Centriolar Lengthening.” *Molecular Syndromology*. https://doi.org/10.1159/000479666.
Cunha-Ferreira, Inês, Inês Bento, Ana Pimenta-Marques, Swadhin Chandra Jana, Mariana Lince-Faria, Paulo Duarte, Joana Borrego-Pinto, et al. 2013. “Regulation of Autophosphorylation Controls PLK4 Self-Destruction and Centriole Number.” *Current Biology*. https://doi.org/10.1016/j.cub.2013.09.037.
Cunha-Ferreira, Inês, Ana Rodrigues-Martins, Inês Bento, Maria Riparbelli, Wei Zhang, Ernest Laue, Giuliano Callaini, David M. Glover, and Mónica Bettencourt-Dias. 2009. “The SCF/Slimb Ubiquitin Ligase Limits Centrosome Amplification through Degradation of SAK/PLK4.” *Current Biology*. https://doi.org/10.1016/j.cub.2008.11.037.
Dammermann, Alexander, Thomas Müller-Reichert, Laurence Pelletier, Bianca Habermann, Arshad Desai, and Karen Oegema. 2004. “Centriole Assembly Requires Both Centriolar and Pericentriolar Material Proteins.” *Developmental Cell*. https://doi.org/10.1016/j.devcel.2004.10.015.
Debec, Alain, William Sullivan, and Monica Bettencourt-Dias. 2010. “Centrioles: Active Players or Passengers during Mitosis?” *Cellular and Molecular Life Sciences*. https://doi.org/10.1007/s00018-010-0323-9.
Delattre, Marie, Sebastian Leidel, Khursheed Wani, Karine Baumer, Jeannine Bamat, Heinke Schnabel, Richard Feichtinger, Ralf Schnabel, and Pierre Gönczy. 2004. “Centriolar SAS-5 Is Required for Centrosome Duplication in C. Elegans.” *Nature Cell Biology*. https://doi.org/10.1038/ncb1146.
Dzhindzhev, Nikola S., George Tzolovsky, Zoltan Lipinszki, Mohammed Abdelaziz, Janus Debski, Michal Dadlez, and David M. Glover. 2017. “Two-Step Phosphorylation of Ana2 by Plk4 Is Required for the Sequential Loading of Ana2 and Sas6 to Initiate Procentriole Formation.” *Open Biology*. https://doi.org/10.1098/rsob.170247.

Dzhindzhev, Nikola S., George Tzolovsky, Zoltan Lipinszki, Sandra Schneider, Ramona Lattao, Jingyan Fu, Janusz Debski, Michal Dadlez, and David M. Glover. 2014. "Plk4 Phosphorylates Ana2 to Trigger SAS6 Recruitment and Procentriole Formation." *Current Biology*. https://doi.org/10.1016/j.cub.2014.08.061.

Dzhindzhev, Nikola S., Quan D. Yu, Kipp Weiskopf, George Tzolovsky, Ines Cunha-Ferreira, Maria Riparbelli, Ana Rodrigues-Martins, Monica Bettencourt-Dias, Giuliano Callaini, and David M. Glover. 2010. "Asterless Is a Scaffold for the Onset of Centriole Assembly." *Nature*. https://doi.org/10.1038/nature09445.

Firat-Karalar, Elif Nur, Navin Rauniyar, John R. Yates, and Tim Stearns. 2014. "Proximity Interactions among Centrosome Components Identify Regulators of Centriole Duplication." *Current Biology*. https://doi.org/10.1016/j.cub.2014.01.067.

Fong, Chii Shyang, Minhee Kim, T. Tony Yang, Jung Chi Liao, and Meng Fu Bryan Tsou. 2014. "SAS-6 Assembly Templated by the Lumen of Cartwheel-Less Centrioles Precedes Centriole Duplication." *Developmental Cell*. https://doi.org/10.1016/j.devcel.2014.05.008.

Galletta, Brian J., Carey J. Fagerstrom, Todd A. Schoborg, Tiffany A. McLamarrah, John M. Ryniawec, Daniel W. Buster, Kevin C. Slep, Gregory C. Rogers, and Nasser M. Rusan. 2016. "A Centrosome Interactome Provides Insight into Organelle Assembly and Reveals a Non-Duplication Role for Plk4." *Nature Communications*. https://doi.org/10.1038/ncomms12476.

Ganem, Neil J., Susana A. Godinho, and David Pellman. 2009. "A Mechanism Linking Extra Centrosomes to Chromosomal Instability." *Nature*. https://doi.org/10.1038/nature08136.

Gartenmann, Lisa, Alan Wainman, Maryam Qurashi, Rainer Kaufmann, Sebastian Schubert, Jordan W. Raff, and Ian M. Dobbie. 2017. "A Combined 3D-SIM/SMLM Approach Allows Centriole Proteins to Be Localized with a Precision of ~4–5 Nm." *Current Biology*. https://doi.org/10.1016/j.cub.2017.08.009.

Gergely, Fanni. 2014. "Small Organelle, Big Responsibility: The Role of Centrosomes in Development and Disease." *Philosophical Transactions of the Royal Society of London. Series B, Biological Sciences*. https://doi.org/10.1098/rstb.2013.0468.

Godinho, Susana A., Remigio Picone, Mithila Burute, Regina Dagher, Ying Su, Cheuk T. Leung, Kornelia Polyak, Joan S. Brugge, Manuel Théry, and David Pellman. 2014. "Oncogene-like Induction of Cellular Invasion from Centrosome Amplification." *Nature*. https://doi.org/10.1038/nature13277.

Gönczy, Pierre. 2012. "Towards a Molecular Architecture of Centriole Assembly." *Nature Reviews Molecular Cell Biology*. https://doi.org/10.1038/nrm3373.

Gopalakrishnan, Jayachandran, Vito Mennella, Stephanie Blachon, Bo Zhai, Andrew H. Smith, Timothy L. Megraw, Daniela Nicastro, Steven P. Gygi, David A. Agard, and Tomer Avidor-Reiss. 2011. "Sas-4 Provides a Scaffold for Cytoplasmic Complexes and Tethers Them in a Centrosome." *Nature Communications*. https://doi.org/10.1038/ncomms1367.

Goryachev, Andrew B., and Marcin Leda. 2017. "Many Roads to Symmetry Breaking: Molecular Mechanisms and Theoretical Models of Yeast Cell Polarity." *Molecular Biology of the Cell*. https://doi.org/10.1091/mbc.e16-10-0739.

Guderian, G., J. Westendorf, A. Uldschmid, and E. A. Nigg. 2010. "Plk4 Trans-Autophosphorylation Regulates Centriole Number by Controlling TrCP-Mediated Degradation." *Journal of Cell Science*. https://doi.org/10.1242/jcs.068502.

Gudi, Radhika, Courtney J. Haycraft, P. Darwin Bell, Zihai Li, and Chenthamarakshan Vasu. 2015. "Centrobin-Mediated Regulation of the Centrosomal Protein 4.1-Associated Protein

(CPAP) Level Limits Centriole Length during Elongation Stage." *Journal of Biological Chemistry*. https://doi.org/10.1074/jbc.M114.603423.

Guichard, P., V. Hamel, M. Le Guennec, N. Banterle, I. Iacovache, V. Nemcíková, I. Flückiger, et al. 2017. "Cell-Free Reconstitution Reveals Centriole Cartwheel Assembly Mechanisms." *Nature Communications*. https://doi.org/10.1038/ncomms14813.

Gupta, Gagan D., Étienne Coyaud, João Gonçalves, Bahareh A. Mojarad, Yi Liu, Qianzhu Wu, Ladan Gheiratmand, et al. 2015. "A Dynamic Protein Interaction Landscape of the Human Centrosome-Cilium Interface." *Cell*. https://doi.org/10.1016/j.cell.2015.10.065.

Habedanck, Robert, York Dieter Stierhof, Christopher J. Wilkinson, and Erich A. Nigg. 2005. "The Polo Kinase Plk4 Functions in Centriole Duplication." *Nature Cell Biology*. https://doi.org/10.1038/ncb1320.

Hatch, Emily M., Anita Kulukian, Andrew J. Holland, Don W. Cleveland, and Tim Stearns. 2010. "Cep152 Interacts with Plk4 and Is Required for Centriole Duplication." *Journal of Cell Biology*. https://doi.org/10.1083/jcb.201006049.

Hatzopoulos, Georgios N., Michèle C. Erat, Erin Cutts, Kacper B. Rogala, Leanne M. Slater, Philip J. Stansfeld, and Ioannis Vakonakis. 2013. "Structural Analysis of the G-Box Domain of the Microcephaly Protein CPAP Suggests a Role in Centriole Architecture." *Structure*. https://doi.org/10.1016/j.str.2013.08.019.

Hoffert, J. D., T. Pisitkun, G. Wang, R.-F. Shen, and M. A. Knepper. 2006. "Quantitative Phosphoproteomics of Vasopressin-Sensitive Renal Cells: Regulation of Aquaporin-2 Phosphorylation at Two Sites." *Proceedings of the National Academy of Sciences*. https://doi.org/10.1073/pnas.0600895103.

Holland, Andrew J., and Don W. Cleveland. 2014. "Polo-like Kinase 4 Inhibition: A Strategy for Cancer Therapy?" *Cancer Cell*. https://doi.org/10.1016/j.ccr.2014.07.017.

Holland, Andrew J., Daniele Fachinetti, Quan Zhu, Manuel Bauer, Inder M. Verma, Erich A. Nigg, and Don W. Cleveland. 2012. "The Autoregulated Instability of Polo-like Kinase 4 Limits Centrosome Duplication to Once per Cell Cycle." *Genes and Development*. https://doi.org/10.1101/gad.207027.112.

Holland, Andrew J., Weijie Lan, Sherry Niessen, Heather Hoover, and Don W. Cleveland. 2010. "Polo-like Kinase 4 Kinase Activity Limits Centrosome Overduplication by Autoregulating Its Own Stability." *Journal of Cell Biology*. https://doi.org/10.1083/jcb.200911102.

Hudson, J. W., A. Kozarova, P. Cheung, J. C. Macmillan, C. J. Swallow, J. C. Cross, and J. W. Dennis. 2001. "Late Mitotic Failure in Mice Lacking Sak, a Polo-like Kinase." *Current Biology*. https://doi.org/10.1016/S0960-9822(01)00117-8.

Hung, L.-Y. 2004. "Identification of a Novel Microtubule-Destabilizing Motif in CPAP That Binds to Tubulin Heterodimers and Inhibits Microtubule Assembly." *Molecular Biology of the Cell*. https://doi.org/10.1091/mbc.e04-02-0121.

Hussein, D, and S S Taylor. 2002. "Farnesylation of Cenp-F Is Required for G2/M Progression and Degradation after Mitosis." *J Cell Sci*.

Huttlin, Edward L., Mark P. Jedrychowski, Joshua E. Elias, Tapasree Goswami, Ramin Rad, Sean A. Beausoleil, Judit Villén, Wilhelm Haas, Mathew E. Sowa, and Steven P. Gygi. 2010. "A Tissue-Specific Atlas of Mouse Protein Phosphorylation and Expression." *Cell*. https://doi.org/10.1016/j.cell.2010.12.001.

Izquierdo, Denisse, Won Jing Wang, Kunihiro Uryu, and Meng Fu Bryan Tsou. 2014. "Stabilization of Cartwheel-Less Centrioles for Duplication Requires CEP295-Mediated Centriole-to-Centrosome Conversion." *Cell Reports*.

https://doi.org/10.1016/j.celrep.2014.07.022.
Jakobsen, Lis, Katja Vanselow, Marie Skogs, Yusuke Toyoda, Emma Lundberg, Ina Poser, Lasse G. Falkenby, et al. 2011. "Novel Asymmetrically Localizing Components of Human Centrosomes Identified by Complementary Proteomics Methods." *EMBO Journal*. https://doi.org/10.1038/emboj.2011.63.
Johnson, Eric F., Kent D. Stewart, Keith W. Woods, Vincent L. Giranda, and Yan Luo. 2007. "Pharmacological and Functional Comparison of the Polo-like Kinase Family: Insight into Inhibitor and Substrate Specificity." *Biochemistry*. https://doi.org/10.1021/bi7008745.
Kemp, Catherine A., Kevin R. Kopish, Peder Zipperlen, Julie Ahringer, and Kevin F. O'Connell. 2004. "Centrosome Maturation and Duplication in C. Elegans Require the Coiled-Coil Protein SPD-2." *Developmental Cell*. https://doi.org/10.1016/S1534-5807(04)00066-8.
Kettenbach, Arminja N., Tuobin Wang, Brendan K. Faherty, Dean R. Madden, Stefan Knapp, Chris Bailey-Kellogg, and Scott A. Gerber. 2012. "Rapid Determination of Multiple Linear Kinase Substrate Motifs by Mass Spectrometry." *Chemistry and Biology*. https://doi.org/10.1016/j.chembiol.2012.04.011.
Khodjakov, Alexey, and Conly L. Rieder. 2001. "Centrosomes Enhance the Fidelity of Cytokinesis in Vertebrates and Are Required for Cell Cycle Progression." *Journal of Cell Biology*. https://doi.org/10.1083/jcb.153.1.237.
Kim, Minhee, Brian P. O'Rourke, Rajesh Kumar Soni, Prasad V. Jallepalli, Ronald C. Hendrickson, and Meng Fu Bryan Tsou. 2016. "Promotion and Suppression of Centriole Duplication Are Catalytically Coupled through PLK4 to Ensure Centriole Homeostasis." *Cell Reports*. https://doi.org/10.1016/j.celrep.2016.06.069.
Kim, T.-S., J.-E. Park, A. Shukla, S. Choi, R. N. Murugan, J. H. Lee, M. Ahn, et al. 2013. "Hierarchical Recruitment of Plk4 and Regulation of Centriole Biogenesis by Two Centrosomal Scaffolds, Cep192 and Cep152." *Proceedings of the National Academy of Sciences*. https://doi.org/10.1073/pnas.1319656110.
Kirkham, Matthew, Thomas Müller-Reichert, Karen Oegema, Stephan Grill, and Anthony A. Hyman. 2003. "SAS-4 Is a C. Elegans Centriolar Protein That Controls Centrosome Size." *Cell*. https://doi.org/10.1016/S0092-8674(03)00117-X.
Kitagawa, D., G. Kohlmaier, D. Keller, P. Strnad, F. R. Balestra, I. Fluckiger, and P. Gonczy. 2011. "Spindle Positioning in Human Cells Relies on Proper Centriole Formation and on the Microcephaly Proteins CPAP and STIL." *Journal of Cell Science*. https://doi.org/10.1242/jcs.089888.
Kitagawa, Daiju, Ioannis Vakonakis, Natacha Olieric, Manuel Hilbert, Debora Keller, Vincent Olieric, Miriam Bortfeld, et al. 2011. "Structural Basis of the 9-Fold Symmetry of Centrioles." *Cell*. https://doi.org/10.1016/j.cell.2011.01.008.
Klebba, Joseph E., Daniel W. Buster, Annie L. Nguyen, Stephen Swatkoski, Marjan Gucek, Nasser M. Rusan, and Gregory C. Rogers. 2013. "Polo-like Kinase 4 Autodestructs by Generating Its Slimb-Binding Phosphodegron." *Current Biology*. https://doi.org/10.1016/j.cub.2013.09.019.
Kleylein-Sohn, Julia, Jens Westendorf, Mikael Le Clech, Robert Habedanck, York Dieter Stierhof, and Erich A. Nigg. 2007. "Plk4-Induced Centriole Biogenesis in Human Cells." *Developmental Cell*. https://doi.org/10.1016/j.devcel.2007.07.002.
Kohlmaier, Gregor, Jadranka Lončarek, Xing Meng, Bruce F. McEwen, Mette M. Mogensen, Alexander Spektor, Brian D. Dynlacht, Alexey Khodjakov, and Pierre Gönczy. 2009. "Overly Long Centrioles and Defective Cell Division upon Excess of the SAS-4-Related

Protein CPAP." *Current Biology*. https://doi.org/10.1016/j.cub.2009.05.018.
Kratz, A.-S., F. Barenz, K. T. Richter, and I. Hoffmann. 2015. "Plk4-Dependent Phosphorylation of STIL Is Required for Centriole Duplication." *Biology Open*. https://doi.org/10.1242/bio.201411023.
Laufer, Radoslaw, Bryan Forrest, Sze Wan Li, Yong Liu, Peter Sampson, Louise Edwards, Yunhui Lang, et al. 2013. "The Discovery of PLK4 Inhibitors: (E)-3-((1H-Indazol-6-Yl)Methylene) Indolin-2-Ones as Novel Antiproliferative Agents." *Journal of Medicinal Chemistry*. https://doi.org/10.1021/jm400380m.
Leda, Marcin, Andrew J. Holland, and Andrew B. Goryachev. 2018. "Autoamplification and Competition Drive Symmetry Breaking: Initiation of Centriole Duplication by the PLK4-STIL Network." *IScience*. https://doi.org/10.1016/j.isci.2018.10.003.
Leidel, Sebastian, Marie Delattre, Lorenzo Cerutti, Karine Baumer, and Pierre Gönczy. 2005. "SAS-6 Defines a Protein Family Required for Centrosome Duplication in C. Elegans and in Human Cells." *Nature Cell Biology*. https://doi.org/10.1038/ncb1220.
Leidel, Sebastian, and Pierre Gönczy. 2003. "SAS-4 Is Essential for Centrosome Duplication in C. Elegans and Is Recruited to Daughter Centrioles Once per Cell Cycle." *Developmental Cell*. https://doi.org/10.1016/S1534-5807(03)00062-5.
Lettman, Molly M., Yao Liang Wong, Valeria Viscardi, Sherry Niessen, Sheng hong Chen, Andrew K. Shiau, Huilin Zhou, Arshad Desai, and Karen Oegema. 2013. "Direct Binding of SAS-6 to ZYG-1 Recruits SAS-6 to the Mother Centriole for Cartwheel Assembly." *Developmental Cell*. https://doi.org/10.1016/j.devcel.2013.03.011.
Levine, Michelle S., Bjorn Bakker, Bram Boeckx, Julia Moyett, James Lu, Benjamin Vitre, Diana C. Spierings, et al. 2017. "Centrosome Amplification Is Sufficient to Promote Spontaneous Tumorigenesis in Mammals." *Developmental Cell*. https://doi.org/10.1016/j.devcel.2016.12.022.
Levine, Michelle S., and Andrew J. Holland. 2018. "The Impact of Mitotic Errors on Cell Proliferation and Tumorigenesis." *Genes and Development*. https://doi.org/10.1101/gad.314351.118.
Lin, Yi Nan, Chien Ting Wu, Yu Chih Lin, Wen Bin Hsu, Chieh Ju C. Tang, Ching Wen Chang, and Tang K. Tang. 2013. "CEP120 Interacts with CPAP and Positively Regulates Centriole Elongation." *Journal of Cell Biology*. https://doi.org/10.1083/jcb.201212060.
Lin, Yu Chih, Ching Wen Chang, Wen Bin Hsu, Chieh Ju C. Tang, Yi Nan Lin, En Ju Chou, Chien Ting Wu, and Tang K. Tang. 2013. "Human Microcephaly Protein CEP135 Binds to HSAS-6 and CPAP, and Is Required for Centriole Assembly." *EMBO Journal*. https://doi.org/10.1038/emboj.2013.56.
Liu, Yi, Gagan D. Gupta, Deepak D. Barnabas, Fikret G. Agircan, Shahid Mehmood, Di Wu, Etienne Coyaud, et al. 2018. "Direct Binding of CEP85 to STIL Ensures Robust PLK4 Activation and Efficient Centriole Assembly." *Nature Communications*. https://doi.org/10.1038/s41467-018-04122-x.
Lopes, Carla A.M., Swadhin Chandra Jana, Inês Cunha-Ferreira, Sihem Zitouni, Inês Bento, Paulo Duarte, Samuel Gilberto, et al. 2015. "PLK4 Trans-Autoactivation Controls Centriole Biogenesis in Space." *Developmental Cell*. https://doi.org/10.1016/j.devcel.2015.09.020.
McLamarrah, Tiffany A., Daniel W. Buster, Brian J. Galletta, Cody J. Boese, John M. Ryniawec, Natalie Ann Hollingsworth, Amy E. Byrnes, et al. 2018. "An Ordered Pattern of Ana2 Phosphorylation by Plk4 Is Required for Centriole Assembly." *Journal of Cell Biology*. https://doi.org/10.1083/jcb.201605106.

Moyer, Tyler C., Kevin M. Clutario, Bramwell G. Lambrus, Vikas Daggubati, and Andrew J. Holland. 2015. "Binding of STIL to Plk4 Activates Kinase Activity to Promote Centriole Assembly." *Journal of Cell Biology* 209 (6): 863–78. https://doi.org/10.1083/jcb.201502088.

Nakamura, Takanori, Haruo Saito, and Mutsuhiro Takekawa. 2013. "SAPK Pathways and P53 Cooperatively Regulate PLK4 Activity and Centrosome Integrity under Stress." *Nature Communications*. https://doi.org/10.1038/ncomms2752.

Nigg, Erich A., and Andrew J. Holland. 2018. "Once and Only Once: Mechanisms of Centriole Duplication and Their Deregulation in Diseases." *Nature Reviews Molecular Cell Biology*. https://doi.org/10.1038/nrm.2017.127.

Nigg, Erich A., and Jordan W. Raff. 2009. "Centrioles, Centrosomes, and Cilia in Health and Disease." *Cell*. https://doi.org/10.1016/j.cell.2009.10.036.

Novak, Zsofia A A., Alan Wainman, Lisa Gartenmann, and Jordan W W. Raff. 2016. "Cdk1 Phosphorylates Drosophila Sas-4 to Recruit Polo to Daughter Centrioles and Convert Them to Centrosomes." *Developmental Cell*. https://doi.org/10.1016/j.devcel.2016.05.022.

O'Connell, Kevin F., Cathy Caron, Kevin R. Kopish, Daryl D. Hurd, Kenneth J. Kemphues, Yongjing Li, and John G. White. 2001. "The C. Elegans Zyg-1 Gene Encodes a Regulator of Centrosome Duplication with Distinct Maternal and Paternal Roles in the Embryo." *Cell*. https://doi.org/10.1016/S0092-8674(01)00338-5.

Ohta, Midori, Tomoko Ashikawa, Yuka Nozaki, Hiroko Kozuka-Hata, Hidemasa Goto, Masaki Inagaki, Masaaki Oyama, and Daiju Kitagawa. 2014. "Direct Interaction of Plk4 with STIL Ensures Formation of a Single Procentriole per Parental Centriole." *Nature Communications*. https://doi.org/10.1038/ncomms6267.

Park, Suk Youl, Jung Eun Park, Tae Sung Kim, Ju Hee Kim, Mi Jeong Kwak, Bonsu Ku, Lan Tian, et al. 2014. "Molecular Basis for Unidirectional Scaffold Switching of Human Plk4 in Centriole Biogenesis." *Nature Structural and Molecular Biology*. https://doi.org/10.1038/nsmb.2846.

Peel, N., M. Dougherty, J. Goeres, Y. Liu, and K. F. O'Connell. 2012. "The C. Elegans F-Box Proteins LIN-23 and SEL-10 Antagonize Centrosome Duplication by Regulating ZYG-1 Levels." *Journal of Cell Science*. https://doi.org/10.1242/jcs.097105.

Pelletier, Laurence, Nurhan Özlü, Eva Hannak, Carrie Cowan, Bianca Habermann, Martine Ruer, Thomas Müller-Reichert, and Anthony A. Hyman. 2004. "The Caenorhabditis Elegans Centrosomal Protein SPD-2 Is Required for Both Pericentriolar Material Recruitment and Centriole Duplication." *Current Biology*. https://doi.org/10.1016/j.cub.2004.04.012.

Puklowski, Anja, Yahya Homsi, Debora Keller, Martin May, Sangeeta Chauhan, Uta Kossatz, Viktor Grünwald, et al. 2011. "The SCF-FBXW5 E3-Ubiquitin Ligase Is Regulated by PLK4 and Targets HsSAS-6 to Control Centrosome Duplication." *Nature Cell Biology*. https://doi.org/10.1038/ncb2282.

Rogers, Gregory C., Nasser M. Rusan, David M. Roberts, Mark Peifer, and Stephen L. Rogers. 2009. "The SCF Slimb Ubiquitin Ligase Regulates Plk4/Sak Levels to Block Centriole Reduplication." *Journal of Cell Biology*. https://doi.org/10.1083/jcb.200808049.

Rothbauer, Ulrich, Kourosh Zolghadr, Serge Muyldermans, Aloys Schepers, M. Cristina Cardoso, and Heinrich Leonhardt. 2007. "A Versatile Nanotrap for Biochemical and Functional Studies with Fluorescent Fusion Proteins." *Molecular & Cellular Proteomics*. https://doi.org/10.1074/mcp.m700342-mcp200.

Schmidt, Thorsten I., Julia Kleylein-Sohn, Jens Westendorf, Mikael Le Clech, Sébastien B. Lavoie, York Dieter Stierhof, and Erich A. Nigg. 2009. "Control of Centriole Length by CPAP and CP110." *Current Biology*. https://doi.org/10.1016/j.cub.2009.05.016.

Serçin, Özdemirhan, Jean Christophe Larsimont, Andrea E. Karambelas, Veronique Marthiens, Virginie Moers, Bram Boeckx, Marie Le Mercier, Diether Lambrechts, Renata Basto, and Cédric Blanpain. 2016. "Transient PLK4 Overexpression Accelerates Tumorigenesis in P53-Deficient Epidermis." *Nature Cell Biology*. https://doi.org/10.1038/ncb3270.

Sharma, Ashwani, Amol Aher, Nicola J. Dynes, Daniel Frey, Eugene A. Katrukha, Rolf Jaussi, Ilya Grigoriev, et al. 2016. "Centriolar CPAP/SAS-4 Imparts Slow Processive Microtubule Growth." *Developmental Cell*. https://doi.org/10.1016/j.devcel.2016.04.024.

Silkworth, William T., Isaac K. Nardi, Lindsey M. Scholl, and Daniela Cimini. 2009. "Multipolar Spindle Pole Coalescence Is a Major Source of Kinetochore Mis-Attachment and Chromosome Mis-Segregation in Cancer Cells." *PLoS ONE*. https://doi.org/10.1371/journal.pone.0006564.

Sir, Joo Hee, Monika Pütz, Owen Daly, Ciaran G. Morrison, Mark Dunning, John V. Kilmartin, and Fanni Gergely. 2013. "Loss of Centrioles Causes Chromosomal Instability in Vertebrate Somatic Cells." *Journal of Cell Biology*. https://doi.org/10.1083/jcb.201309038.

Sonnen, K. F., A.-M. Gabryjonczyk, E. Anselm, Y.-D. Stierhof, and E. A. Nigg. 2013. "Human Cep192 and Cep152 Cooperate in Plk4 Recruitment and Centriole Duplication." *Journal of Cell Science*. https://doi.org/10.1242/jcs.129502.

Sonnen, Katharina F., Lothar Schermelleh, Heinrich Leonhardt, and Erich A. Nigg. 2012. "3D-Structured Illumination Microscopy Provides Novel Insight into Architecture of Human Centrosomes." *Biology Open*. https://doi.org/10.1242/bio.20122337.

Stevens, Naomi R., Jeroen Dobbelaere, Kathrin Brunk, Anna Franz, and Jordan W. Raff. 2010. "Drosophila Ana2 Is a Conserved Centriole Duplication Factor." *Journal of Cell Biology*. https://doi.org/10.1083/jcb.200910016.

Stevens, Naomi R., Hélio Roque, and Jordan W. Raff. 2010. "DSas-6 and Ana2 Coassemble into Tubules to Promote Centriole Duplication and Engagement." *Developmental Cell*. https://doi.org/10.1016/j.devcel.2010.11.010.

Sur, Surojit, Raymond Pagliarini, Fred Bunz, Carlo Rago, Luis A Diaz, Kenneth W Kinzler, Bert Vogelstein, and Nickolas Papadopoulos. 2009. "A Panel of Isogenic Human Cancer Cells Suggests a Therapeutic Approach for Cancers with Inactivated P53." *Proceedings of the National Academy of Sciences of the United States of America*. https://doi.org/10.1073/pnas.0813333106.

Swallow, Carol J., Michael A. Ko, Najeeb U. Siddiqui, John W. Hudson, and James W. Dennis. 2005. "Sak/Plk4 and Mitotic Fidelity." *Oncogene*. https://doi.org/10.1038/sj.onc.1208275.

Tang, Chieh Ju C., Ru Huei Fu, Kuo Sheng Wu, Wen Bin Hsu, and Tang K. Tang. 2009. "CPAP Is a Cell-Cycle Regulated Protein That Controls Centriole Length." *Nature Cell Biology*. https://doi.org/10.1038/ncb1889.

Tang, Chieh Ju C., Shin Yi Lin, Wen Bin Hsu, Yi Nan Lin, Chien Ting Wu, Yu Chih Lin, Ching Wen Chang, Kuo Sheng Wu, and Tang K. Tang. 2011. "The Human Microcephaly Protein STIL Interacts with CPAP and Is Required for Procentriole Formation." *EMBO Journal*. https://doi.org/10.1038/emboj.2011.378.

Taus, Thomas, Thomas Köcher, Peter Pichler, Carmen Paschke, Andreas Schmidt, Christoph Henrich, and Karl Mechtler. 2011. "Universal and Confident Phosphorylation Site Localization Using PhosphoRS." *Journal of Proteome Research*.

https://doi.org/10.1021/pr200611n.
Tsou, Meng Fu Bryan, and Tim Stearns. 2006. “Controlling Centrosome Number: Licenses and Blocks.” *Current Opinion in Cell Biology*. https://doi.org/10.1016/j.ceb.2005.12.008.
Vulprecht, J., A. David, A. Tibelius, A. Castiel, G. Konotop, F. Liu, F. Bestvater, et al. 2012. “STIL Is Required for Centriole Duplication in Human Cells.” *Journal of Cell Science*. https://doi.org/10.1242/jcs.104109.
Wong, Yao Liang, John V. Anzola, Robert L. Davis, Michelle Yoon, Amir Motamedi, Ashley Kroll, Chanmee P. Seo, et al. 2015. “Reversible Centriole Depletion with an Inhibitor of Polo-like Kinase 4.” *Science*. https://doi.org/10.1126/science.aaa5111.
Zheng, X., L. M. Gooi, A. Wason, E. Gabriel, N. Z. Mehrjardi, Q. Yang, X. Zhang, et al. 2014. “Conserved TCP Domain of Sas-4/CPAP Is Essential for Pericentriolar Material Tethering during Centrosome Biogenesis.” *Proceedings of the National Academy of Sciences*. https://doi.org/10.1073/pnas.1317535111.
Zheng, Xiangdong, Anand Ramani, Komal Soni, Marco Gottardo, Shuangping Zheng, Li Ming Gooi, Wenjing Li, et al. 2016. “Molecular Basis for CPAP-Tubulin Interaction in Controlling Centriolar and Ciliary Length.” *Nature Communications*. https://doi.org/10.1038/ncomms11874.

Curriculum Vitae

Tyler C. Moyer

Contact Information
- **email:** tylermoyer2011@gmail.com
- **phone:** 570-329-6851
- **address:** 2710 Fait Avenue, Baltimore, MD 21224

EDUCATION

Johns Hopkins School of Medicine // Baltimore, MD **2013-2019**
- Ph.D. Candidate in Department of Molecular Biology and Genetics
- NSF Graduate Research Fellow

Bucknell University// Lewisburg, PA **2007-2011**
- B.S. in Cell Biology/Biochemistry
- GPA: 3.93/4.0, Graduated *summa cum laude*

RESEARCH EXPERIENCE

PhD Candidate, Johns Hopkins School of Medicine **2013-present**
Laboratory of Dr. Andrew Holland
Molecular mechanisms controlling mammalian centriole and centrosome copy number.

- Implemented CRISPR/Cas9 genome engineering technology to build novel cell lines in order to more acutely probe the function of regulatory kinases and molecular complexes of unknown function.
- Optimized lab protocols for protein expression and purification in multiple systems.
- Presented research regularly at group meetings, departmental seminars, and regional conferences
- Collaborated with local, national, and international scientists to study multiple aspects of centriole biology.
- Mentored both rotation and undergraduate students.

Graduate Intern, AstraZeneca **Feb 2019-April 2019**
Department of Cell Culture and Fermentation Sciences
Optimization of monoclonal antibody production in CHO cells

- Contributed to a team of researchers aiming to use CRISPR/Cas9 genome engineering technology to generate novel cell lines with the goal of increased monoclonal antibody production.

Undergraduate Researcher, Bucknell University **2009-2011**
Department of Chemistry, Laboratory of Dr. Thomas Selby
Active site analysis of the phosphatidylinositol-specific phospholipase C from Streptomyces antibioticus

- Purified and characterized an enzyme with targeted mutations to uncover the mechanism of a novel transition state.

LEADERSHIP EXPERIENCE

Physical Science Teacher. Pine Bluff School District. Pine Bluff, AR **2011-2012**

- Taught six periods per day of Physical Science, collaborated with fellow science teachers to plan lessons and laboratory exercises. Maintained laboratory inventory
- Trained by Teach for America, a non-profit organization aiming to close the educational achievement gap in low-income communities

Field Executive. Chi Phi Fraternity. Suwanee, GA **2012-2013**

- Traveled to various college campuses as a leadership consultant promoting leadership practices, accountability, risk and social event management, ethical decision making, budgeting, fundraising, campus and community relations, service and philanthropy, and recruitment.
- Facilitated and organized various educational leadership programs throughout the country for undergraduate and alumni members.

SELECTED AWARDS & HONORS

2015 National Science Foundation Graduate Research Fellows Program Fellowship
2011 Bucknell Prize in Cell Biology/Biochemistry
2011 University Prize for Men
2011 Louis W. Robey Prize (given to graduating male who best exemplifies the pillars of a Bucknell Education)
2010 Greek Leader of the Year

PUBLICATIONS

Moyer, T.C., Holland, A.J. Plk4 phosphorylates STIL to promote CPAP binding and procentriole assembly. In revision at **eLife**.

Kodani, A., **Moyer, T.C.**, Chen, A., Ryu, S., Holland, A.J., Walsh, C.A., Reiter, J.F. SFI1 recruits USP9X to stabilize the microcephaly protein STIL. Accepted at **J. Cell Biol**. 2019

Lambrus, B.*, **Moyer, T.C.*,** and A.J. Holland. 2018. Applying the auxin-inducible degradation (AID) system for rapid protein depletion in mammalian cells. ***Methods in Cell Biology***. doi: 10.1016/bs.mcb.2018.03.004.

Zitouni, S., Francia, M.E., Leal, F., Montenegro Gouveia, S., Nabais, C., Duarte, P., Gilberto, S., Brito, D., **Moyer, T.**, Kandels-Lewis, S., Ohta, M., Kitagawa, D., Holland, A.J., Karsenti, E., Lorca, T., Lince-Faria, M., Bettencourt-Dias, M. 2016. CDK1 Prevents Unscheduled PLK4-STIL Complex Assembly in Centriole Biogenesis. **Current Biology** 26(9):1127-37.

Moyer, T.C., K.M. Clutario, B.G. Lambrus, V. Daggubati, and A.J. Holland. 2015. Binding of STIL to Plk4 activates kinase activity to promote centriole assembly. **J. Cell Biol**. 209:863–78.

Moyer, T.C. and A.J. Holland. 2015. Generation of a conditional analog-sensitive kinase in human cells using CRISPR/Cas9-mediated genome engineering. **M. Cell Biol**. 129:19-36.

PRESENTATIONS

Moyer, T.C., A.J. Holland. (2018, April) Building the Centriole: How Plk4 initiates centriole duplication. Research seminar given at the American Society for Cell Biology Mid-Atlantic Mitosis and Meiosis local meeting, Baltimore, MD. (invited talk)

Moyer, T.C., A.J. Holland. (2017, May). Plk4 kinase activity is regulated through various methods to ensure faithful centriole duplication. Poster session presented at the National Cancer Institute Centriole and Cilia Meeting, Frederick, MD. (poster)

Moyer, T.C., A.J. Holland. (2016, July). Optimizing methods for the generation of conditional Auxin-Inducible Degron-tagged genes using CRISPR/Cas9. Poster session presented at the Cold Spring Harbor Genome Engineering: The CRISPR/Cas Revolution Annual Meeting, Cold Spring Harbor, NY (poster)

Moyer, T.C., K.M. Clutario, B.G. Lambrus, V. Daggubati, and A.J. Holland. (2015, December). Binding of STIL to Plk4 activates kinase activity to promote centriole assembly. Poster session presented at the American Society for Cell Biology Annual Convention, San Diego, CA (poster)

Moyer, T.C. "Molecular Control of Centriole Duplication Timing." National Cancer Institute, Frederick, MD. 27 March 2015. Research Seminar. (invited talk)

Moyer, T.C., K.M. Clutario, A.J. Holland. (2014, December). Chemical genetic analysis of Polo-like kinase 4 activity. Poster session presented at the American Society for Cell Biology Annual Convention, Philadelphia, PA. (poster)